

**THERAPEUTIC TARGETING AND CLINICAL
ASSESSMENT OF THE TUMOUR VASCULATURE**

Quan Sing Ng

**A thesis submitted for the degree of Doctor of Medicine
University of London**

2007



UMI Number: U591359

All rights reserved

INFORMATION TO ALL USERS

The quality of this reproduction is dependent upon the quality of the copy submitted.

In the unlikely event that the author did not send a complete manuscript and there are missing pages, these will be noted. Also, if material had to be removed, a note will indicate the deletion.



UMI U591359

Published by ProQuest LLC 2013. Copyright in the Dissertation held by the Author.
Microform Edition © ProQuest LLC.

All rights reserved. This work is protected against
unauthorized copying under Title 17, United States Code.



ProQuest LLC
789 East Eisenhower Parkway
P.O. Box 1346
Ann Arbor, MI 48106-1346

STATEMENT OF ORIGINALITY

The work presented in this thesis is my own.

Name: Quan Sing Ng **Signature:**

ABSTRACT

The tumour vascular network is essential for tumour growth. Over the next few years, the use of vascular targeting drugs in the treatment of patients with cancer will escalate, which in turn will increase demand for non-invasive methods of assessing tumour vasculature. A perfusion CT technique was developed, allowing measurement of tumour vascular leakage (K) and blood volume (BV) of entire large tumours. This technique is shown to improve on measurement repeatability compared to conventional single level techniques, and can be used to measure tumour vascular changes following anti-cancer treatment.

Ionising radiation has been shown to act synergistically with the vascular disrupting agent Combretastatin A4 Phosphate (CA4P) in animal tumour models. Patients with advanced non-small cell lung cancer were treated with fractionated radiotherapy in combination with CA4P. Radiation alone increases tumour K and BV, especially at the tumour rim, and appears to enhance the vascular disrupting activity of CA4P. The increase in K after radiotherapy correlates with subsequent decrease in BV after CA4P, and a sustained reduction in tumour BV was achieved with this combination.

Nitric oxide (NO) is an important signalling molecule responsible for maintaining the vasodilator tone in tumour vessels, as well as having pro-angiogenic properties. As part of a phase I study, patients with cancer were treated with the

nitric oxide synthase inhibitor N-nitro L-arginine (LNNA). Patients with measurable tumours were scanned using perfusion CT, and all patients demonstrated sustained reductions in tumour BV, demonstrating for the first time in man that NO inhibition has tumour anti-vascular activity.

In summary, perfusion CT is a repeatable technique that can be used to measure vascular changes in whole tumours following therapy. The results presented here have provided further evidence that targeting the tumour vasculature is a promising approach in the treatment of cancer.

ACKNOWLEDGEMENTS

First and foremost, this work would not have been possible without the goodwill and selflessness of the patients at Mount Vernon Cancer Centre.

I am also indebted to the following:

Professor Peter Hoskin, my mentor and supervisor, for his inspirational guidance and cheerful encouragement throughout.

Dr Vicky Goh, for her unfailing support, generosity and enthusiasm.

Sister Jessica Milner, for organising and caring for the patients.

Professor Michele Saunders, for her sound advice and encouragement.

Dr Anwar Padhani, for his insightful comments.

Professor Vincent Cunningham, for patiently explaining the Patlak model.

Professor Gillian Tozer, for her invaluable observations.

Ms Jackie Anderson for providing exceptional administrative support.

Radiographers at the Paul Strickland Scanner Centre, for always accommodating the patients even at the last minute.

Si Min, for always being there when I needed her.

TABLE OF CONTENTS

STATEMENT OF ORIGINALITY	2
ABSTRACT	3 – 4
ACKNOWLEDGEMENTS	5
LIST OF FIGURES	11 – 19
LIST OF TABLES	20
CHAPTER 1 INTRODUCTION	21 – 66
1.1 TARGETING THE TUMOUR VASCULATURE	
1.2 TUMOUR VASCULAR BIOLOGY	
1.2.1 Tumour angiogenesis	
1.2.2 The role of nitric oxide	
1.3 VASCULAR TARGETING DRUGS	
1.3.1 A brief history	
1.3.2 Anti-angiogenic agents	
1.3.3 Small molecule vascular disrupting agents	
1.3.3.1 Flavanoids	
1.3.3.2 Tubulin binding drugs	
1.3.3.2.1 CA4P	
1.3.3.2.1.1 Combination therapy with CA4P	
1.3.3.2.2 Oxi-4503	
1.3.3.2.3 AVE8062 (formerly AC7700)	
1.3.3.2.4 ZD6126	
1.4 FUNCTIONAL IMAGING OF TUMOUR VASCULATURE	

- 1.4.1 PET
- 1.4.2 DCE-MRI
- 1.4.3 Perfusion CT
- 1.5 AIM

CHAPTER 2 VOLUMETRIC PERFUSION COMPUTED 67 – 83
TOMOGRAPHY

- 2.1 INTRODUCTION
- 2.2 VOLUMETRIC PERFUSION CT METHODOLOGY
 - 2.2.1 Image acquisition
 - 2.2.2 Data post-processing and analysis
 - 2.2.3 Patlak analysis
- 2.3 DISCUSSION

CHAPTER 3 MEASUREMENT REPEATABILITY OF 84 – 113
VOLUMETRIC PERFUSION COMPUTED
TOMOGRAPHY

- 3.1 INTRODUCTION
- 3.2 AIM
- 3.3 PATIENTS AND METHODS
 - 3.3.1 Study design
 - 3.3.2 Volumetric perfusion CT
 - 3.3.3 Statistical analysis

- 3.4 RESULTS
- 3.4.1 Within subject measurement repeatability
- 3.4.2 Whole tumour versus four levels versus single level perfusion CT measurements
- 3.4.3 Observer variability
- 3.5 DISCUSSION

CHAPTER 4 TUMOUR VASCULAR EFFECTS OF 114 – 129
FRACTIONATED RADIOTHERAPY IN
HUMAN NON-SMALL CELL LUNG CANCER

- 4.1 INTRODUCTION
- 4.2 AIM
- 4.3 PATIENTS AND METHODS
- 4.3.1 Study Design
- 4.3.2 Volumetric perfusion CT
- 4.3.3 Statistical analysis
- 4.4 RESULTS
- 4.4.1 Whole tumour vascular changes
- 4.4.2 Vascular changes in the tumour rim compared to the centre
- 4.5 DISCUSSION

CHAPTER 5 TUMOUR VASCULAR EFFECTS OF 130 – 149

**COMBRETASTATIN A4 PHOSPHATE
IN COMBINATION WITH RADIOTHERAPY**

5.1 INTRODUCTION

5.2 AIM

5.3 PATIENTS AND METHODS

5.3.1 Study design

5.3.2 Volumetric perfusion CT

5.3.3 Statistical analysis

5.4 RESULTS

5.4.1 Vascular changes from the whole tumour during the first week of
treatment

5.4.2 Vascular changes in the tumour rim compared to the centre during
the first week of treatment

5.4.3 Vascular changes from the whole tumour during the second week
of treatment

5.4.4 Vascular changes from the whole tumour during the third week of
treatment

5.5 DISCUSSION

CHAPTER 6 TUMOUR VASCULAR EFFECTS OF 150 – 168

NTRIC OXIDE SYNTHESIS INHIBITION

6.1 INTRODUCTION

6.2	AIM
6.3	PATIENTS AND METHODS
6.3.1	Study design
6.3.2	Pharmacokinetics
6.3.3	Volumetric perfusion CT
6.3.4	Statistical analysis
6.4	RESULTS
6.4.1	Cardiovascular changes following L-NNA
6.4.2	Pharmacokinetics
6.4.3	Tumour vascular changes following L-NNA
6.5	DISCUSSION

CHAPTER 7	FINAL DISCUSSION AND CONCLUSION	169 – 175
APPENDIX 1		176 – 177
REFERENCES		178 – 220
PUBLICATIONS		221

LIST OF FIGURES

Chapter 1

- Figure 1.1 Synthesis of NO and citrulline from arginine catalysed by the enzyme nitric oxide synthase (NOS).
- Figure 1.2 Mechanism of action of NO on the tumour vasculature and tumour cells resulting in both tumour progression (a), and tumour regression (b).
- Figure 1.3 The chemical structures of FAA (a), and DMXAA (b).
- Figure 1.4 The chemical structure of colchicine.
- Figure 1.5 Tubulin binding agents bind to tumour endothelial cell tubulin (a), resulting in depolymerisation of microtubules, leading to rounding up of the shape of endothelial cells (b). This causes an increase in vascular resistance, permeability, and interstitial fluid pressure, resulting in vascular collapse (c). This can lead to blood cell rouleaux formation, activation of the coagulation cascade, thrombus formation, and tumour haemorrhagic necrosis (d). (Reproduced from Siemman 2002).
- Figure 1.6 The chemical structure of CA4.
- Figure 1.7 The chemical structure of Oxi-4503.
- Figure 1.8 The chemical structure of ZD6126.
- Figure 1.9 A simple two compartmental model valid for both CT and MRI. During the first pass, the contrast agent is transiently confined to

the intravascular space. In the delayed phase, the contrast agent passes through into the extravascular space by simple diffusion (K or K_{trans}), which is gradually balanced by the rate it is transferred back into the intravascular space (K_2 or K_{ep}).

Figure 1.10 Multi-detector CT (MDCT) allows improved spatial resolution, faster scanning time, and the ability to acquire a larger volume (a), compared to single-detector CT where the image slice position has to be determined prior to scanning (b). (Images adapted from www.ctisus.org).

Chapter 2

Figure 2.1 The 16-detector row computed tomography (CT) scanner used in this research study.

Figure 2.2 This series shows the reformatted pre-contrast and eight post-contrast images from a single 10mm axial level; all images are at a similar position along the z-axis of the patient.

Figure 2.3 Image from a single 10mm axial level shows the region of interest drawn freehand around a lung tumour using a mouse and electronic cursor, together with the corresponding coloured parametric map. Each pixel within the tumour map represents a vascular parameter value, in this case, the transfer constant K ; the colour scale indicates red pixels as high K values and purple pixels as low K values.

Figure 2.4 Coloured parametric maps from multiple contiguous axial levels encompassing the whole lung tumour. Each pixel location within the tumour region of interest (ROI) corresponds to a single quantitative vascular parameter value, in this case, the transfer constant K . A global value representing the vascular parameter for the entire tumour can therefore be calculated by taking the median value of all pixels involved.

Figure 2.5 Patlak plot is shown for a study patient. The transfer constant K is derived from the gradient of the line, and relative blood volume (BV) from the y-intercept.

Chapter 3

Figure 3.1 A region of interest (ROI) was drawn freehand around the lung tumour in a study patient and coloured parametric maps of the vascular parameter, in this case, the transfer constant (K) are automatically generated by the perfusion software for this 10mm tumour coverage (a). By repeating the process for another three adjacent tumour levels in the same patient, and amalgamating data from all individual pixels from the four levels, tumour K values can be derived from a 40mm z-axis coverage (b). The colour scale indicates red pixels as high K values and purple pixels as low K values.

Figure 3.2 Bland-Altman agreement plot (a) of the difference between the two scans against the mean of the transfer constant (K) values from the two scans. The mean difference is indicated by the solid line. The two outer dotted lines represent the 95% limits of agreement, which define the range within which most differences between repeated K measurements made on the same subject will lie. Scatter plot (b) of K measurements from the two scans, with a line of perfect agreement, which represents the line all points would lie on if both measurements gave the same reading. This plot provides a visual demonstration of how precise the two sets of measurements are. The closer the measurements lie to this line of equality, the better the agreement.

Figure 3.3 Bland-Altman agreement plot (a) of the difference between the two scans against the mean of the blood volume (BV) values from the two scans. The mean difference is indicated by the solid line. The two outer dotted lines represent the 95% limits of agreement, which define the range within which most differences between repeated BV measurements made on the same subject will lie. Scatter plot (b) of BV measurements from the two scans, with a line of perfect agreement, which represents the line all points would lie on if both measurements gave the same reading. This plot provides a visual demonstration of how precise the two sets of measurements are.

The closer the measurements lie to this line of equality, the better the agreement.

Figure 3.4 Scatter plots of consecutive patients showing the absolute difference from repeated scans for blood volume (BV) (a) and transfer constant (K) (b). Outliers were identified as having differences greater than twice the standard deviation of the differences from all 18 patients.

Figure 3.5 Bland-Altman agreement plots (a) of the difference in transfer constant (K) between the two scans against the mean of the K values for a 10mm, 40mm and whole tumour coverage. The narrowing of the 95% limits of agreement with whole tumour coverage compared to 10mm and 40mm coverage indicates an improvement in measurement repeatability. Scatter plots (b) of K measurements from the two scans with a line of perfect agreement, for a 10mm, 40mm and whole tumour coverage. As tumour coverage increases from 10mm to 40mm to whole tumour, the measurements become closer to the line of equality, indicating an improvement in agreement, and hence the precision of the measurements.

Figure 3.6 Bland-Altman agreement plots (a) of the difference in blood volume (BV) between the two scans against the mean of the BV values for a 10mm, 40mm and whole tumour coverage. The narrowing of the 95% limits of agreement with whole tumour coverage compared to

10mm and 40mm coverage indicates an improvement in measurement repeatability. Scatter plots (b) of BV measurements from the two scans with a line of perfect agreement, for a 10mm, 40mm and whole tumour coverage. As tumour coverage increases from 10mm to 40mm to whole tumour, the measurements become closer to the line of equality, indicating an improvement in agreement, and hence the precision of the measurements.

Chapter 4

Figure 4.1 Line graphs showing mean changes (± 1 standard error) in whole tumour vascular blood volume (BV) (a) and transfer constant (K) (b) after fractionated radiotherapy. Measurements are derived from pixel-by-pixel analysis of whole lung tumour volumes and included pixels from both the more vascularised tumour rim as well as the relatively poorly perfused tumour centre.

Figure 4.2 Coloured parametric maps depicting vascular blood volume (BV) at three contiguous axial levels from a lung tumour, at baseline (a) and after four fractions (18Gy total dose) of radiation therapy (b). Baseline tumour vascularity was spatially heterogeneous with the tumour rim being more vascular than the centre. A greater increase in BV after radiotherapy is observed at the tumour rim compared to the centre.

Figure 4.3 Line graphs showing mean changes (± 1 standard error) in tumour blood volume (BV) (a) and transfer constant (K) (b) at the tumour rim and the tumour centre following fractionated radiation therapy. Increases in both vascular parameters were greater at the tumour rim compared to the tumour centre.

Chapter 5

Figure 5.1 CT images of a lung tumour from three representative axial levels showing coloured parametric map of transfer constant (K) at baseline (a) and after two fractions (9Gy total dose) of radiotherapy (b). Increases in K were seen predominantly at the rim of the tumour.

Figure 5.2 CT images of a lung tumour from three representative axial levels showing coloured parametric map of tumour blood volume (BV) before CA4P (a), 4 hours (b), and 72 hours (c) after a single dose of CA4P. Reduction in BV seen after CA4P at 4 hours was sustained to 72 hours and most evident at the tumour rim.

Figure 5.3 Line graphs showing individual changes in tumour transfer constant (K) after two fractions of radiotherapy (RT) (a), and tumour blood volume (BV) at four and 72 hours after combretastatin A4 Phosphate (CA4P) (b). The six patients who had increases in K after RT had a vascular response to CA4P

Figure 5.4 Regression plot showing change in whole tumour blood volume (BV) after combretastatin A4 Phosphate (CA4P) against change in the transfer constant (K) after radiotherapy. Increase in K after radiotherapy correlated to reduction in BV after CA4P ($r=0.77$, $p=0.026$).

Figure 5.5 Line graphs showing mean vascular changes (± 1 standard error) at the tumour rim and the tumour centre for transfer constant (K) after two fractions of radiotherapy (a), and blood volume (BV) at four and 72 hours after combretastatin A4 phosphate (CA4P) (b). Changes in both vascular parameters were greater at the tumour rim compared to the tumour centre.

Figure 5.6 Changes in mean (± 1 standard error) tumour blood volume (BV) and transfer constant (K) during the course of treatment.

Chapter 6

Figure 6.1 Mean cardiovascular changes ($\pm 95\%$ confidence intervals) in systolic blood pressure (SBP), diastolic blood pressure (DBP) and pulse rate (HR) after a single dose of N-nitro L-arginine (L-NNA).

Figure 6.2 Relationship between N-nitro L-arginine (L-NNA) dose in mg/kg and L-NNA plasma area under the curve (AUC) (a), and peak concentration (b).

Figure 6.3 Typical plasma profile after 0.9mg/kg of N-nitro L-arginine (L-NNA)

Figure 6.4 Coloured parametric maps of tumour blood volume (BV) representing three contiguous axial levels of a lung tumour before (a), and one hour after a single 0.5mg/kg infusion of N-nitro L-arginine (L-NNA) (b). Each pixel within the tumour map represents a single vascular parameter value; the colour scale indicates red pixels as high BV values and purple pixels as low BV values.

Figure 6.5 Line graph showing tumour vascular changes for all eight patients at baseline and one hour after N-nitro L-arginine (L-NNA) and the corresponding boxplots at baseline, one hour and 24 hours after L-NNA for blood volume (BV) (a), percentage of non-enhancing pixels (b), and transfer constant (K) (c). Significant reductions in BV and increases in non-perfused pixels were observed after L-NNA. Changes in K were not statistically significant.

Figure 6.6 Relationship between plasma N-nitro L-arginine (L-NNA) area under the curve (AUC) and reduction in tumour blood volume (BV) at 24 hours after L-NNA.

LIST OF TABLES

Chapter 1

Table 1.1 Anti-angiogenic agents in clinical trial

Chapter 3

Table 3.1 Repeatability statistics from paired studies performed on 18 patients measuring whole tumour blood volume (BV) and transfer constant (K)

Table 3.2 Repeatability statistics from 10mm, 40mm and whole tumour measurements

Table 3.3 Inter- and Intra-observer agreement from ten patients for whole tumour transfer constant (K) and blood volume (BV) measurements

Chapter 4

Table 4.1 Mean (\pm standard deviation) values for tumour transfer constant (K) and blood volume (BV) at baseline and after fractionated radiotherapy

Chapter 5

Table 5.1 Treatment schedule for study patients receiving combretastatin A4 Phosphate (CA4P) at 50mg/m² in combination with radiotherapy (RT) at 4.5Gy per fraction.

CHAPTER 1

INTRODUCTION

1.1 Targeting the tumour vasculature

The tumour vasculature is an attractive target for anti-cancer therapy for several reasons. First, tumour cells rely on an intact vascular network for survival. The tumour blood supply provides oxygen and nutrients and enables removal of toxic waste products. Solid tumours cannot grow and metastasise without their own blood supply. Second, tumour vessels are readily accessible to blood-borne anti-cancer agents, as the cells to be targeted are next to the blood stream. This minimises problems with drug delivery. Third, a single tumour vessel might provide the blood supply for thousands of tumour cells, and theoretically, blockage or destruction of this single vessel will lead to significant tumour cell death downstream. Finally, endothelial cells that line tumour blood vessels have not undergone malignant transformation, and are less likely to become drug resistant due to genetic mutations.

Drugs that target the tumour vasculature are broadly divided into anti-angiogenic agents that prevent new vessel formation, and vascular disrupting agents that selectively destroy existing tumour vessels. There is also evidence that conventional treatment modalities such as radiotherapy and chemotherapy have vascular effects that contribute to their anti-tumour activity. Over the next few

years, there will be an increase in the number of vascular targeting drugs that enter the clinic, which will provide the impetus for further development of non-invasive methods of assessing the tumour vascularity *in vivo*. Functional imaging using computed tomography (CT), magnetic resonance imaging (MRI), and positron emission tomography (PET), can be used to measure surrogate markers of tumour vascular physiology including blood flow, blood volume, and permeability, and thus provide the clinical tools needed to study the tumour vascular environment.

The aim of this work is to measure the vascular changes that occur in human tumours after anti-cancer therapy using a novel functional CT technique. It is hoped that this work will contribute to increasing our understanding of tumour vascular biology, the role of the tumour vasculature in cancer, and lead to the development of novel strategies in cancer therapy.

1.2 Tumour vascular biology

Most solid tumours begin as an avascular group of cells relying on simple diffusion as a means of acquiring nutrition. In order for tumours to grow beyond a few millimetres in diameter, they need to develop their own viable blood supply, which is essential to the process of tumour growth, proliferation, and metastasis (Folkman 1992). The process of tumour neo-vascularisation involves angiogenesis, the development of new vessels by sprouting from pre-existing

ones, and possibly vasculogenesis, *de novo* vascular formation through the recruitment of circulating endothelial progenitor cells. The tumour vasculature is morphologically and functionally distinct. Tumour vessels are thin and tortuous, and are characterised by a relatively high endothelial cell proliferation rate, incomplete endothelium, relative absence of smooth muscle or pericyte investiture, hyper-permeability, high interstitial fluid pressure, and spatially and temporally heterogeneous microcirculation (Jain 1987, Boucher et al 1990, Dvorak et al 1991, Eberhard et al 2000, Hashizume et al 2000, Baluk et al 2003).

1.2.1 Tumour angiogenesis

Tumour angiogenesis is believed to be regulated by a dynamic balance between pro-angiogenic and anti-angiogenic factors. The initiation of tumour angiogenesis involves the switch to an angiogenic phenotype (Hanahan and Folkman 1996). This angiogenic switch can be triggered by the activation of oncogenes, and inactivation of tumour suppressor genes. The tumour microenvironment also plays a part in disrupting this tightly regulated equilibrium, and hypoxia, glucose deprivation, and low pH, can lead to the initiation of angiogenesis (Raben et al 2003). Cancer cells stimulate angiogenesis by the increased production of pro-angiogenic factors, and a decrease in the physiologic levels of endogenous anti-angiogenic factors. The overall process of tumour angiogenesis involves the breakdown of basement membrane and the extracellular matrix by matrix metalloproteinase enzymes (MMP), migration and proliferation of endothelial

cells, organisation of endothelial cells into hollow tubes, formation of new networks of blood vessels, and investment with smooth muscle cells or pericytes.

Regulators involved in inducing angiogenesis include vascular endothelial growth factor (VEGF), acidic and basic fibroblast growth factors (FGF), platelet derived growth factor (PDGF), angiopoietins (Ang-1 and Ang-2), epidermal growth factor (EGF), placental growth factor (PIGF), interleukin-8, integrins, and tumour necrosis factor alpha (TNF- α). PDGF is produced by endothelial and other cells and plays a central role in the recruitment of pericytes and smooth muscle cells (Gerhardt and Betsholtz 2003). The angiopoietins are ligands to the vascular specific receptor tyrosine kinase Tie-2, which when activated, stabilises the growing neovascular network (Thurston 2003). Integrins are present on endothelial cells and mediate endothelial cell-extracellular matrix interactions, adhesion and migration (Hodivala-Dilke et al 2003). Some of the known naturally occurring inhibitors of angiogenesis include thrombospondin-1 (TSP-1), angiostatin, endostatin, transforming growth factor beta (TGF- β), and tissue inhibitor of metalloproteinase-1, -2, and -3 (TIMP-1, TIMP-2 and TIMP-3).

VEGF is probably the most widely studied pro-angiogenic factor (Veikkola et al 2000). The VEGF molecule is a homodimer glycoprotein with several different isoforms, which mediates angiogenesis by acting on high affinity transmembrane tyrosine kinase receptors. VEGFR-1 and VEGFR-2 are found on vascular endothelial cells while VEGFR-3 is expressed on the lymphatic endothelium.

Originally identified as vascular permeability factor (Senger et al 1983), VEGF promotes angiogenesis by inducing capillary vessel permeability allowing plasma proteins such as fibrin to leak into the extravascular space, leading to clotting of extravasated fibrinogen and introduction of a provisional plasma-derived matrix. This provides a favourable environment for activated endothelial cells to migrate into and proliferate, once basement membrane breakdown has occurred. Functional vessels subsequently result from re-canalisation of these endothelial cells (Veikkola et al 2000).

1.2.2 The role of nitric oxide

Furchgott and Zawadzki (1980) first described the significance of endothelial cells in arterial smooth muscle relaxation, and hypothesised that the vasodilatory properties of acetylcholine were dependent on the release of a substance from endothelial cells termed endothelium derived relaxing factor (EDRF). Moncada and colleagues (Palmer et al 1987) demonstrated that nitric oxide (NO) released from vascular endothelial cells is indistinguishable from EDRF in terms of biological activity, stabilisation by superoxide dismutase, and susceptibility to inhibition by haemoglobin. They went on to identify L-arginine as the precursor to the synthesis of NO, as well as the enzyme nitric oxide synthase (NOS), which is able to generate NO and L-citrulline from L-arginine (Moncada et al 1989).

NO is now recognised as a ubiquitous signalling molecule that is implicated in a wide range of pathological and physiological processes. The formation of NO

from arginine is catalysed by the nitric oxide synthase (NOS) enzymes (Alderton et al 2001) (Figure 1.1).

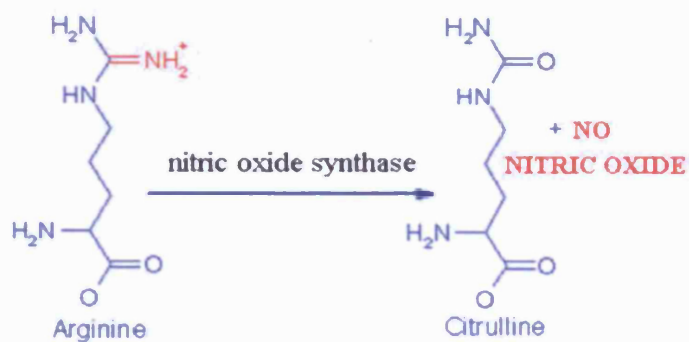


Figure 1.1 Synthesis of NO and citrulline from arginine catalysed by the enzyme nitric oxide synthase (NOS)

Three distinct isoforms of NOS have been identified: neuronal NOS (nNOS, also known as NOS1), inducible NOS (iNOS, also NOS2), and endothelial NOS (eNOS, also NOS3). nNOS and eNOS are constitutively expressed enzymes (cNOS), that are activated by increased intracellular concentrations of calcium (Ca^{2+}). Ca^{2+} binds to calmodulin and the resulting complex activates nNOS or eNOS to produce low levels of NO, which mediates several physiological processes by activation of guanylate cyclase, causing an increase in cGMP. iNOS contains tightly bound calmodulin and is not dependent on intracellular Ca^{2+} . Transcription of the iNOS gene is induced by inflammatory cytokines

(including TNF α and IFN γ), endotoxins, hypoxia and oxidative stress to produce physiologically high levels of NO. Inhibitory cytokines include TGF β , IL-4, IL-10, and macrophage deactivating factor (MDF). In general, NO derived from eNOS has been implicated in tumour angiogenesis, as well as maintaining the vasodilator tone of tumour blood vessels, while iNOS induced NO mediates neoplastic transformation.

The biological role of NO in tumourigenesis is complex and NO has been implicated in both inhibition and promotion of tumour growth (Fukumara et al 2006, Bonavida et al 2006) (Figure 1.2). The actions of NO appear to be dependent on its local concentration, cell type, cellular genetics and redox status. NO can induce tumour progression directly through induction of DNA damage, tumour cell invasion, proliferation, and migration, and indirectly through increased tumour blood flow and angiogenesis. On the other hand, high levels of NO are cytotoxic and can induce tumour cell apoptosis. Increased expression of NOS has been demonstrated in experimental tumour models, and higher levels of NOS expression in human tumours may be correlated with worse prognosis (Thomsen et al 1994, Cobbs et al 1995, Vakkala et al 2000, Klotz et al 1998, Fujimoto et al 1997, Gallo et al 1998).

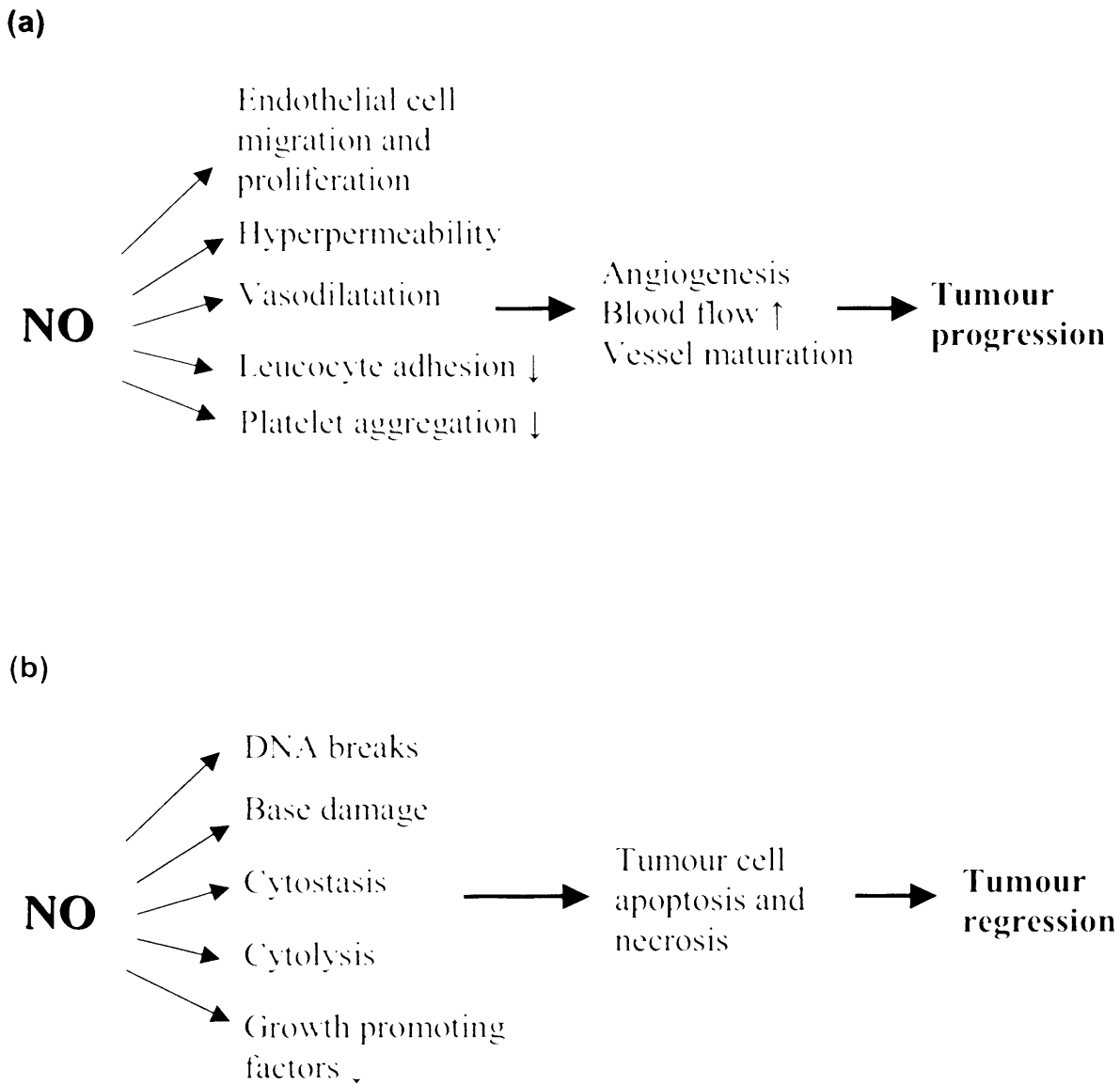


Figure 1.2 Mechanism of action of NO on the tumour vasculature and tumour cells resulting in both tumour progression (a), and tumour regression (b).

NO plays an important role in tumour vascular biology. NO induces endothelial cell proliferation, migration and differentiation (Ziche et al 1994, Kawasaki et al 2003). It has been shown to modulate blood flow and maintain the vasodilator tone of tumour vessels (Peterson 1991). NO is known to act downstream from many pro-angiogenic factors including VEGF which activate endothelial NOS in vascular endothelial cells (Ziche et al 1997, Veikkola et al 2000, Fukumara et al 2001). NO mediates VEGF induced hyper-permeability in tumour vessels and contributes to the development of the extracellular matrix (Fukumara et al 2001). NO might also have a role in the regulation of endogenous inhibitors of angiogenesis, and low levels of NO have been shown to suppress TSP-1 expression (Ridnour et al 2005).

NO delivered exogenously from NO donor agents or by endogenous induction, has been reported as a hypoxic cell radiosensitiser and also as a radiosensitiser of oxygenated cells, which might be due to an increase in DNA damage mediated by reactive oxygen and nitrogen species (Mitchell et al 1993, Griffin et al 1996, Janssens et al 1998, Policastro et al 2006). The vasodilatory effects of NO may also contribute to increasing oxygenation of hypoxic tumour cells and enhancing radiotherapeutic efficacy. NO has also been found to mediate chemosensitivity in tumour cells, and hypoxia-induced drug resistance appears to result, in part, from downstream suppression of endogenous NO production (Matthews et al 2001). NO mimetics have been shown to reduce chemoresistance to doxorubicin in breast and prostate cancer cells (Frederiksen

et al 2003, Muir et al 2006). NO induced vasodilatation may also improve cytotoxic drug delivery to tumours. However, the potential therapeutic role of NO and NOS inhibition in cancer patients remains to be evaluated.

1.3 Vascular targeting drugs

1.3.1 A brief history

It was first suggested more than 160 years ago, that the tumour vasculature was a potential target for the treatment of cancer. It was reported that occasionally, solid tumours could be eradicated when their circulation was interrupted (Walshe 1844). In the 1970s, Folkman and colleagues hypothesised that tumours needed to develop their own blood supply in order to grow, and that tumour growth could be arrested if the factors promoting angiogenesis could be blocked (Folkman 1971). A soluble factor was isolated from animal and human tumours, which was termed tumour-angiogenic factor, and shown to be mitogenic to endothelial cells and responsible for formation of new capillaries (Folkman et al 1971). It is now well recognised that tumour angiogenesis is a critical event in tumour growth and this has led to the identification of a large number of pro-angiogenic growth factors that can act directly on surface receptors on the vascular endothelium (e.g. vascular endothelial growth factor, VEGF), or indirectly via other cell types to activate further growth factor production (e.g. transforming growth factor- β , TGF- β). The VEGF-neutralising antibody bevacizumab was the first anti-angiogenic agent to be approved by the United States Food and Drug

Administration (FDA) in February 2004, although in the United Kingdom, it is not currently recommended by the National Institute for Health and Clinical Excellence (NICE).

In the early 1980s, Denekamp proposed that it might be possible to exploit the functional and morphological differences between tumour and normal blood vessels and therefore selectively target the existing tumour blood supply. It was also suggested that the anti-tumour effects of radiation and cytotoxic drugs could be partially due to damage to the tumour vasculature (Denekamp 1982 and 1984). Distinct from anti-angiogenic agents, which aim to prevent tumour neo-vascularisation, vascular disrupting agents (VDA) aim to cause a rapid shutdown of the established vasculature, resulting in secondary tumour cell death. Two classes of VDAs are being developed. Ligand-directed VDAs use antibodies or peptides to target markers on the tumour endothelium which are selectively up-regulated. These markers include molecules involved with angiogenesis, cell adhesion, and pro-thrombotic change. Low molecular weight VDAs exploit the differences between normal and tumour endothelium to induce vascular shutdown of tumour blood vessels. Several low molecular weight VDAs are currently in clinical trials including the tubulin binding drugs, combretastatin A4 phosphate (CA4P), Oxi 4503 and ZD6126, and the flavanoid, 5,6-dimethylxanthone-4-acetic acid (DMXAA). These are more advanced in clinical development and will be discussed in greater detail in a later section.

1.3.2 Anti-angiogenic agents

The anti-angiogenic approach involves blocking the ability of endothelial cells to break down the surrounding matrix, inhibiting normal endothelial cells directly, and blocking factors that stimulate angiogenesis. Clinical strategies to interfere with VEGF signalling include the use of neutralising antibodies (e.g. Bevacizumab), the VEGF trap which uses a soluble VEGF receptor, and inhibition of the VEGF receptor tyrosine kinase (e.g. ZD6474). A list of anti-angiogenic agents in clinical trials is shown in Table 1.1 (from the United States National Cancer Institute, <http://www.cancer.gov/clinicaltrials/developments/anti-angio-table>). Some of these agents have unknown mechanisms of actions (e.g. Thalidomide) but have been shown to have anti-angiogenic properties in pre-clinical testing. More recently, some agents have been developed, which have multiple targets. For example, BIBF1120 (Boehringer Ingelheim) is an oral triple angiokinase inhibitor with activity against VEGFR, PDGFR, and FGFR.

Table 1.1 Anti-angiogenic agents in clinical trial

Drug	Clinical stage	Mechanism
<i>Drugs that block matrix breakdown</i>		
Dalteparin	Phase 2/3	Heparin binding growth factor inhibitor
Suramin	Phase 1/2	Heparin binding growth factor inhibitor
<i>Drugs that directly inhibit endothelial cells</i>		
ABT-510	Phase 1/2	Thrombospondin-1 mimetic
Lenalidomide	Phase 3	Cytokine and immunomodulator
LY317615	Phase 2/3	Protein kinase C beta inhibitor
Thalidomide	Phase 3	Cytokine and immunomodulator
Soy Isoflavone	Phase 2	Soy protein isolate
<i>Drugs that block activators of angiogenesis</i>		
AMG-706	Phase 1/2	VEGFR/ PDGFR/Kit/Ret
Bevacizumab	Phase 3	Monoclonal antibody to VEGF
AZD2171	Phase 2/3	VEGFR-1,2,3
Bay 43-9006	Phase 3	RAF/VEGFR/PDGFR
PI-88	Phase 2	Heparanase/VEGF/FGF-1,2

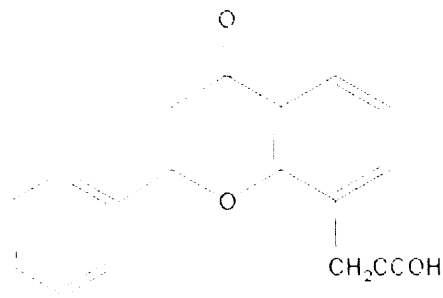
PTK787/ZK 222584	Phase 1/2	VEGFR-1,2,3
SU11248	Phase 3	VEGFR/PDGFR/KIT/FLT3
XL184	Phase 1	VEGFR-2/Met/KIT/FLT3/Tie-2
ZD6474	Phase 2/3	VEGFR-2/EGFR
BIBF1120	Phase 1/2	VEGFR/FGFR/PDGFR
VEGF trap	Phase 2/3	VEGFR-1,2 fused to Fc IgG1
<i>Drugs that inhibit endothelial cell function</i>		
ATN-161	Phase 1/2	$\alpha_v\beta_1$ -integrin inhibitor
EMD-121974	Phase 1/2	$\alpha_v\beta_3/\alpha_v\beta_5$ -integrin inhibitor
Celecoxib	Phase 2/3	COX-2 inhibitor

1.3.3 Small molecule vascular disrupting agents

1.3.3.1 Flavanoids

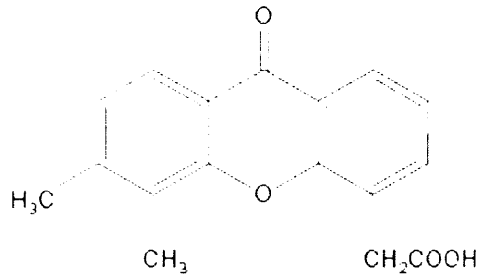
Flavone acetic acid (FAA) was originally developed as an anti-inflammatory drug and was found to have significant anti-vascular and anti-tumour activity in murine tumours (Corbett et al 1986, Kerr et al 1989). The toxicity and lack of anti-tumour activity in phase 1 and 2 clinical studies (Havlin et al 1991, Kaye et al 1990, Kerr et al 1989, Weiss et al 1988, Kerr et al 1987) led to the development of the active and more potent analogue, DMXAA (Antisoma) (Figure 1.3).

(a)



FAA

(b)



DMXAA

Figure 1.3 The chemical structures of FAA (a), and DMXAA (b).

The exact mechanism of action of DMXAA is unknown but is thought to involve the production of a range of cytokines and anti-vascular agents (Baguley 2003). DMXAA may upregulate nuclear-factor $\kappa\beta$ (NF $\kappa\beta$) gene transcription on vascular endothelial and tumour cells, leading to production of tumour necrosis factor and other cytokines (Karin et al 2000, Woon et al 2002). DMXAA has a direct effect on the tumour vascular endothelium causing DNA strand breaks and endothelial

cell apoptosis, increase in permeability, platelet activation and release of serotonin (5HT), and a rapid decrease in blood flow (Lash et al 1998, Ching et al 2002, Baguley et al 1997, Zwi et al 1994). This is followed by the production of tumour necrosis factor alpha (TNF α), which is crucial to the vascular disrupting activity, as well as toxicity of DMXAA (Baguley 2003). Indeed, the lack of anti-tumour activity by FAA was thought to be due to a species-specific difference in the ability to induce TNF α , as FAA is unable to induce TNF α in human mononuclear cell lines in contrast to its activity in murine cell lines (Ching et al 1994). Other cytokines and mediators implicated in the anti-vascular activity of DMXAA include interferon- γ , mRNA for interferon- α , chemokine interferon-inducible protein-10, and nitric oxide (Pang et al 1998, Cao et al 2001). The anti-tumour efficacy of DMXAA has been shown to be enhanced by radiation, cytotoxics, bioreductive agents, and immunomodulatory agents (Cliffe et al 1994, Pruijij et al 1997, Wilson et al 1998, Pedley et al 1996, Pedley et al 1999).

The effects of DMXAA on tumour perfusion were studied in animal tumour models. Using the $^{86}\text{RbCl}$ extraction technique, DMXAA was shown to cause a 79% reduction in tumour perfusion, with no recovery even after 24 hours (Murata et al 2001). Reduction in blood flow after DMXAA was also shown to correspond to onset of hypoxia in the murine RIF-1 tumours, the MDAH-MCa-4 mouse mammary carcinomas, and in NZMN10 human melanoma xenografts (Siim et al 2000). Using MRI, DMXAA treated FaDu and A253 xenografts showed a 78% and 49% reduction in vascular perfusion respectively. CD31-immunostaining of

tumour sections revealed three-fold and two-fold reductions in microvessel density respectively 24 hours after treatment (Seshadri et al 2006). Similarly, MRI studies on the rat GH3 prolactinomas, showed a reduction in MR vascular parameters 24 hours after treatment with 350 mg/kg DMXAA. However, at 200mg/kg, no changes in MR parameters were observed despite histological evidence of tumour necrosis and a significant increase in plasma 5-hydroxyindoleacetic acid (5-HIAA) (McPhail et al 2006).

Two phase-I trials were conducted in parallel by Cancer Research UK in New Zealand and the UK. In the UK study, DMXAA was given weekly at doses ranging from 6 to 4900mg/m² to 46 patients. The maximum tolerated dose was established at 3700mg/m²; dose-limiting toxicities in the form of urinary incontinence, visual disturbance, and anxiety were observed at the highest dose level (Rustin et al 2003). In the New Zealand study, a total of 63 patients received DMXAA every three weeks as a 20 minute infusion. Dose-limiting toxicities were observed at 4900mg/m², including confusion, tremor, slurred speech, visual disturbance, anxiety, urinary incontinence and possible left ventricular failure. Transient prolongation of the corrected cardiac QT interval was seen in 13 patients evaluated at doses of 2000mg/m² and above. A patient with metastatic cervical carcinoma achieved an unconfirmed partial response at 1100mg/m², progressing after eight courses (Jameson et al 2003). Patients from these two studies underwent MRI examinations, demonstrating reductions in MR vascular parameters across a wide range of dose levels (Galbraith et al 2002). A

further phase 1 study was carried out to identify the optimal dose of DMXAA for combination studies (McKeage et al 2006). Fifteen patients received weekly DMXAA at doses ranging from 300 to 3000mg/m². The recommended dose was 1200m/m² because this dose produced no significant effect on heart rate-corrected cardiac QT interval, produced near maximum levels of 5-HIAA, achieved DMXAA plasma concentrations within the preclinical therapeutic range, and was well tolerated.

Phase 1b/2 combination studies of DMXAA are underway. In two separate studies, patients with recurrent ovarian carcinomas and patients with advanced (stage IIIB and IV) non-small cell lung cancer respectively were randomised to receive carboplatin, and paclitaxel, with or without DMXAA. Preliminary data reported no significant additional toxicity with DMXAA, and encouraging early response rates (Gabra et al 2006, McKeage et al 2006).

1.3.3.2 Tubulin binding drugs

The mechanism of action of tubulin binding drugs has been extensively studied (Attard et al 2006). Microtubules are formed from the polymerisation of soluble tubulin heterodimers. They form the backbone of the cellular cytoskeleton, and have a wide range of cellular functions. They are involved in the transport of organelles, transmitters and receptors down neuronal axons. They form mitotic spindles that transport daughter chromosomes to separate poles of the dividing cell during mitosis. Drugs that interfere with microtubule function cause mitotic

arrest leading to cellular apoptosis, which is thought to be the primary anti-neoplastic action of tubulin binding drugs. Examples of tubulin binding drugs are commonly used chemotherapeutic agents like the vinca alkaloids (vincristine, vinblastine etc.), and the taxanes (paclitaxel, docetaxel etc.).

Early studies with the tubulin-binding, anti-inflammatory drug colchicine demonstrated that it induces haemorrhagic necrosis in tumours by damaging the tumour vasculature (Ludford 1945, Ludford 1948) (Figure 1.4).

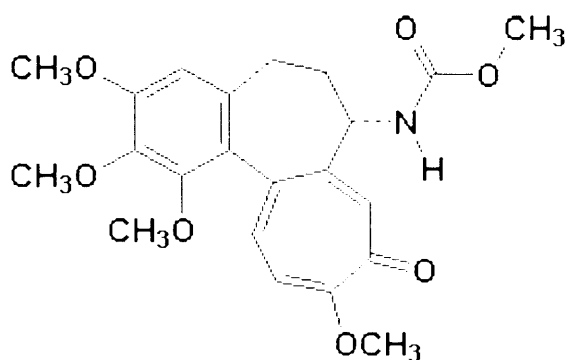


Figure 1.4 The chemical structure of colchicine.

Clinical studies confirmed the vascular disrupting activity of colchicine but only at toxic and potentially lethal doses (Seed 1940). Similarly, the vinca alkaloids have been shown to have anti-vascular activity but only at doses close to their

maximum tolerated dose (MTD) (Baguley et al 1991, Hill et al 1993, Hill et al 1994). Newer agents have since been developed, that can induce vascular damage in tumours at doses much lower than the MTD. These novel tubulin binding agents work by acting near the colchicine binding site of the β -subunit of endothelial cell tubulin, resulting in depolymerisation of microtubules and disorganisation of actin and tubulin, leading to changes in the three-dimensional shape of newly formed endothelial cells. These cells are particularly sensitive to the effects of tubulin binding agents because they lack a well developed actin cytoskeleton and pericytic infiltration that can help maintain its shape. The rounding-up of the shape of endothelial cells can cause an increase in vascular resistance, as well as a rapid increase in vascular permeability. The tumour microcirculation already possesses a high interstitial fluid pressure, and the leakage of plasma proteins into the extracellular space can further exacerbate the interstitial pressure, leading to vascular collapse. The loss of fluid from the vascular space can also cause an increase in haematocrit and consequently increase viscous resistance to blood flow. Exposure of the basement membrane to flowing blood can also initiate the coagulation cascade leading to thrombus formation and reduction in tumour blood flow (Tozer et al 2005) (Figure 1.5).




Figure 1.5 Tubulin binding agents bind to tumour endothelial cell tubulin (a), resulting in depolymerisation of microtubules, leading to rounding up of the shape of endothelial cells (b). This causes an increase in vascular resistance, permeability, and interstitial fluid pressure, resulting in vascular collapse (c). This can lead to blood cell rouleaux formation, activation of the coagulation cascade, thrombus formation, and tumour haemorrhagic necrosis (d). (Reproduced from Siemann 2002).

1.3.3.2.1 CA4P

CA4P (OxiGene) is the first small molecule tubulin binding agent that displays potent and selective toxicity towards tumour vasculature below its MTD (Figure 1.6).

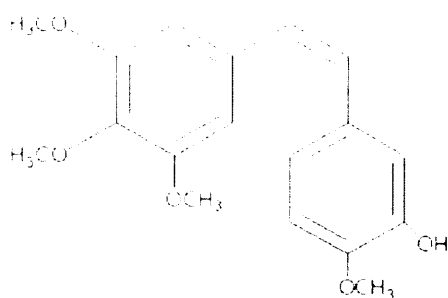


Figure 1.6 The chemical structure of CA4.

CA4P is a synthetic, water soluble, phosphorylated prodrug of the natural product combretastatin A4 (CA4), which was originally isolated from the bark of the African bush willow, *Combretum caffrum*. *In vitro*, the parent CA4 is a strong tubulin-binding agent that has potent activity in preventing tubulin polymerisation and microtubule assembly. Although the exact mechanism for the anti-vascular effects of CA4P remains under investigation, preclinical evidence suggests that it may be a consequence of endothelial cell shape changes and cell damage.

In experimental tumours, CA4P activates the Rho/Rho-kinase pathway, causing microtubule depolymerisation and remodelling of the actin cytoskeleton, resulting in an acute change in endothelial cell shape, and acute increase in vascular permeability (Tozer et al 2005, Kanthou and Tozer 2002, Tozer et al 2001, Galbraith et al 2001). CA4P disrupts the molecular engagement of the endothelial cell-specific junctional molecule vascular endothelial-cadherin (VE-cadherin) *in vitro* and *in vivo* in mice, leading to increase in vascular permeability (Vincent et al 2005). The increase in tumour vascular permeability can result in leakage of plasma proteins into the extracellular space. This causes a further increase in the high interstitial fluid pressure, which results in vascular collapse. Indeed, tumours which are more permeable appear to be more susceptible to the vascular shutdown caused by CA4P (Beauregard et al 2001). The loss of fluid from the vascular space can also cause an increase in haematocrit and consequently increase viscous resistance to blood flow. The reduction in blood flow by CA4P has also been shown to be enhanced by nitric oxide synthase inhibition, suggesting that nitric oxide is involved in the mechanism of action of CA4P (Parkins et al 2000, Davis et al 2002).

In pre-clinical studies, CA4P induces an acute vascular shutdown at less than 10% of the MTD (Dark et al 1997). Using the ⁸⁶RbCl extraction technique, a 50-60% reduction in tumour perfusion was observed in tumours after a single intra-peritoneal administration of 100mg/kg of CA4P, which was associated with a greater than 90% loss of functional vascular volume within six hours post-

treatment (Chaplin et al 1999). Similar findings have been demonstrated in the murine adenocarcinoma CaNT using Hoeschst 33342 dye (Chaplin and Hill 2002).

Vascular changes after CA4P in animal tumour models have also been studied using functional imaging. DCE-MRI and spectroscopy (MRS) were used to demonstrate reductions in perfusion at the central regions of the tumour after CA4P which corresponded to haemorrhagic necrosis seen on histological section (Beauregard et al 1998). Using DCE-MRI, tumour perfusion in rodent tumours were measured after receiving CA4P (30mg/kg), and showed significant decreases at 90 minutes. Twenty-four hours after CA4P, the centre of the tumour remained necrotic while there was re-perfusion at the rim of the tumour to baseline levels suggesting that CA4P selectively targets the necrotic cells in the tumour centre (Zhao et al 2005). This rim of surviving cells is thought to be a consequence of the shared normal vessel circulation between the perimeter of tumours and neighbouring normal tissue. More recently, it was demonstrated that the viable tumour rim might be the result of circulating endothelial progenitor cells which home to the rim following CA4P treatment (Shaked et al 2006).

Phase I human studies of CA4P used weekly for three weeks with a one week break have been completed (Rustin et al 2003). CA4P was rapidly dephosphorylated to the active compound, which was further metabolised to the glucuronide. The only toxicity that possibly was related to the drug dose up to

40mg/m² was tumour pain. Dose-limiting toxicity (DLT) was reversible ataxia in two patients treated at 114mg/m², and vasovagal syncope and motor neuropathy in two patients treated at 88mg/m². One patient suffered fatal ischemia in previously irradiated bowel at 52mg/m². Other drug-related grade 2 or higher toxicities seen in more than one patient were pain, lymphopaenia, fatigue, anaemia, diarrhoea, hypertension, hypotension, vomiting, visual disturbance, and dyspnoea.

A separate phase 1 study looking at the cardiovascular safety profile of CA4P reported significant increases in corrected QT intervals (QTc) on 12-lead electrocardiogram (ECG) at three and four hours after administering CA4P (Cooney et al 2004). Two patients also had ECG changes consistent with acute coronary syndrome within 24 hours of CA4P infusion. Preliminary report from a subsequent study has shown that the increase in QTc was transient, with partial recovery by six hours after CA4P (Ng et al 2005). However, it is now recommended that patients receiving CA4P should not have significant cardiac medical history or prolonged QTc at baseline.

Functional imaging studies were incorporated into the phase 1 trials to evaluate the tumour vascular effects of CA4P. Using DCE MRI, Galbraith et al (2003) showed that CA4P caused significant reductions in tumour K_{trans} in six of 16 patients treated at 46.8mg/m², with a significant group mean reduction of 37% at 4 hours after treatment, with partial recovery by 24hours. The mean reduction in

tumour initial area under the gadolinium–diethylenetriamine pentaacetic acid concentration-time curve (AUC) was 33% at 4 hours, again with some recovery by 24 hours demonstrating a transient vascular shutdown. No significant reductions in DCE-MRI vascular parameters were seen in muscle or in kidney. Visual inspection of tumour perfusion parameter maps provided preliminary evidence for the selective targeting of CA4P to the central region of the tumour. A further 13 patients on this study were scanned using H₂¹⁵O PET and C¹⁵O PET (Anderson et al 2003); reductions of 49% and 15% were seen in tumour perfusion and blood volume respectively 30 minutes after CA4P administration. Again, there was limited recovery of tumour blood volume and perfusion by 24 hours. Vascular changes were also observed in spleen and kidney at 30 minutes after CA4P, with recovery by 24 hours.

1.3.3.2.1.1 Combination therapy with CA4P

CA4P appears to selectively disrupt the vasculature in the tumour centre resulting in haemorrhagic necrosis, while leaving a rim of viable tumour cells at the periphery that can re-vascularise and proliferate. The partial recovery in tumour vascularity after single agent CA4P, and the lack of objective response in phase I human studies strongly suggests that in order to optimise the therapeutic effects of CA4P, it needs to be combined with another treatment modality that can target the surviving tumour rim. This viable rim is vascularised and well oxygenated and is likely to be in a state of rapid proliferation, thus lending itself well to tumour cell killing by conventional therapies.

CA4P has been shown to enhance the tumour cytotoxic effects of conventional chemotherapeutic agents. Tumour growth was impeded when CA4P was combined with 5-fluorouracil in experimental murine colon adenocarcinoma (Grosios et al 2000). In the resistant medullary thyroid carcinoma model in mice, the combination of CA4P and doxorubicin extended the tumour doubling time compared to untreated controls (Nelkin and Ball 2001). CA4P when combined with cisplatin caused increased tumour cell death secondary to haemorrhagic necrosis in rodent (KHT sarcoma), human breast (SKBR3) and ovarian (OW-1) tumour models (Siemann et al 2002). In a xenograft model of Kaposi's sarcoma grown in athymic mice, significant tumour growth delay was achieved when CA4P was combined with cisplatin (Li et al 2002). CA4P when combined with irinotecan also significantly increased the tumour volume doubling time in the experimental rhabdomyosarcoma tumour model in rats (Wildiers et al 2004).

CA4P in combination with other novel agents has also been studied. Using the SW1222 colorectal xenografts, antibody-targeted radioimmunotherapy was shown to be more effective against the well perfused tumour rim but was less effective at the more hypoxic centre, producing tumour regressions for approximately 35 days. When ¹³¹I-labeled anti-carcinoembryonic antigen IgG, was combined with CA4P, complete cures were obtained (Pedley et al 2001). The spatial distribution of this combination was also studied and revealed that radioimmunotherapy effectively treated the tumour rim only, while CA4P targeted

the tumour centre (Pedley et al 2002). More recently, it was demonstrated that treatment of tumour-bearing mice with CA4P leads to an acute mobilisation of circulating endothelial progenitor cells (CEP), which home to the viable tumour rim. Disruption of this CEP spike by anti-angiogenic drugs resulted in marked reductions in tumour rim size and blood flow as well as enhanced anti-tumour activity (Shaked et al 2006).

CA4P has been shown to enhance or act synergistically with radiation (Siemann and Horsman 2002, Li et al 1998, Murata et al 2001). Radiotherapy is known to be effective at the tumour rim where blood flow and oxygenation is relatively normal (Steel 1983). In addition, a high oxygen tension relative to the more hypoxic tumour core lends itself well to radiation treatment where tumour damaging free radical formation is largely oxygen dependent. Ionising radiation treatment targets the richly oxygenated areas of tumours, whereas the more hypoxic inner region of tumours frequently remains relatively unaffected and will continue to survive and grow. Thus, combining CA4P with radiotherapy might provide the potential synergy that is required to treat the whole tumour.

Pre-clinical studies have demonstrated synergy between CA4P and radiation. In nude mice bearing the murine adenocarcinoma CaNT, CA4P was combined with a fractionated radiation schedule, and demonstrated a 63% increase in tumour regression compared to radiation alone. Furthermore, 50% of the tumour bearing animals achieved a complete response, which was not observed with radiation or

CA4P alone (Chaplin et al 1999). In both the KHT sarcoma and the C3H mammary carcinoma in mice, CA4P combined with radiation caused an increase in tumour necrosis (Murata 2001). In the rat rhabdomyosarcoma model, CA4P significantly enhanced the growth delay effects of ionising radiation, with the greatest effects being seen with large tumours (Landuyt et al 2001). In KHT sarcoma-bearing mice, CA4P administered after radiation treatment significantly reduced tumour cell survival compared to radiation alone (Li et al 1998).

The possibility that CA4P might affect radiation damage in normal tissue was assessed by Murata et al (2001) using mouse normal foot skin, a well established sensitive endpoint representative of acute morbidity. The results showed that CA4P given 30 minutes post irradiation significantly improved tumour response to radiation as evidenced by the increased induction of tumour necrosis but did not enhance radiation-induced skin damage. These observations suggest that CA4P preferentially targets the tumour vasculature and that the enhancement of radiation damage in tumours is associated with such vascular changes.

The apparent concern in such combination studies is the potential induction of hypoxia by CA4P rendering the tumour radioresistant, and the effects of vascular shutdown hindering delivery of systemic cytotoxic drugs to the tumour. In the C3H mammary carcinoma, tumour hypoxia measured with the Eppendorf oxygen electrode increased within one hour of CA4P, and was sustained up to six hours,

with partial recovery at 12 and 24 hours (Horsman et al 1998). More recently, it was shown using ^{19}F MRI oximetry and DCE-MRI that CA4P induces hypoxia and reduced perfusion in the syngeneic 13762NF rat breast carcinoma within 90 minutes of treatment (Zhao et al 2005). The initial changes in oxygenation in the tumour centre and periphery were parallel but by 24 hours, there was significant re-perfusion and re-oxygenation at the periphery of the tumour, while the centre remained hypoxic. The spatial and temporal effects of CA4P might therefore explain the dependence of timing and scheduling of the anti-tumour activity of CA4P when combined with radiotherapy and chemotherapy. In the C3H mammary carcinoma, improvement in tumour control was only observed when CA4P was administered at the same time or after radiation (Murata et al 2001, Horsman and Murata 2002). In a variety of tumour models, tumour cell death was significantly enhanced without increase in bone marrow toxicity when CA4P was administered one to three hours after cisplatin but not when it was given one hour before cisplatin (Siemann et al 2002). In contrast, the combination of irinotecan and CA4P did not appear to be affected by scheduling in causing tumour growth delay in the rhabdomyosarcoma tumour model in WAG/Rij rats (Wildiers et al 2004).

The importance of scheduling was demonstrated in a phase 1 dose-escalating combination study of CA4P and carboplatin (Bilenker et al 2005). In this study, CA4P was administered one hour after carboplatin on a 21 day treatment cycle and failed to reach therapeutic doses of either CA4P or carboplatin because of

dose-limiting thrombocytopenia. Pharmacokinetic interaction between the two drugs was suggested to be the reason for the greater exposure of carboplatin (as area under the curve) causing increased thrombocytopenia. Also, CA4P has previously been shown using $H_2^{15}O$ PET to transiently reduce kidney perfusion in patients, with full recovery by 24 hours (Anderson et al 2003). Therefore, CA4P when administered one hour after carboplatin, might have affected renal excretion of carboplatin and increased its toxic side effects. A similar study combining CA4P with paclitaxel, carboplatin, or both is ongoing (Rustin et al 2005). In this study, CA4P was administered to patients 18 to 22 hours prior to receiving chemotherapy. Preliminary results reported that dose escalation reached therapeutic levels of CA4P and both cytotoxic agents without enhancement of chemotherapy related toxicity.

The rationale for combination therapy with CA4P therefore stems from their different and potentially complementary mechanisms and site of action and their non-overlapping toxicity profiles. Careful timing and sequencing of these agents is critical to treatment success. Presently, early phase clinical trials of CA4P in combination with radiotherapy, chemotherapy, immunotherapy, and anti-angiogenic agents are underway.

1.3.3.2.2 Oxi-4503

Oxi-4503 (OxiGene) is the diphosphate prodrug form of combretastatin A1 which has been reported to have more potent anti-vascular and anti-tumour effects than CA4P (Figure 1.7).

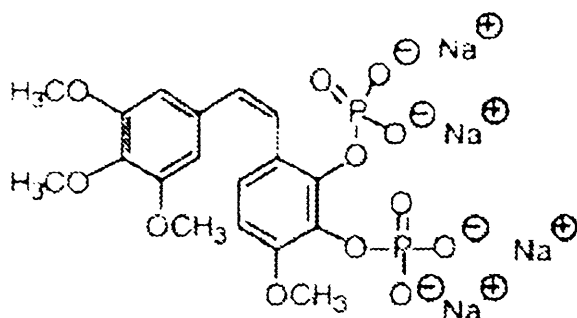


Figure 1.7 The chemical structure of Oxi-4503.

In murine breast adenocarcinoma CaNT, Oxi4503 at a dose of 1 mg/kg induced a greater than 50% reduction in functional vascular volume, which increased to 80% or more following doses of 10, 25 and 50 mg/kg. In contrast, CA4P induced approximately 40% vascular shutdown at 50 mg/kg, but had no measurable effect at 10 mg/kg. In addition, Oxi4503 but not CA4P induced significant tumour growth retardation at comparable doses (Hill et al 2002). Similar reductions in blood flow measured using intravenous injections of fluorescence beads, and tumour growth were observed in mice tumours after Oxi4503. In this study, the spatial heterogeneity in tumour blood flow was studied using quantitative fluorescence microscopy, and showed that Oxi4503 had greater vascular

disrupting effects at the tumour periphery than CA4P, where only central regions were affected (Hua et al 2003). The additional potency of Oxi4503 compared to CA4P, may be due to the rate of dephosphorylation, or the production of a quinine metabolite with enhanced cytotoxic activity (Thorpe et al 2003). Oxi4503 is currently in phase 1 clinical trials.

1.3.3.2.3 AVE8062 (formerly AC7700)

AVE8062 (Aventis) is a synthetic water soluble combretastatin A4 derivative, that has been shown in animal tumour models to have potent anti-vascular and anti-tumour activity (Hori et al 1999, Hori et al 2002). The mechanisms of action of AVE8062 was evaluated using intravital microscopy, which showed that AVE8062 induced a powerful and long-lasting constriction of host arterioles, so that complete stasis of blood flow occurred in downstream vessels, which supplied blood to tumours, resulting in complete vascular thrombosis (Hori et al 2003). Preliminary results from a phase 1 clinical trial of AVE8062 administered once weekly for 3 weeks every 28 days, reported asymptomatic systolic hypotension in patients. A change in DCE-MRI vascular parameters was also observed (Tolcher et al 2003).

1.3.3.2.4 ZD6126

ZD6126 (Astra Zeneca) is a phosphate prodrug of the tubulin binding agent ZD6126 phenol (N-acetylcolchicinol) (Figure 1.8).

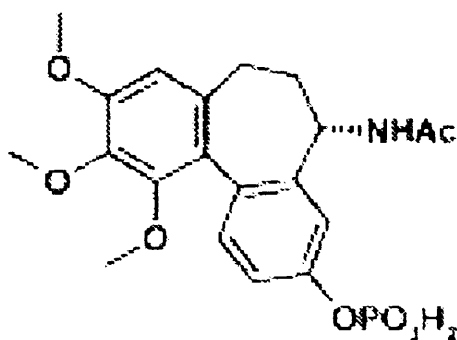


Figure 1.8 The chemical structure of ZD6126.

In vivo studies of ZD6126 were carried out in a range of tumour models, and showed that at doses 8 to 16 times lower than the MTD, ZD6126 causes vascular shutdown leading to extensive tumour necrosis, and was able to achieve growth delay in certain tumours (Blakley et al 2002). Similar findings were observed in the CH3 mouse mammary carcinoma where ZD6126 induced a significant decrease in tumour perfusion and oxygenation, and a significantly increased necrotic fraction (Horsman and Murata 2003). Functional imaging studies using MR studies were also performed to assess the vascular effects of ZD6126. In the rat GH3 prolactinomas and murine RIF-1 fibrosarcomas a dose-dependent decrease in MR vascular parameters was observed after ZD6126 (Robinson et al 2003). In the GH3 prolactinoma, 50 mg/kg of ZD6126 resulted in a decrease in MR vascular parameters, with no recovery of perfusion even at 96 hours (McIntyre et al 2004). ZD6126 has also been shown to enhance the therapeutic effects of chemotherapy, radiotherapy, and anti-angiogenic agents

(Siemman and Rojiani 2002, Siemman and Rojiani 2002, Horsman and Murata 2003, Raben et al 2004, Cionini et al 2004).

In clinical studies, the tumour anti-vascular activity of ZD6126 was demonstrated using DCE-MRI. In 9 patients, at doses of 80mg/m² and higher, MR vascular parameters after ZD6126 treatment were reduced to 36-72% of the baseline values (Evelhoch et al 2004). Preliminary data from a phase 1 dose-escalating study of ZD6126 on a 21 day cycle was reported, with one patient experiencing grade 2 ischaemic changes on 12-lead electrocardiogram (ECG) and grade 3 elevation in troponin I with subsequent demonstration of coronary artery disease (Gadgeel et al 2002). A completed phase 1 study with 32 patients receiving weekly ZD6126 (Beerepoot et al 2006), also reported a patient with a history of ischaemic heart disease developing acute myocardial infarction two weeks after drug discontinuation. Dose limiting toxicities were hypoxia caused by pulmonary embolism and an asymptomatic decrease in left ventricular ejection fraction at 28 mg/m². In this study, circulating endothelial cells, which were measured as a pharmacodynamic marker of vascular damage, were shown to increase after infusion of ZD6126.

1.4 Functional imaging of tumour vasculature

Over the next few years, an increasing number of vascular targeting drugs will be used in the treatment of patients with cancer, which in turn will increase demand

for non-invasive methods of assessing tumour vascularity *in vivo*. There are several reasons for this. First, these drugs may not alter tumour size as a consequence of their action; thus, conventional criteria for therapeutic response assessment, based on tumour size change, may be inappropriate (World Health Organisation 1979, Therasse et al 2000, Kerbel and Folkman 2000). Second, functional imaging can provide pharmacodynamic information related to drug mechanism of action which, in early clinical trials of new therapeutic agents can support the decision to go ahead and develop larger phase 3 clinical studies with clinically relevant end-points. Third, vascular targeting drugs tend to have a wider therapeutic window than conventional drugs. Thus, in early-phase dose-finding trials, relying solely on toxicity-based criteria to define a dose has been suboptimal. Biologic changes, assessed by these imaging methods, can be used to show proof of principle of drug activity, and a lower dose than defined using toxicity-based criteria may be selected for further study. Finally, functional imaging techniques may have an advantage over the current standard of quantification in histological studies of angiogenesis using microvessel density counting, which is invasive and limited by random sampling errors and observer variability.

Several imaging modalities can assess the vascular function of human tumours. Apart from cost and logistics issues, the choice of modality will depend on our understanding of both the drug mechanism and the capabilities and limitations of the imaging technique. Perfusion CT (also known as dynamic contrast enhanced

CT), dynamic contrast enhanced magnetic resonance imaging (DCE-MRI), and positron emission tomography (PET) are the imaging techniques most commonly used in the clinical evaluation of vascular targeting drugs.

1.4.1 PET

Positron emission tomography (PET) can be used to quantify tumour physiological characteristics such as glucose metabolism, blood flow and blood volume, which are relevant to tumour angiogenesis and its therapy (Laking and Price 2003). Proton rich isotopes act as PET radiotracers that decay by positron (positively charged electron) emission. When its kinetic energy is dispersed, the positron combines with a normal electron and the two particles are annihilated. They are converted to two gamma ray photons of equal energy which are emitted 180 degrees apart, and are detected coincidentally with a PET camera, which is a ring-shaped array comprising a large number of scintillation detectors. When two scintillation detectors, separated 180 degrees apart are stimulated simultaneously, they will transmit a coincident signal. Using tomographic reconstruction algorithms, the spatiotemporal distribution of the positron emitter can be localised three-dimensionally.

PET with [18F]-fluorodeoxyglucose (^{18}F FDG), has been advocated as a tool to monitor clinical and sub-clinical responses after cancer treatment (Young et al 1999). In most malignant tissues, there is increased cellular uptake and accumulation of phosphorylated FDG by hexokinase. FDG-6-phosphate is not

metabolised intracellularly due to the position of the ^{18}F label and is therefore biochemically trapped. Measuring the uptake of FDG serves as a proxy for glucose metabolism. ^{18}F FDG PET has been shown to be superior to conventional response criteria using CT in monitoring response to imatinib therapy in patients with gastrointestinal stromal tumours (Antoch et al 2004). ^{18}F FDG PET is also widely used in the diagnosis, prognostication and therapeutic monitoring of a wide variety of cancers (Weber 2005). Agents that deprive tumours of blood supply also impact metabolism and their therapeutic efficacy are therefore potentially measurable using FDG-PET. ^{15}O -labeled water (H_2^{15}O) is freely diffusible into and out of tissue water, is biologically and metabolically inert, and can be used to measure tissue perfusion. ^{15}O -labeled carbon monoxide (C^{15}O) binds irreversibly with haemoglobin to form C^{15}O -Hb carboxyhaemoglobin, which stays within the vascular space and can be used to measure vascular blood volume. H_2^{15}O and C^{15}O PET have been used to assess tumour vascular response following CA4P in a phase 1 clinical trial (Anderson et al 2003). Hypoxia imaging is also possible using tracers that are trapped within cells in the reduced state (Krause et al 2006). ^{18}F -fluoromisonidazole (^{18}F -MISO) has a high accumulation in hypoxic tissue that is proportional to the hypoxic fraction of the tumour. ^{18}F -MISO has been used to measure hypoxia in human cancers including lung, head and neck, renal, brain and rectal tumours, and has been used to monitor the effects of cancer therapy (Krause et al 2006). Copper $^{60,-62,-64}$ labelled methylthiosemicarbazone (Cu-ATSM) has also been developed for hypoxic imaging. ATSM compounds are freely diffusible, and are

rapidly taken up by hypoxic cells but are quickly washed out of normoxic cells, and have the potential advantage of a more rapid visualisation of hypoxia signal. Patients with lung cancer were investigated with (^{60}Cu) ATSM PET prior to receiving therapy (chemotherapy only, radiotherapy only or chemo-radiotherapy). Non-responders were shown to have a significantly higher (^{60}Cu) ATSM uptake than in responders (Dehdashti et al 2003). Tracers have also been used to label specific organic compounds in the angiogenic pathway, such as VEGF, potentially allowing for the direct imaging of tumour angiogenesis (Li et al 2001). The major limitations of PET are relatively poor spatial resolution, limited clinical availability, high radiation dose and the expense in using and logistical difficulty in producing short-lived isotopes.

1.4.2 DCE-MRI

DCE-MRI is relatively well established in imaging angiogenesis (Padhani 2003). It does not employ ionising radiation, therefore allowing repeated examinations, and this is particularly suited to early phase dose finding trials. DCE-MRI measurements of tumour perfusion have also been correlated against histological markers of angiogenesis in a variety of tumours (Buckley et al 1997, Hawighorst et al 1997). DCE-MRI is essentially a single level technique although multiple slices can be examined. DCE-MRI measures the change in signal intensity over a period of time as the contrast agent passes through the tumour vasculature. It is able to distinguish between malignant and benign tissues because their vasculature is morphologically and functionally different. A

significant disadvantage of MRI is that the relationship between MR signal intensity change and contrast agent concentration, particularly for large vessels, is not easily defined. The signal intensity is dependent on multiple factors including the tissue T1 relaxation time, contrast agent dose, rate of injection, the chosen imaging sequence and parameters.

Vascular parameters may be evaluated by two MR sequences. T1 weighted sequences reflect microvessel perfusion, permeability and extracellular leakage space. T2* weighted sequences reflect tissue perfusion and blood volume. In T1 sequences, the change in the signal intensity of the commonly used paramagnetic contrast agent, gadolinium–diethylenetriamine pentaacetic acid (Gd-DTPA), measured over several minutes can be analysed using pharmacokinetic models. Gd-DTPA is neither freely diffusible nor a pure blood pool agent, and therefore the transfer constant (K_{trans}) of Gd-DTPA from the plasma into the extracellular space will be affected by permeability changes as well as perfusion changes. In extra-cranial tumours, due to high microvessel permeability, blood perfusion will be the dominant factor and K_{trans} approximates to the blood flow per unit volume of tissue. Other vascular parameters measurable using T1 weighted sequences are the extracellular leakage space (v_e), and the rate of contrast return into the vasculature (k_{ep}) (Figure 1.9). T2* weighted sequences monitor the passage of contrast through the vascular space, and the loss of signal intensity is dependent on the vascular concentration of the contrast agent, and microvessel size and density. Kinetic

modelling of the signal intensity change allows the relative quantification of blood volume (rBV), mean transit time (MTT), and blood flow (rBF).

Hypoxic imaging with MR is possible with blood oxygen level dependent (BOLD) MRI, which uses endogenous deoxyhaemoglobin as the source of contrast. Deoxyhaemoglobin increases the MR transverse relaxation rate $R2^*$ ($=1/T2^*$) of water in blood and in the surrounding tissue, therefore acting as an intrinsic contrast agent. Deoxyhaemoglobin concentration changes with oxygen content but it is also affected by tissue perfusion. The major advantage of BOLD MRI is that there is no need to administer contrast material, and therefore it can be repeated as needed.

1.4.3 Perfusion CT

Perfusion CT allows direct quantification of vascular function, as there is a direct linear relationship between enhancement change and iodine concentration. For example, at 80kV, 1mg/ml iodine is equivalent to a Hounsfield Unit (HU) change of 43HU. This is a significant advantage over DCE-MRI where the relationship between MR signal intensity change and contrast agent concentration is complex. Perfusion CT assessment of tumour vascularity is possible by tracking the temporal changes in tissue attenuation, as intravenously administered low molecular weight (<1kD) iodinated contrast media travels by blood flow to the tissue, and by rapid diffusion, leaks out from the vascular space into the extravascular space. To date, different image acquisition protocols, image

analysis methods, and a variety of pharmacokinetic models exist for the quantification of physiologically based vascular parameters (Miles 2003, Dawson 2006). In general, a non-contrast enhanced baseline image is acquired, followed by a series of repeated images after intravenous contrast medium administration. There is an initial vascular phase when the contrast media remains transiently in the intravascular space. During this first pass, contrast enhancement reflects tissue perfusion (blood flow per unit volume or mass of tissue) and blood volume. A typical scanning protocol would involve acquisition of up to 60 images, at a frequency of one image every second. Delayed phase studies are performed when the contrast agent passes through into the extravascular space. Delayed enhancement is determined by the rate constant of the transfer of contrast media into the extravascular space (transfer constant, K). K is a function of both tissue blood flow and the permeability surface product (PS); the latter is defined as the product of permeability and the total surface area of capillary endothelium in a unit mass of tissue. Whether K is dominated by flow or PS may be altered according to the experimental conditions. Delayed phase studies allow larger volumes to be covered, and images are obtained at a lower frequency but over a longer period (Figure 1.9).

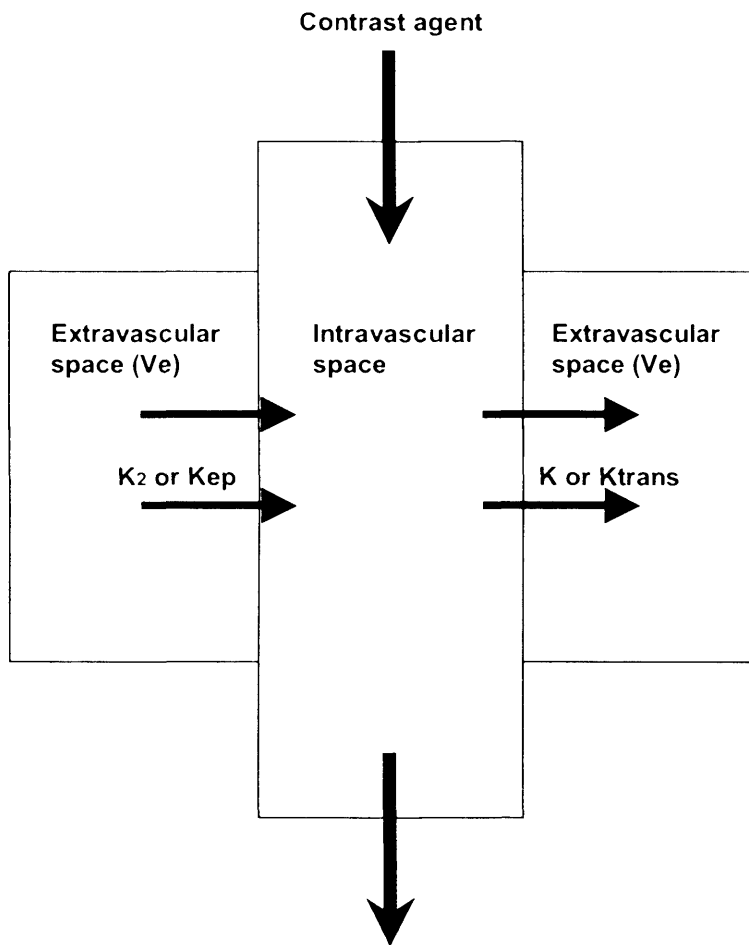


Figure 1.9 A simple two compartmental model valid for both CT and MRI. During the first pass, the contrast agent is transiently confined to the intravascular space. In the delayed phase, the contrast agent passes through into the extravascular space by simple diffusion (K or K_{trans}), which is gradually balanced by the rate it is transferred back into the intravascular space (K₂ or K_{ep}).

The limitations of perfusion CT include radiation exposure, the need for intravenous injections of contrast media, and the risk of hypersensitivity reactions. Perfusion CT measurements, like MRI, are also currently limited to a single axial level, limiting tumour coverage in heterogeneous tumours. Perfusion CT has several advantages over DCE-MRI in imaging the tumour vasculature. As mentioned previously, the reliable linear relationship between enhancement, measured as HU, and contrast concentration, allows straightforward quantification, compared to MR where quantification remains problematic. CT is widely accessible, relative cost effective, and commercial perfusion software is now available, and can be easily incorporated into existing CT protocols for day-to-day oncological imaging. There are also anatomical regions where CT is preferable to MR, for example the lung, where respiratory motion can produce artefacts that would interfere with MR evaluation. The introduction of multi-detector CT (MDCT) has stimulated further interest in perfusion CT techniques. Unlike single detector CT, where the image slice position has to be determined prior to scanning, MDCT allows the CT scanner to acquire more than one slice simultaneously (Figure 1.10). The advantages of MDCT are improved spatial resolution, reduced scanning time, and the ability to scan a larger tissue volume. The use of perfusion CT to obtain tumour vascular measurements will be further described in Chapter 2.




Figure 1.10 Multi-detector CT (MDCT) allows improved spatial resolution, faster scanning time, and the ability to acquire a larger volume (a), compared to single-detector CT where the image slice position has to be determined prior to scanning (b). (Images adapted from www.ctisus.org)

1.5 Aim

There are three main objectives to this work. The first is to develop a repeatable clinical perfusion CT method that will allow quantification of tumour vascularity in whole tumours. The second is to assess the vascular changes that occur after treatment with fractionated radiotherapy alone and in combination with the vascular disrupting agent CA4P. The final objective is to measure the vascular changes that occur after treatment with the NOS inhibitor L-NNA.

CHAPTER 2

VOLUMETRIC PERFUSION COMPUTED TOMOGRAPHY

2.1. Introduction

Perfusion CT (also known as dynamic contrast enhanced CT) provides a quantitative and non-invasive method for studying tumour vascular function. CT is widely available and perfusion CT has been used increasingly as a clinical tool for monitoring responses to treatment with vascular targeting drugs (Thomas et al 2003, Xiong et al 2004, Willett et al 2004). It has been validated against a variety of techniques including microspheres, xenon CT and ^{15}O labelled- H_2O PET (Gobbel et al 1991, Gobel et al 1993, Cenic et al 1999, Gillard et al 2000, Wintermark et al 2001, Purdie et al 2001) and has been correlated against histological markers of angiogenesis (Jinzaki et al 2000, Tateishi et al 2002, Yi et al 2004, Wang et al 2006). Up to now, CT assessment of tumour vascular parameters has been limited to a single tumour level, though a number of contiguous axial images at the same tumour level can be acquired with multi-detector row scanners, depending on the row configuration. For example, with a 16-detector row scanner, a z-axis coverage up to 24mm is possible, and with a 64-detector scanner, a maximum coverage of 4cm is achievable.

However, it is well recognised that tumour vasculature exhibits spatial heterogeneity; blood flow can vary in different locations within a single tumour

depending on the tumour microenvironment (Chaplin et al 1995, Kimura et al 1996). Therefore, single level measurements of tumour vascularity will only provide a limited sample of the entire region of interest and may be unrepresentative of the tumour as a whole, especially in larger tumours. Greater tumour coverage has the potential to compensate for this heterogeneity, and hence to reduce measurement variability. In collaboration with Siemens Medical Solutions (Forchheim, Germany), a CT technique was developed that allows evaluation of tumour vascularity in entire tumour volumes.

2.2 Volumetric perfusion CT methodology

2.2.1 Image acquisition

Patients were scanned using a 16-detector row CT scanner (Sensation 16, Siemens Medical Solutions, Forchheim, Germany) (Figure 2.1). No additional patient preparation was required over and above that for a routine thoracic CT examination. An 18-gauge cannula was placed into an antecubital fossa vein while the patient lay supine on the scanner table. The majority of patients recruited into this study had lung cancer, and in order to minimise movement, all patients were carefully instructed on the correct breath-holding technique prior to scanning, and were allowed to practise several times. All scans were performed using breath-hold at tidal expiratory volume, as a consistent tumour position and coverage were more achievable in expiration than inspiration in our patient group.

There was also direct communication between the patients and the radiographer at all times during scanning using a microphone and speaker.



Figure 2.1 The 16-detector row computed tomography (CT) scanner used in this research study

An initial non-contrast breath-hold helical scan was performed ensuring that the entire lung tumour was encompassed, using the following imaging parameters: 80kV, 120mAs, table feed 30mm, rotation time 0.5seconds, detector width 1.5mm, reconstruction width 2mm, field of view 500mm, matrix 512mm. This non-contrast scan provided baseline images, and was used to plan the subsequent perfusion study. The level of the aortic arch was identified from these scans. A single axial scan was performed at the level of the aortic arch, to allow a region of interest (ROI) to be placed within the aorta for a subsequent contrast medium bolus tracking scan (CARE bolus, Siemens Medical Solution, Forchheim, Germany). Contrast of 108ml iobitridol 300mg iodine/ml (Xenetix 300, Guerbet, Paris, France) was administered using a dual headed pump injector (Injekttron CT2, Medtron, Saarbrucken, Germany), with a decreasing bolus infusion (32ml at 4 ml/s for 8 seconds, 16mls at 2ml/s for 8 seconds, and 60mls at 1ml/s for 60 seconds), and followed by a saline flush (20mls at 1ml/s for 20 seconds). The rationale for the multi-phasic contrast infusion protocol was to optimise experimental conditions for subsequent quantitative analysis of vascularity using Patlak based analysis (Patlak et al 1983, Patlak and Blasberg 1985).

Placement of a circular region of interest (mean area 1.5 cm²) within the boundaries of the aorta allowed the time to aortic peak enhancement to be identified. A contrast medium bolus tracking scan (CARE bolus, Siemens Medical Solution, Forchheim, Germany), located at the level of the aortic arch, was commenced at the same time as contrast agent administration. The dynamic

study was manually triggered when peak aortic enhancement was identified on the bolus tracking enhancement graphs visualised on the console screen, and enhancement seen to fall; this was typically started within 3 to 5 seconds of the peak. This study, encompassing the entire tumour, consisted of a total of 8 breath-hold helical acquisitions in expiration using the following parameters: 80kV, 120mAs, table feed 30mm, rotation time 0.5seconds, detector width 1.5mm, reconstruction width 2mm ,SFOV 500mm, matrix 512mm. 80kV was chosen in preference to the standard 120kV to minimise radiation dose, as available data from the cranial circulation shows that there is no significant change in image quality at 80kV, despite a lower dose (Wintermark et al 2000). A further advantage of using 80kV for perfusion assessment is the better X-ray absorption of iodine at a lower kV. In between each of these 8 acquisitions, the patient was asked to breathe in and out, and to hold their breath. Total dynamic acquisition time varied from patient to patient depending on the tumour coverage required. Typically, each breath-hold acquisition was in the order of 3 to 6 seconds depending on tumour size, with a 7 second breathing interval between each acquisition, thus the entire dynamic acquisition was of the order of 90 seconds for a large tumour.

2.2.2 Data post-processing and analysis

Data was transferred to a dedicated workstation (Leonardo; Siemens Medical Solutions, Forchheim, Germany). Each dynamic study consisted of nine helical scans (baseline scan and eight post contrast scans), that required post-

processing prior to quantitative analysis. For each scan, the 2mm axial images were reformatted into 10mm axial slices, overlapping by 5mm, using 3D software (3D analysis; Siemens Medical Solutions, Forchheim, Germany), to permit slice-by-slice analysis of the whole tumour within a clinically acceptable time.

These reformatted scans were checked to ensure that the entire tumour had been included. The image corresponding to the same tumour level along the z-axis of the patient was selected from each of the nine scans (one unenhanced and eight post-contrast dynamic scans) so that quantification could be performed for each level along the z-axis until the entire tumour was evaluated. It was possible to select images at a similar position along the tumour z-axis on all nine scans as image reformatting was performed previously from the same position; this was achieved by comparing the tumour position to adjacent anatomical structures. Then, each reformatted 10mm axial image from the same position along the z-axis of the patient from each of the nine helical scans, was saved as a separate series on the workstation, for further analysis (Figure 2.2). Thus for every patient, depending on the tumour size, a number of series were obtained, encompassing the entire tumour; each series consisting of one baseline non-contrast image and eight subsequent dynamic contrast enhanced axial images at the same tumour level.

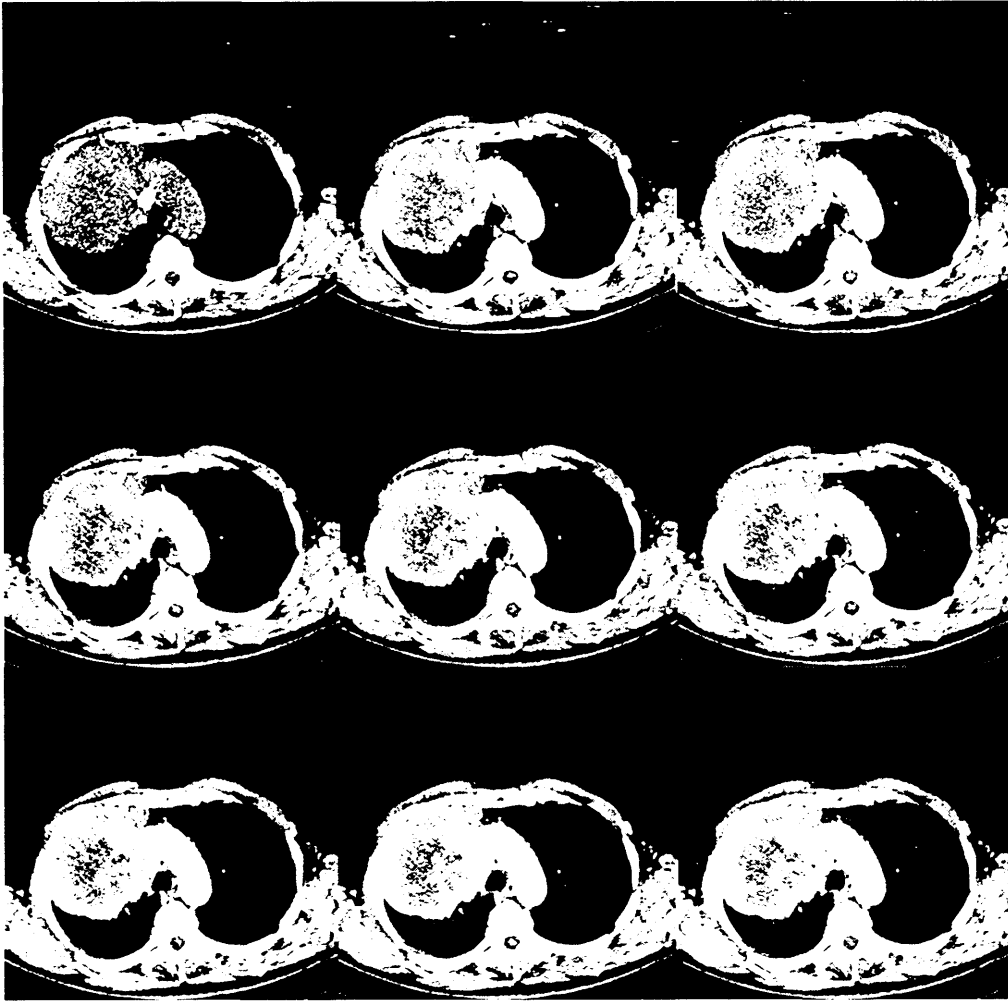


Figure 2.2 This series shows the reformatted pre-contrast and eight post-contrast images from a single 10mm axial level; all images are at a similar position along the z-axis of the patient.

Prototype software (Functional CT; Siemens Medical Solutions, Forchheim, Germany) based on the Patlak model was used for analysis of tumour vascularity. For each patient, the series of reformatted dynamic images, encompassing the whole tumour, were loaded into the software. The arterial input was determined from the bolus tracking scan images for each patient and an arterial time-shift of 3 seconds was employed by the software. A circular region of interest (ROI) was placed within the aorta, using an electronic cursor and mouse. This enabled individualised arterial time enhancement changes to be inputted directly into the software analysis program, and this arterial input information was saved automatically by the software for subsequent quantification of vascular parameters.

A ROI was drawn freehand around the tumour by the observer using an electronic cursor and mouse, taking care to exclude surrounding air, or atelectatic lung tissue. Subsequent software processing was automated: the change in Hounsfield unit over time, following contrast administration, of each pixel within the selected ROI, was transformed to generate coloured functional parametric maps of tissue vascularity based on Patlak analysis for the tumour ROI (Figure 2.3). Each pixel location within the functional map corresponded to a single quantitative value resulting from the mathematical calculation of the data at that location, that is, analysis was on a pixel-by-pixel basis. This process was repeated for each contiguous axial level, until the entire tumour had been covered (Figure 2.4). Finally, a global value representing the vascular parameter

for the entire tumour was calculated by taking the median value of all individual pixels involved.

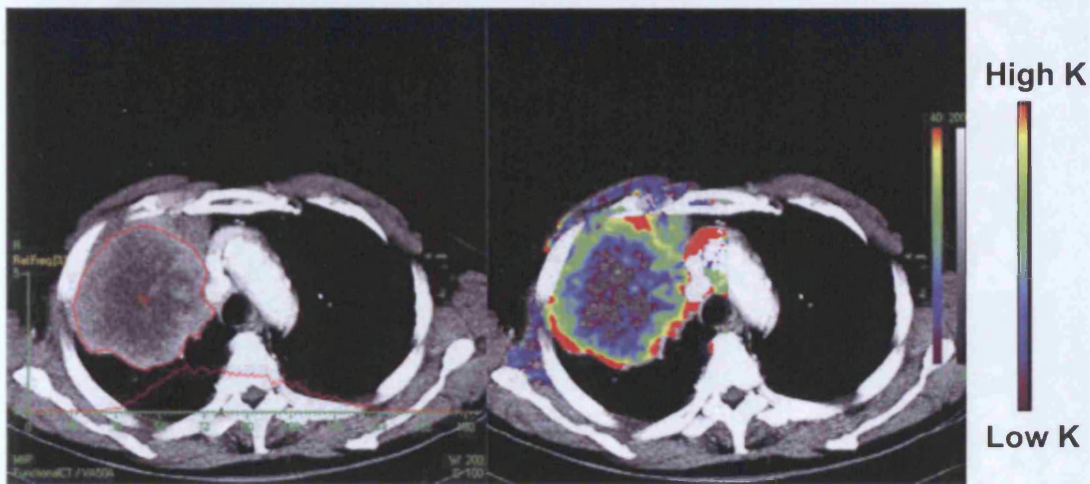


Figure 2.3 Image from a single 10mm axial level shows the region of interest drawn freehand around a lung tumour using a mouse and electronic cursor, together with the corresponding coloured parametric map. Each pixel within the tumour map represents a vascular parameter value, in this case, the transfer constant K ; the colour scale indicates red pixels as high K values and purple pixels as low K values.

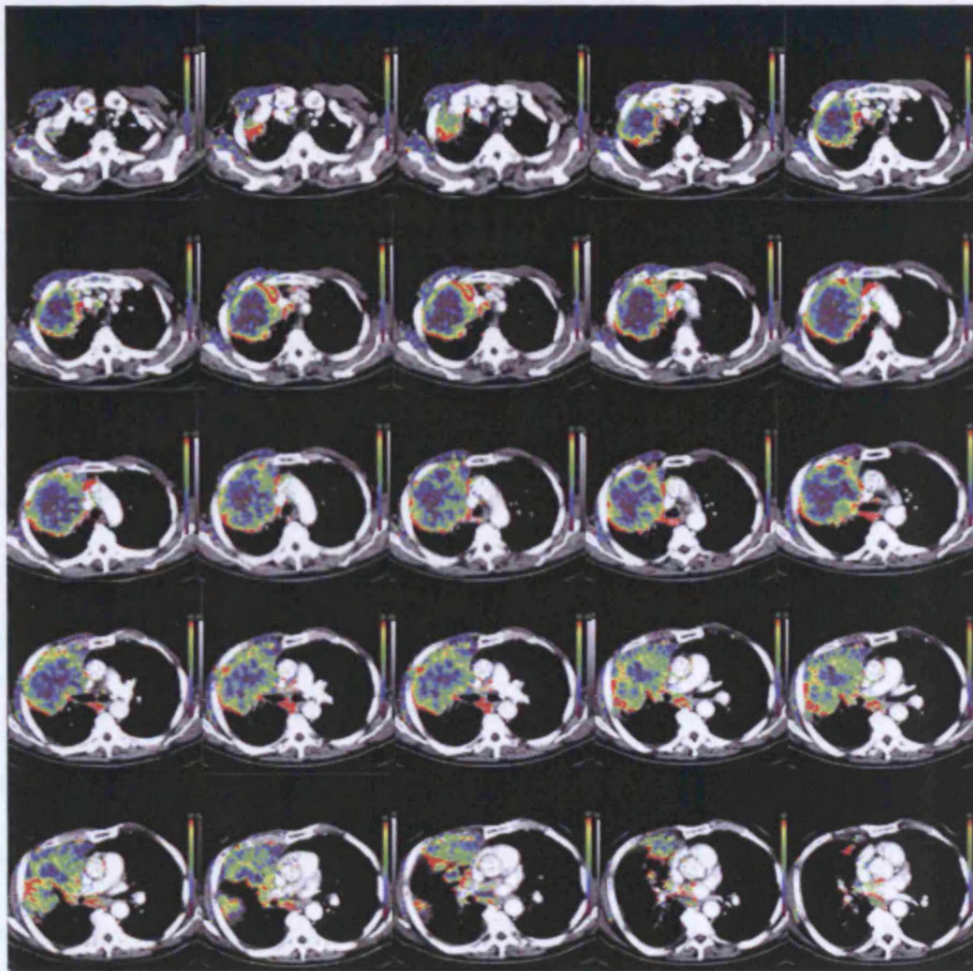


Figure 2.4 Coloured parametric maps from multiple contiguous axial levels encompassing the whole lung tumour. Each pixel location within the tumour region of interest (ROI) corresponds to a single quantitative vascular parameter value, in this case, the transfer constant K . A global value representing the vascular parameter for the entire tumour can therefore be calculated by taking the median value of all pixels involved.

2.2.3 Patlak Analysis

The software used here is based on a simplified Patlak analysis (Patlak et al 1983, Patlak and Blasberg 1985). This model assumes a one-way transfer of contrast from the intravascular into the extravascular-extracellular space. At any time point, the contrast concentration in tissue is equivalent to the sum of the intravascular and extravascular concentration of contrast as denoted by the following equation: $c(t) = BV \cdot b(t) + K \int b(t).dt$, where $c(t)$ is the concentration of contrast within the tissue, BV is the relative blood volume occupied by the vascular space of the tissue, $b(t)$ is the concentration of contrast in blood, and K is the rate constant of transfer of contrast from the intravascular into the extravascular space. Dividing the equation by $b(t)$ produces the linear equation: $c(t)/b(t) = BV + K \int b(t).dt / b(t)$. For systems with irreversible accumulation over the time course of the experiment, a plot of $c(t)/b(t)$ against $\int b(t).dt / b(t)$ results in a linear increase after sufficient equilibration time. By modifying the time axis in this way, Patlak analysis effectively transforms $c(t)/b(t)$ versus time data into that which would have been observed had the arterial input function been constant throughout the experiment, with the terminal slope of the line equal to K (ml/100ml/min) and y-intercept relating to BV (ml/100ml) (Figure 2.5). The multi-phasic bolus infusion was therefore chosen to maintain arterial contrast as constant as possible following bolus loading, thus minimising the transformation required in the Patlak analysis.

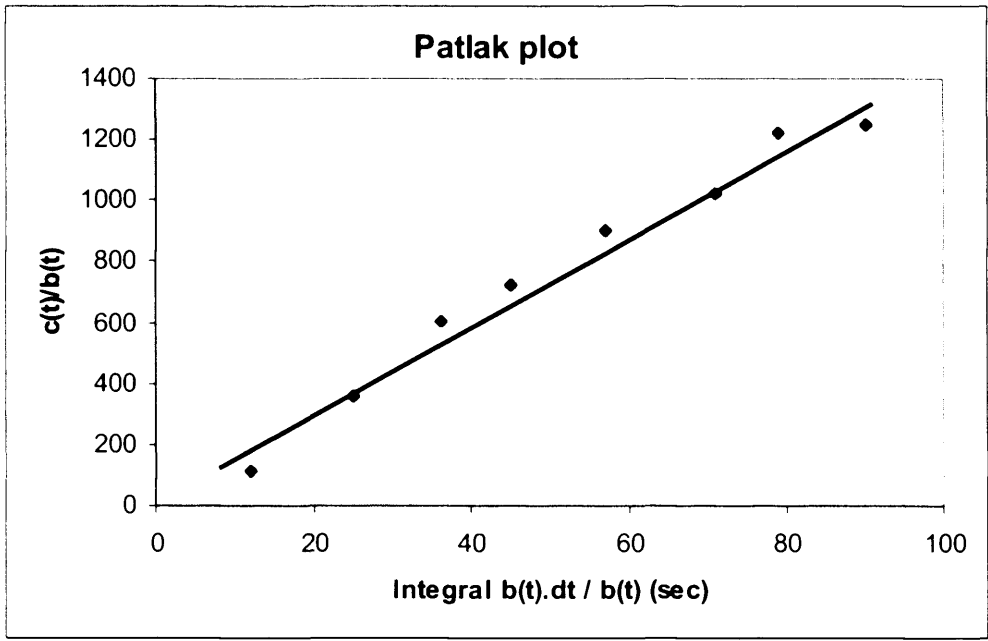


Figure 2.5 Patlak plot is shown for a study patient. The transfer constant K is derived from the gradient of the line, and relative blood volume (BV) from the y-intercept.

2.3 Discussion

Clinical assessment of vascular targeting drugs used in the treatment of cancer has highlighted problems when using conventional response criteria to quantify therapeutic effect (World Health Organisation 1979, Therasse et al 2000, Kerbel et al 2002). Morphological measurements can be unreliable for a number of reasons, especially the time lag between functional and anatomical changes and

difficulties in defining the margins of an infiltrative tumour. Furthermore, tumour shrinkage may not occur with these drugs and therapeutic effect may be underestimated. For example, patients with colorectal cancer treated with the anti-angiogenic agent bevacizumab achieved a five month improvement in overall survival, despite only demonstrating a 10% increase in objective tumour response (Hurwitz et al 2004). Consequently, functional assessment has been advocated, as direct quantification of tumour vascular biology is possible.

CT measurements of tumour vascular parameters are inherently variable due to a combination of intrinsic and extrinsic factors, including cardiac output, technique variability, instrument variability, observer variability, and tumour heterogeneity. It may be possible to compensate for some extrinsic factors, for example, reducing observer variability by using the same observer, and using individualised arterial input function for each patient. However, it is more difficult to compensate for the intrinsic heterogeneity in tumour perfusion as the tumour microcirculation exhibits spatial heterogeneity (Chaplin et al 1995, Kimura et al 1996). Hence, perfusion CT measurement results obtained from a single 2mm axial tumour slice will be different from measurements made on the neighbouring slice or one 10mm away. To compensate for the spatial variation in tumour perfusion, a solution is to increase the tumour volume assessed by perfusion CT.

The use of MDCT allows for improved spatial resolution, reduced scanning time, and the ability to scan a larger tissue volume. By acquiring multiple helical

acquisitions dynamically, assessment of an entire tumour volume is possible, which may decrease measurement error, thus improving measurement reproducibility. This is particularly important when repeated measurements are made on the same patient, for example, when assessing therapeutic drug effects. Furthermore, single level measurements have been problematic for quantitative assessment of perfusion in lung lesions, not least because of image mis-registration from respiratory motion during scan acquisition. For example, Miles et al (2001) reported that six out of 16 CT perfusion studies could not be analysed because of this. Using the described whole tumour helical acquisition technique, it was possible to assess the entire tumour successfully in all studies performed.

Patlak analysis of perfusion CT data has been validated against animal studies (Pollard et al 2004), used to assess kidney function and lymphoma disease activity, and to monitor tumour vascular response to therapy (Dawson and Peters 1993, Ford et al 1996, Dugdale et al 1999, Miles et al 1999, Harvey et al 1999). This simplified analysis assumes a one-way transfer of contrast from the intravascular into the extravascular-extracellular space. The CT iodinated contrast used in clinical practice is freely diffusible between the intravascular and extravascular-extracellular space and does not have intracellular uptake. Previous investigators have not taken into account contrast back-flow (K_2), or intracellular movement (K_3 and K_4), as no intracellular uptake occurs. The amount of back-diffusion depends on the concentration difference between the

extravascular and intravascular compartment. By using a multi-phasic contrast infusion protocol, the intravascular concentration remained high, and back-flow from the extravascular compartment can therefore be minimised, making the above assumption valid. This is especially so during the short acquisition time of about 90 seconds used in this study.

The transfer constant, K , is defined by the equation $K=E \cdot F$ where E , the extraction fraction, is defined by $E=1-e^{-(PS/F)}$, therefore K is a function of both flow (F) and the permeability surface area product (PS) (Renkin 1959, Crone 1963). From the literature in humans, values of F in extra-cranial tumours range from 30 to 100ml/100ml/min in lung cancer, 91.1ml/100ml/min in rectal cancer, and 101.5ml/100ml/min in head and neck cancer, while PS values range from 14.1ml/100ml/min in rectal cancer and 25.3ml/100ml/min in head and neck cancer (Kiessling et al 2004, Gandhi et al 2006, Goh et al 2006). From the data in Chapter 3, the mean K value in untreated lung tumours from 18 patients is 11.1ml/100ml/min. Using the Renkin and Crone equation above, $PS = -F \cdot \ln(1-K/F)$. By inputting F values of between 30 and 100ml/100ml/min, PS values will range from 11.8 to 13.9ml/100/min. Thus the K values measured here for untreated tumours appear to approximate PS and not F . This approximation will hold true as long as tumour blood flow is much higher than PS . However, it is noted that experimental conditions will change following therapy, for example, after radiation treatment, F might increase significantly and K will approximate to PS , or after treatment with a vascular targeting drug, F decreases and K might

then approximate to F . Interpretation of K is therefore dependent on knowledge of drug mechanism of action, which in novel agents, might be limited.

Volumetric perfusion CT is technically feasible and allows the measurement of vascular parameters in entire tumour volumes. However, there are several factors limiting the use of perfusion CT to perform whole tumour vascular measurements in everyday clinical setting. First, currently available CT technology does not allow whole tumour measurements of blood flow, as a much faster scanning speed of up to one scan per second is required. Although this might change with technological advances, the radiation dose implications of volumetric scanning at higher temporal resolution will have to be taken into account in human studies. However, BV is a relatively insensitive vascular parameter, since flow changes with very small changes in vessel calibre, and therefore any BV changes observed, may reflect greater reductions in blood flow. Second, data analysis was performed using prototype software which is not generally available; again, that might change in the near future. The software is also not fully automated. In order to evaluate the entire tumour, regions of interest were drawn manually around the tumour on individual 10mm axial slices overlapping by 5mm, which depending on the size of the tumour can be both time and labour intensive. For example, the average lung tumour diameter in the repeatability study (Chapter 3) is about 8cm, which is divided into 16 contiguous slices; each slice was analysed individually. Also, the variation amongst different observers in defining lung tumour volumes even when following a defined

protocol is well recognised (Senan et al 1999). Finally, the tumour microcirculation is in a continuous state of flux, and perfusion CT vascular measurements merely provide a “snap-shot” of the microvascular function at the point when the scans were acquired. For example, an increase in blood volume in one tumour microregion combined with a similar degree of decrease in another would, using this method, imply no change in blood volume. However, measurements of a global change in tumour vascularity remain valid as response to treatment is based on the whole tumour.

In summary, volumetric perfusion CT permits quantitative whole tumour measurements of vascularity. Whole tumour assessment is a step in the direction for improving the reliability of tumour vascular measurements.

CHAPTER 3

MEASUREMENT REPEATABILITY OF VOLUMETRIC PERFUSION

COMPUTED TOMOGRAPHY

3.1 Introduction

For any clinical measurement method to have practical utility it should be reproducible. Ideally, measurements made by the same method, on the same subjects, but using a different instrument, by different operators, and in different settings should produce identical results (British Standards Institution). However, this is not realistic in routine clinical practice because the measurement result obtained, especially in biological measurements, is often subject to intrinsic and extrinsic sources of variability. Therefore, measurements are considered to be repeatable if the same results are obtained by the same method, on the same subjects, using the same instrument, in the same setting, and within a short interval of time (British Standards Institution). In everyday clinical practice, a measurement method would be considered to be repeatable if the variation observed after repeated measurements on the same patients, and without intervening therapy, is small enough relative to the magnitude of actual biological changes observed following therapy. Extrinsic causes of variation can be due to the measurement instrument itself, the acquisition technique, patient compliance, and the skill and experience of the operator. Inter and intra-observer variation is an important source of measurement variability. It is also recognised that the

tumour blood supply is intrinsically variable, and the tumour microcirculation exhibits spatial and temporal heterogeneity (Kimura et al 1996, Chaplin et al 1995), which contributes to the biological variation affecting measurement results. While the day-to-day variation in functional vascular measurements might be unavoidable, assessment of whole tumour volumes may compensate for spatial heterogeneity. Volumetric perfusion CT allows the measurement of tumour vascular parameters throughout the entire tumour volume, and may potentially improve measurement repeatability as compared to conventional single level imaging techniques. To date, there is little reported data on tumour vascular measurement repeatability using CT, which is clearly relevant to therapeutic assessment where a magnitude of change is measured to assess effect.

3.2 Aim

The aim of this chapter is firstly, to evaluate the repeatability of whole tumour vascular measurements in patients with non-small cell lung cancer using volumetric perfusion CT. Secondly, in order to test the hypothesis that measurement repeatability of perfusion CT improves with greater tumour volume coverage, the vascular measurements derived from a whole tumour volume are compared to measurements from a 40mm z-axis coverage (four contiguous tumour levels), and a 10mm z-axis coverage (single tumour level). Thirdly, to evaluate inter and intra-observer variability of volumetric perfusion CT.

3.3 Patients and Method

3.3.1 Study Design

Local research ethics committee approval was obtained, with explicit approval for radiation exposure of patients for research purposes as required under the Ionising Radiation (Medical Exposure) Regulations (IR(ME)R). Each patient gave written informed consent, which included information on the radiation exposure from the CT examinations (7.5mSv per examination). Eighteen patients (11 males, 7 females, mean age 68 years) with histologically proven, inoperable non-small cell lung cancer (mean tumour size 8.0cm, range 4.9 to 11.8cm) were enrolled into the study. Paired perfusion CT examinations were performed on each of the 18 patients; the second CT study was performed within 24 hours of the first study, without therapeutic intervention, using identical technical parameters.

3.3.2 Volumetric perfusion CT

The CT methodology, image post-processing and data analysis have been described in Chapter 2. Each of the 18 patients had two perfusion CT studies, and as much as possible, images from each tumour slice from both studies were co-registered by comparing the tumour position to adjacent anatomical structures. As before, Patlak analysis (1983 and 1985) was used to quantify (i)

transfer constant (K; ml/100ml/min) which provides information on permeability surface area product and blood flow, and (ii) relative blood volume (BV; ml/100ml) on a pixel-by-pixel basis. Thus quantification of vascular parameters for the whole tumour was carried out on all 36 studies to allow assessment of repeatability

In order to determine if CT vascular measurement repeatability improves with increasing z-axis tumour coverage, additional analysis was carried out on the 18 patients by comparing vascular measurements derived from the whole tumour, to measurements obtained from 40mm z-axis tumour coverage (four contiguous tumour levels), and from 10mm coverage (single tumour level). Following image post-processing, a single central 10mm tumour level was chosen, and using the perfusion software, a region of interest (ROI) was drawn freehand around the tumour. As before, each pixel location within the functional map generated for the ROI corresponded to a single quantitative vascular value resulting from the Patlak calculation of the data at that location. Data was analysed on a pixel-by-pixel basis, and median values of tumour K and BV were derived for this single 10mm tumour level. These values were recorded for each patient. This process was repeated for another three adjacent tumour levels. By amalgamating data from all individual pixels from these three levels and the initial tumour level, a median value for K and BV was calculated, producing values for a z-axis coverage of 40mm (Figure 3.1).

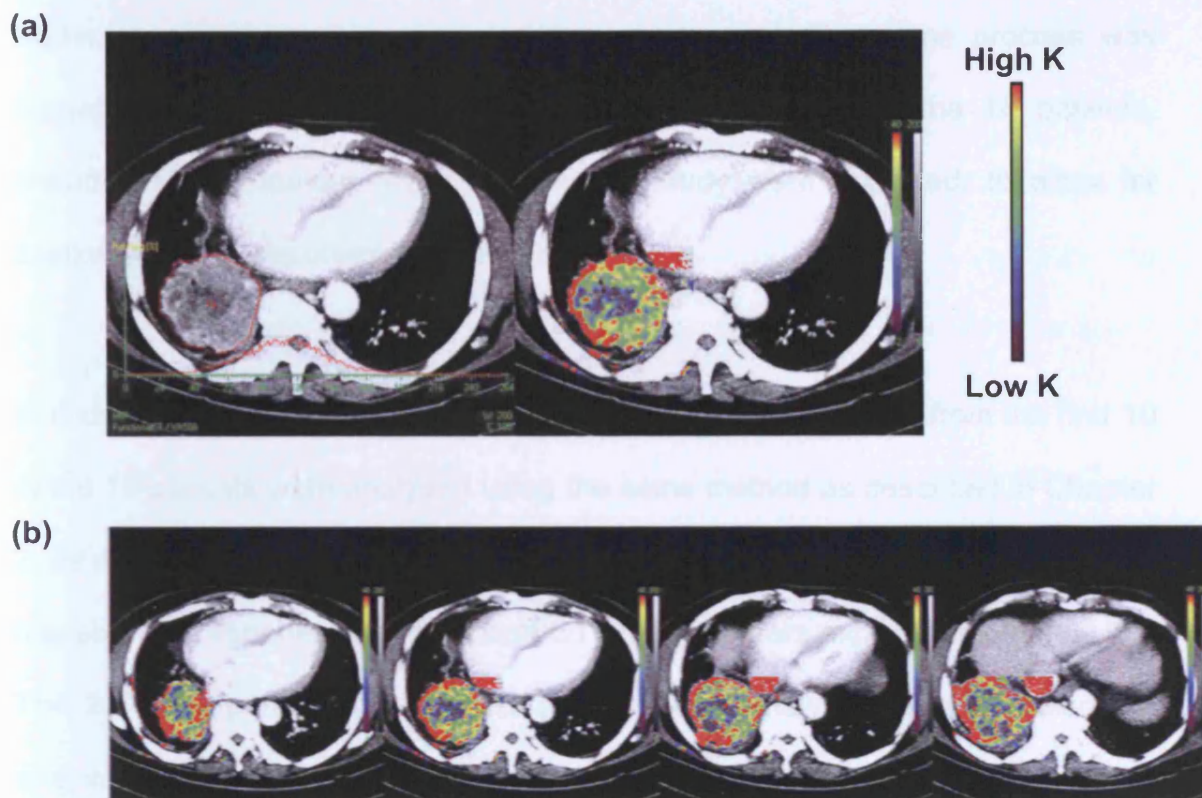


Figure 3.1 A region of interest (ROI) was drawn freehand around the lung tumour in a study patient and coloured parametric maps of the vascular parameter, in this case, the transfer constant (K) are automatically generated by the perfusion software for this 10mm tumour coverage (a). By repeating the process for another three adjacent tumour levels in the same patient, and amalgamating data from all individual pixels from the four levels, tumour K values can be derived from a 40mm z-axis coverage (b). The colour scale indicates red pixels as high K values and purple pixels as low K values.

Again, these values were recorded for each patient. The same process was repeated for the second perfusion CT study from each of the 18 patients, ensuring similar tumour levels as the first study were analysed, to allow for assessment of measurement repeatability.

In order to determine inter-observer variability, the scan images from the first 10 of the 18 patients were analysed using the same method as described in Chapter 2, by a second independent observer (Dr Vicky Goh, Consultant Radiologist) who has six years experience of perfusion CT and nine years experience of chest CT. The 20 scans performed on the 10 patients were analysed by both observers, and values for K and BV were recorded for each study. To determine intra-observer variability, the images from the 20 studies were re-analysed by both observers after an interval of four weeks to reduce recall bias.

3.3.3 Statistical analysis

Statistical analysis was performed using StatsDirect statistical software version 2.3.8 (StatsDirect Ltd, Sale, Cheshire, United Kingdom). Bland and Altman (1986) repeatability statistics were applied as a means of quantifying measurement error of the volumetric perfusion CT technique. The same statistics were applied to assess the inter and intra-observer variability, and used to compare the repeatability of whole tumour volumetric measurements with conventional four and single level measurements

Initial analysis was performed to confirm that the statistical assumptions required for repeatability analysis were upheld. Kendalls τ was used to establish any correlation between the absolute difference and the mean; if the difference appeared to increase when the mean parameter value increased, the data was transformed by natural logarithm. Using Bland and Altman statistics, the mean, standard deviation, mean difference, and 95% limits of agreement for each vascular parameter were established. The following statistical measurements of repeatability were derived:

1. The square root of the mean squared difference (dSD) was calculated, where d is the difference between repeated measurements, and n is the number of patients.

$$dSD = \sqrt{(\sum d^2/n)}$$

2. The within patient standard deviation (WSD) was calculated from:

$$WSD = dSD/\sqrt{2}$$

3. The within patient coefficient of variation (WCV) was calculated by dividing the WSD by the overall mean of each parameter. For logarithmic transformed data, the WCV was calculated from:

$$WCV = \exp(WSD)-1$$

4. The repeatability coefficient (r) was calculated from:

$$r = 2.77 \times WSD (=1.96 \times dSD)$$

For logarithmic transformed data, this can be expressed as a percentage of the mean:

$$\%r = 100 \times \exp(\text{LNmean} \pm r) / \text{mean}$$

5. To calculate the 95% confidence interval (CI) for change which might occur in 'n' patients

$$\text{CI} = \pm (1.96 \times \text{dSD}) / \sqrt{n}$$

For logarithmic transformed data, this can be expressed as a percentage of the mean:

$$\%\text{CI} = 100 \times \exp(\text{LNmean} \pm \text{CI}) / \text{mean}$$

6. The ratio of the between patient variance and within patient variance was assessed using one-way analysis of variance, and tested for significance.
7. The intra-class correlation coefficient was derived.

3.4 Results

3.4.1 Within subject measurement repeatability

All 18 patients completed their scans; all 36 studies were technically adequate, included the entire tumour and were analysed successfully. K values were transformed by natural logarithm because the difference in mean values increased when the mean parameter value increased (Kendalls tau, $p < 0.05$).

The mean, mean difference, 95% limits of agreement and repeatability statistics are presented in Table 3.1. The Bland and Altman agreement plot showing the 95% limits of agreement for K, and the corresponding scatter plot of K values from both scans against the line of perfect agreement are shown in Figure 3.2. The Bland and Altman agreement plot and the corresponding scatter plot of BV are shown in Figure 3.3. Both tumour K and BV showed acceptable agreement between studies as demonstrated by WCV of 10.4% and 23.6% respectively. Intraclass correlation coefficient for K and BV were 0.90 and 0.70 respectively.

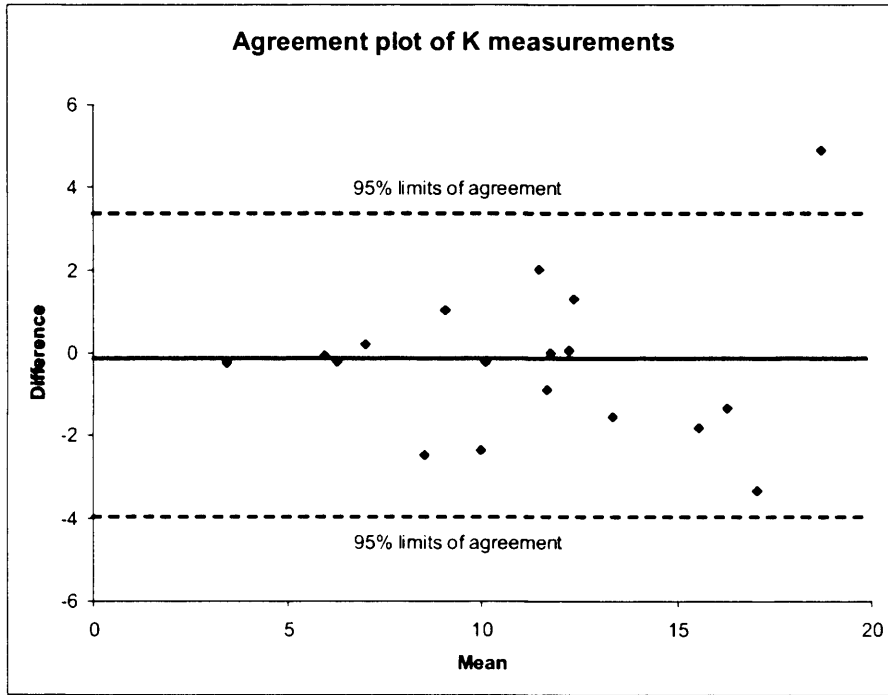
Table 3.1 Repeatability statistics from paired studies performed on 18 patients measuring whole tumour blood volume (BV) and transfer constant (K)

	(a) K (ml/100ml/min)	(b) BV (ml/100ml)
Mean (SD)	11.1 (4.1)	5.6 (2.3)
Mean difference	-0.09	1.0
95% limits of agreement	-4.0 to 3.4	-2.2 to 4.2
WSD	0.10 ^a	1.3
WCV	10.4% ^a	23.6%
Repeatability	0.27 ^a	3.6
ICC	0.90	0.70
Variance ratio	19.5 (p<0.001)	6.0 (p<0.001)

SD – standard deviation; WCV – within subject coefficient of variation; ICC – intraclass correlation coefficient; WSD – within subject standard deviation

^aLn transformed data

(a)



(b)

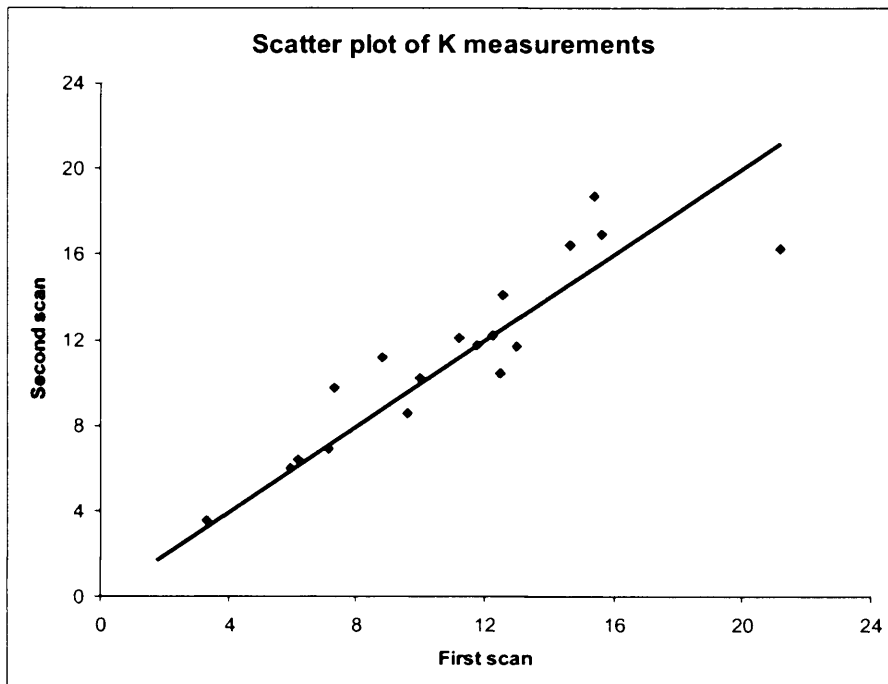
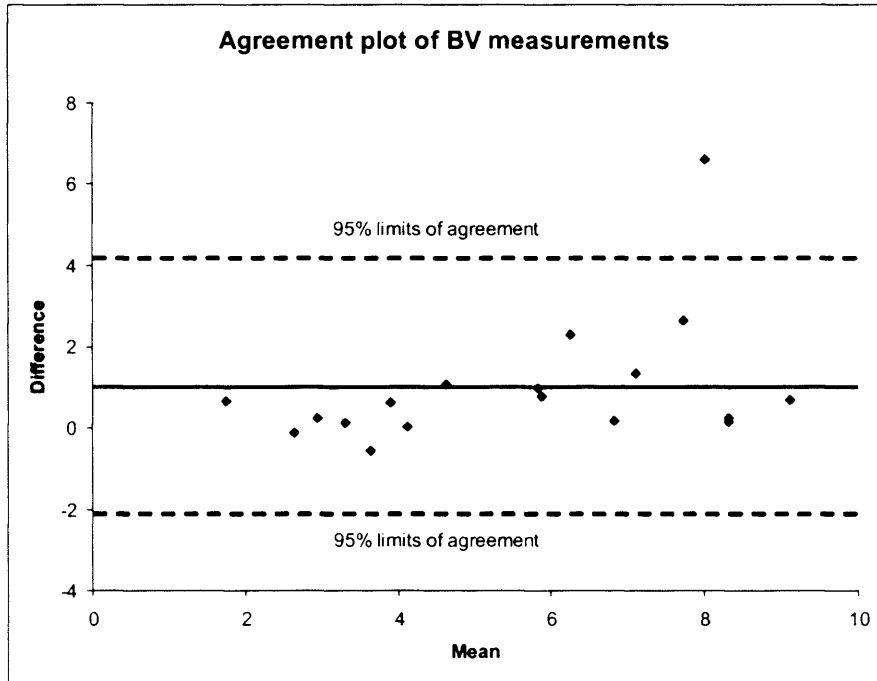


Figure 3.2 Bland-Altman agreement plot (a) of the difference between the two scans against the mean of the transfer constant (K) values from the two scans. The mean difference is indicated by the solid line. The two outer dotted lines represent the 95% limits of agreement, which define the range within which most differences between repeated K measurements made on the same subject will lie. Scatter plot (b) of K measurements from the two scans, with a line of perfect agreement, which represents the line all points would lie on if both measurements gave the same reading. This plot provides a visual demonstration of how precise the two sets of measurements are. The closer the measurements lie to this line of equality, the better the agreement.

(a)



(b)

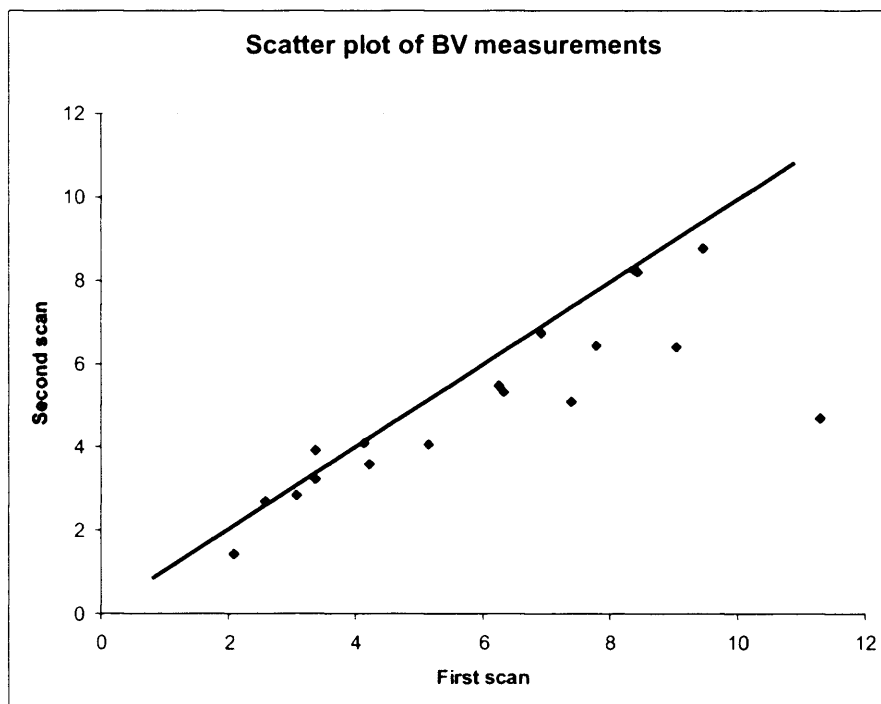
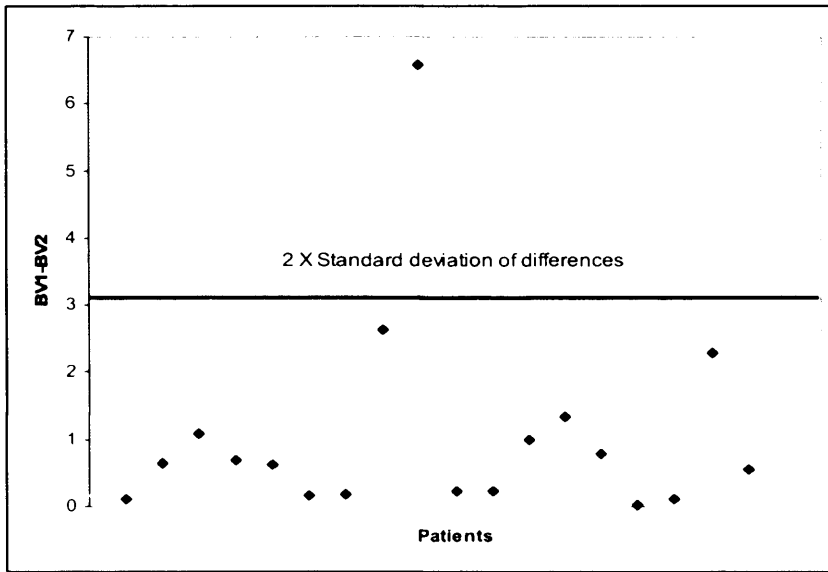


Figure 3.3 Bland-Altman agreement plot (a) of the difference between the two scans against the mean of the blood volume (BV) values from the two scans. The mean difference is indicated by the solid line. The two outer dotted lines represent the 95% limits of agreement, which define the range within which most differences between repeated BV measurements made on the same subject will lie. Scatter plot (b) of BV measurements from the two scans, with a line of perfect agreement, which represents the line all points would lie on if both measurements gave the same reading. This plot provides a visual demonstration of how precise the two sets of measurements are. The closer the measurements lie to this line of equality, the better the agreement.

Apart from demonstrating measurement agreement, the statistics can potentially be used to assess if a change in measurement value following therapy is significant. From the BV repeatability dataset above, a clear outlier was identified which cannot be explained by any technical factors. For this patient, the difference in BV from the two scans was greater than four times the standard deviation of the differences from all patients and was excluded (Figure 3.4). Outliers were also identified from the K repeatability dataset. However, as more than one outlier was present, these data were included. Analysis was therefore carried out on the remaining 17 patients. The 95% limits of change for a group of n patients can be estimated from the value of dSD using the following formula: $(1.96 * dSD) / \sqrt{n}$. The dSD values for BV and logarithmically transformed K are 1.05ml/100ml and 0.13ml/100ml/min respectively. Hence, for a group of 17 patients, any change in tumour BV of more than $\pm 9.2\%$ as a consequence of treatment would be over and above measurement variability, i.e. the probability of this change being random is less than 5%. Similarly, an increase in tumour K of more than 6.5%, or reduction more than 6.1% for a group of 17 patients would be statistically significant at the 5% level; this was asymmetric about the mean as K was logarithmically transformed.

(a)



(b)

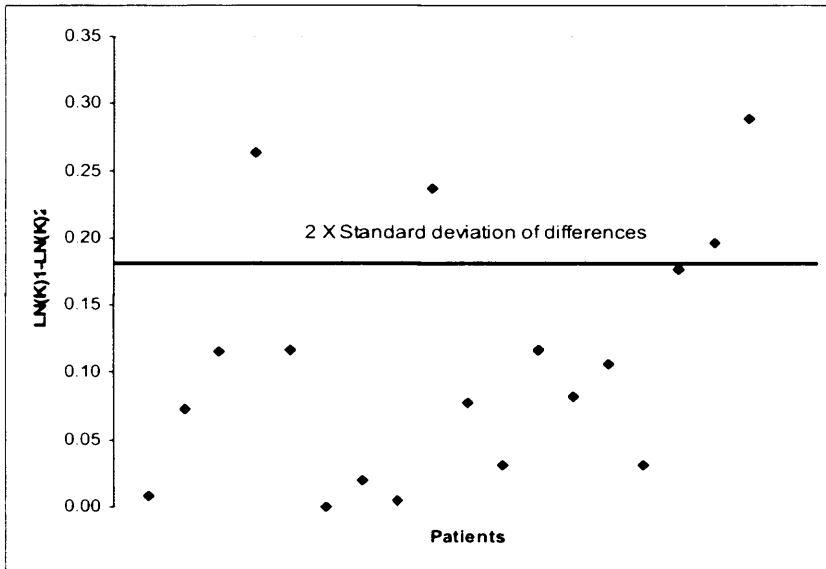


Figure 3.4 Scatter plots of consecutive patients showing the absolute difference from repeated scans for blood volume (BV) (a) and transfer constant (K) (b). Outliers were identified as having differences greater than twice the standard deviation of the differences from all 18 patients.

3.4.2 Whole tumour versus four levels versus single level perfusion CT measurements

Additional analysis was performed on the 18 patients to compare the repeatability of perfusion CT vascular measurements derived from a whole tumour volume and compared to measurements from a 40mm z-axis coverage (four contiguous tumour levels) and a 10mm z-axis coverage (single tumour level). The mean, mean difference, 95% limits of agreement and repeatability statistics for K and BV measurements from 10mm z-axis coverage, 40mm z-axis coverage and the whole tumour for the 10 patients are summarised in Table 3.2. Bland-Altman agreement plots and scatter plots for K and BV are shown in Figure 3.5 and Figure 3.6.

WCV for K measurements was 21.7% from a 10mm coverage, improving to 12.6% for 40mm coverage, and 10.4% for the whole tumour volume. Similarly, the WCV for BV measurements was 38.7% from a 10mm coverage, improving to 29.3% for 40mm coverage, and 23.6% for the whole tumour volume. These results demonstrate that by increasing z-axis coverage from 10mm to 40mm, and ultimately by analysing the whole tumour volume, improvement in repeatability for tumour vascular measurements can be achieved.

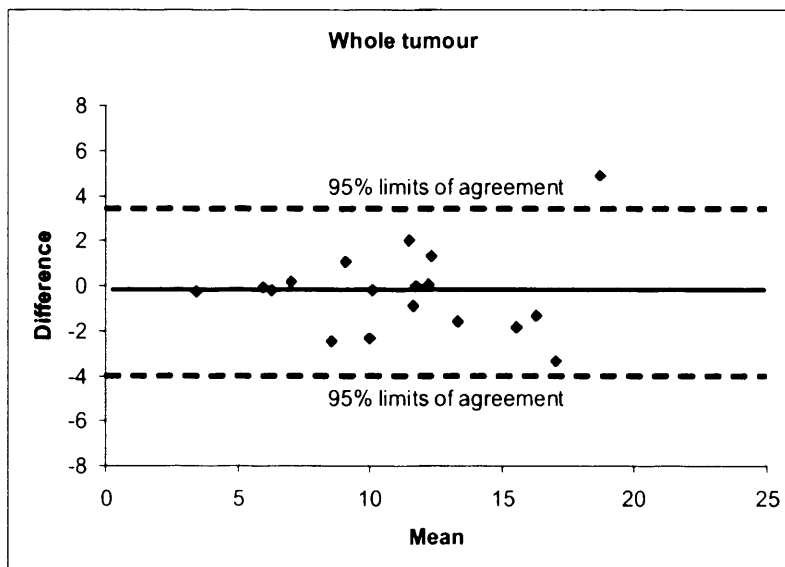
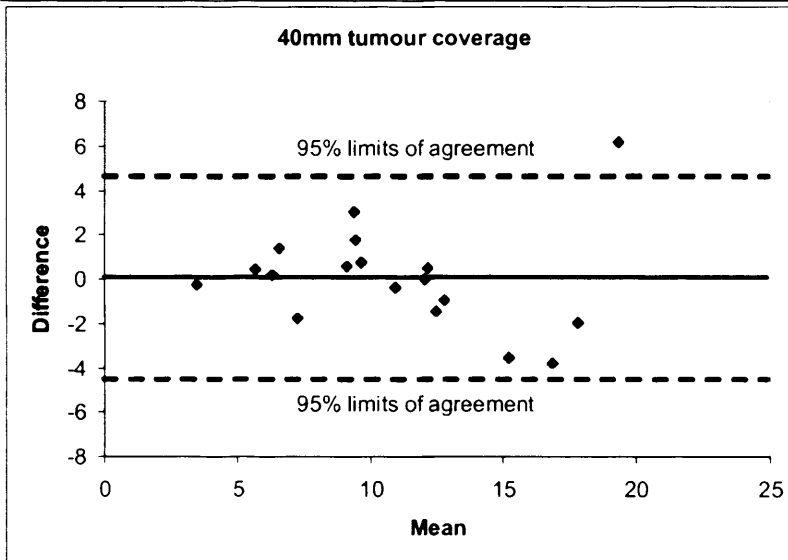
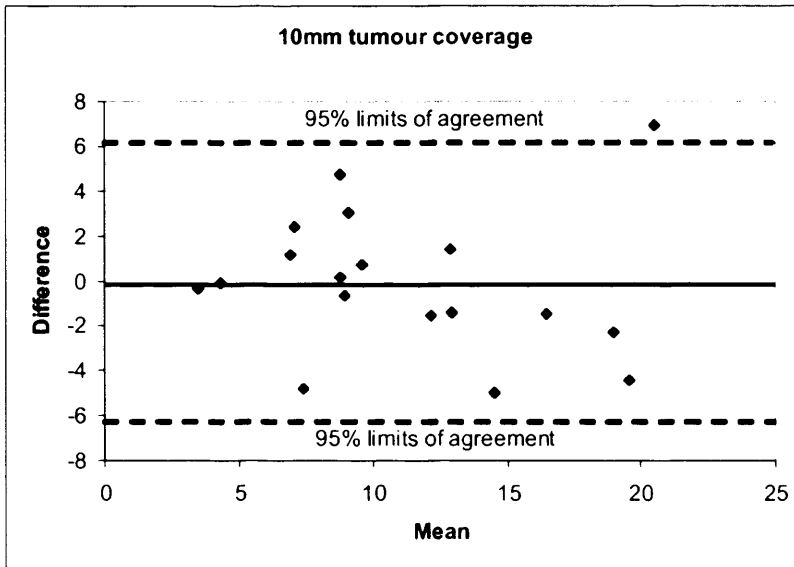
Table 3.2 Repeatability statistics from 10mm, 40mm and whole tumour measurements

	10mm	40mm	Whole tumour
(a) K (ml/100ml/min)			
<i>Mean (SD)</i>	11.2 (5.1)	10.9 (4.4)	11.1 (4.1)
<i>Mean difference</i>	-0.08	0.04	-0.09
<i>95% limits of agreement</i>	-6.3 to +6.1	-4.5 to +4.6	-4.0 to +3.4
<i>WSD^a</i>	0.20	0.12	0.10
<i>WCV^a</i>	21.7%	12.6%	10.4%
<i>Repeatability^a</i>	0.54	0.33	0.27
<i>ICC</i>	0.83	0.87	0.90
<i>Variance ratio</i>	11.0 (p<0.001)	15.1 (p<0.001)	19.5 (p<0.001)
(b) BV (ml/100ml)			
<i>Mean (SD)</i>	5.8 (2.6)	5.5 (2.4)	5.6 (2.3)
<i>Mean difference</i>	1.1	1.1	1.0
<i>95% limits of agreement</i>	-4.8 to +7.0	-3.0 to +5.1	-2.2 to +4.2
<i>WSD</i>	2.2	1.6	1.3
<i>WCV</i>	38.7%	29.3%	23.6%
<i>Repeatability</i>	6.2	4.4	3.6
<i>ICC</i>	0.45	0.62	0.70
<i>Variance ratio</i>	2.8 (p=0.018)	4.5 (p=0.0013)	6.0 (p<0.001)

SD – standard deviation; WCV – within subject coefficient of variation; ICC – intraclass correlation coefficient; WSD – within subject standard deviation

^aLN transformed data

(a)



(b)

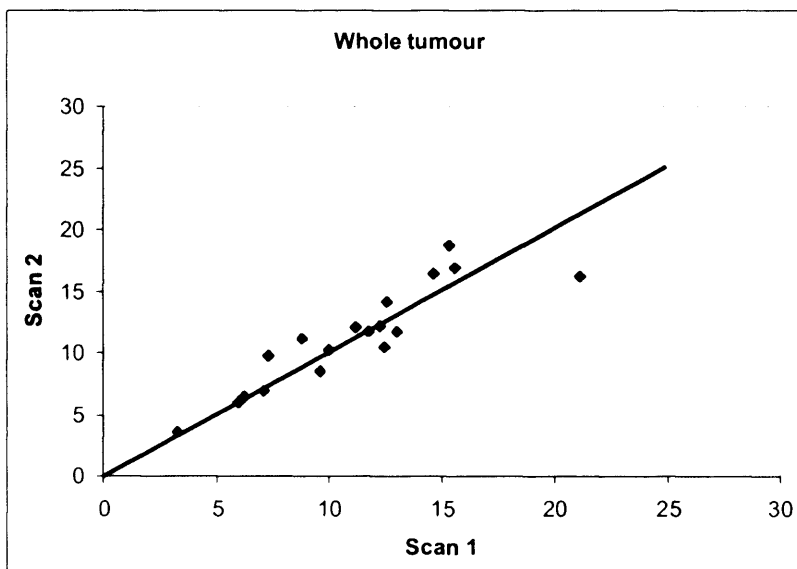
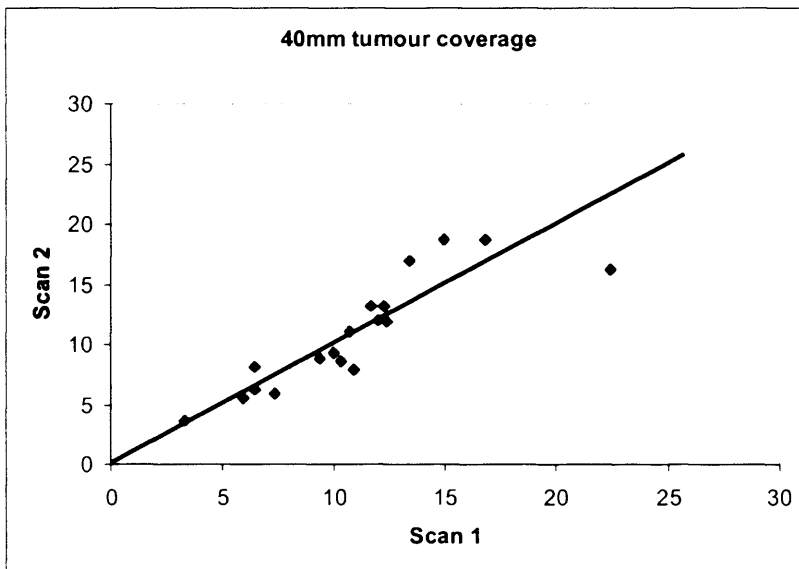
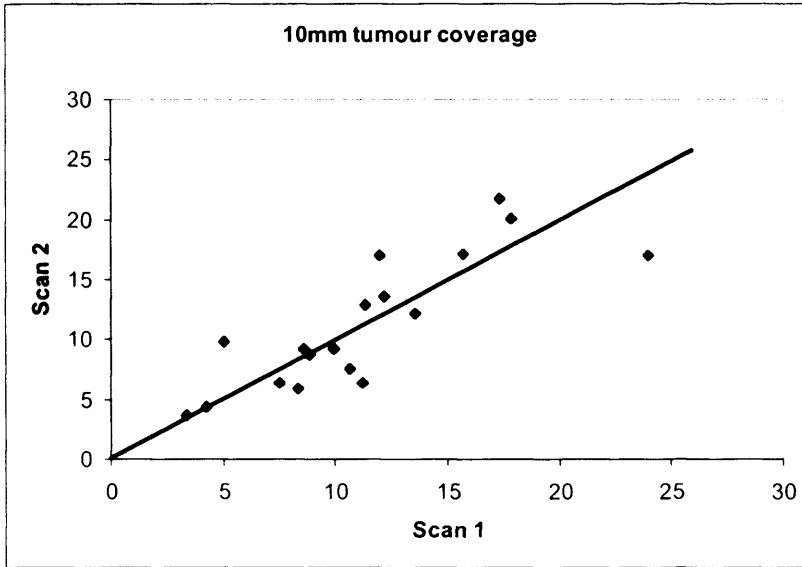
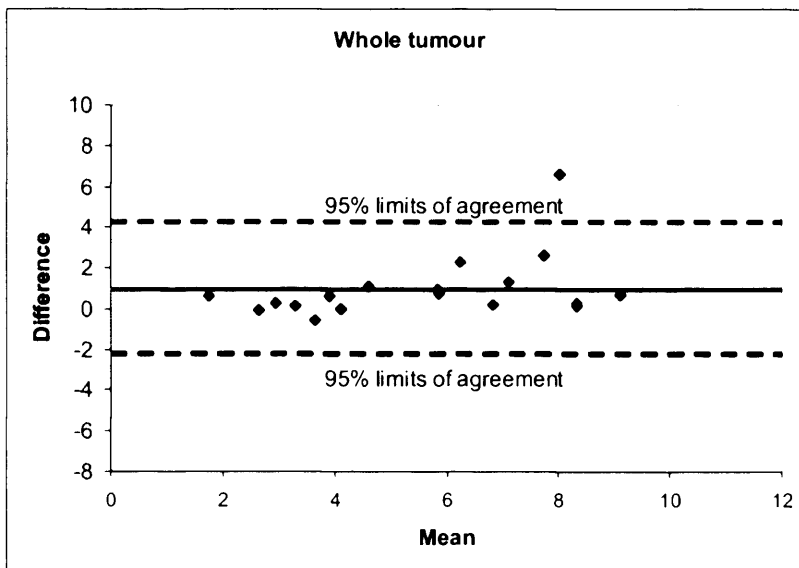
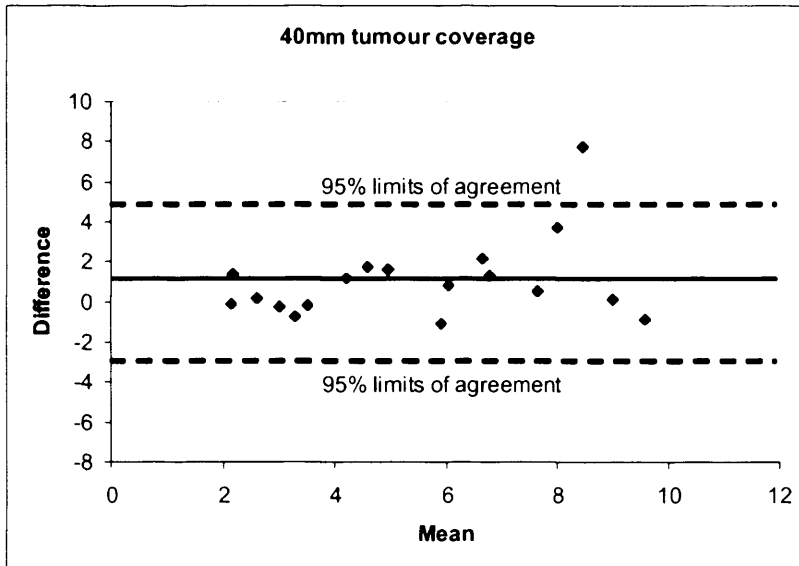
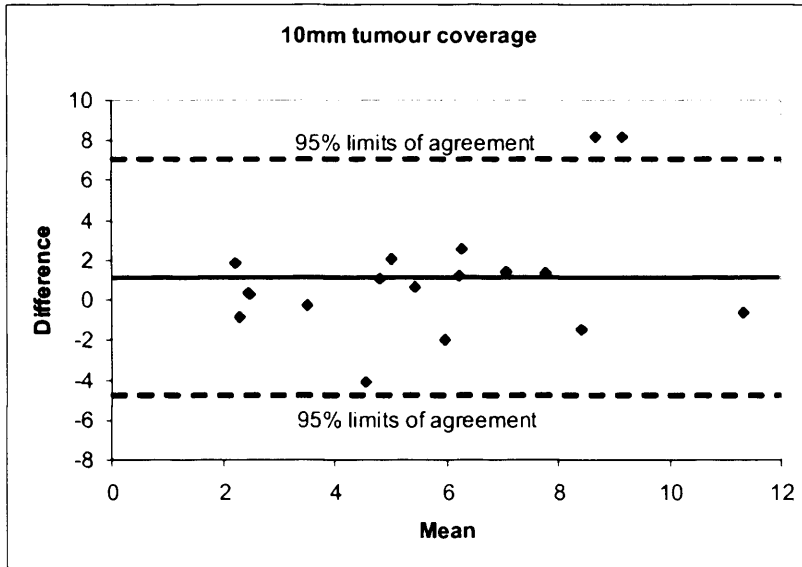


Figure 3.5 Bland-Altman agreement plots (a) of the difference in transfer constant (K) between the two scans against the mean of the K values for a 10mm, 40mm and whole tumour coverage. The narrowing of the 95% limits of agreement with whole tumour coverage compared to 10mm and 40mm coverage indicates an improvement in measurement repeatability. Scatter plots (b) of K measurements from the two scans with a line of perfect agreement, for a 10mm, 40mm and whole tumour coverage. As tumour coverage increases from 10mm to 40mm to whole tumour, the measurements become closer to the line of equality, indicating an improvement in agreement, and hence the precision of the measurements.

(a)



(b)

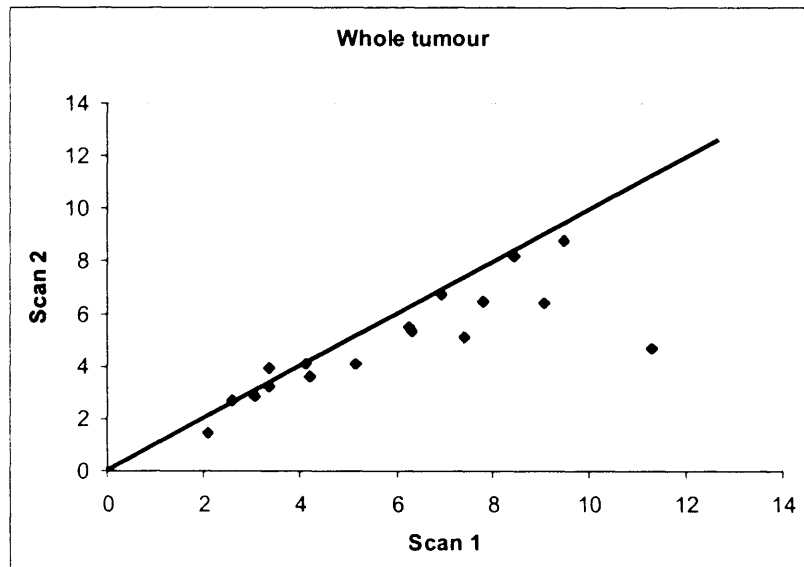
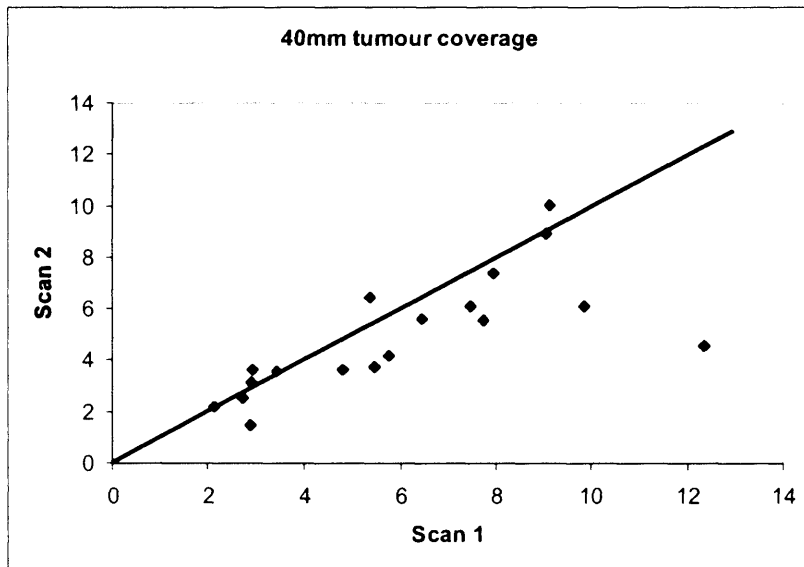
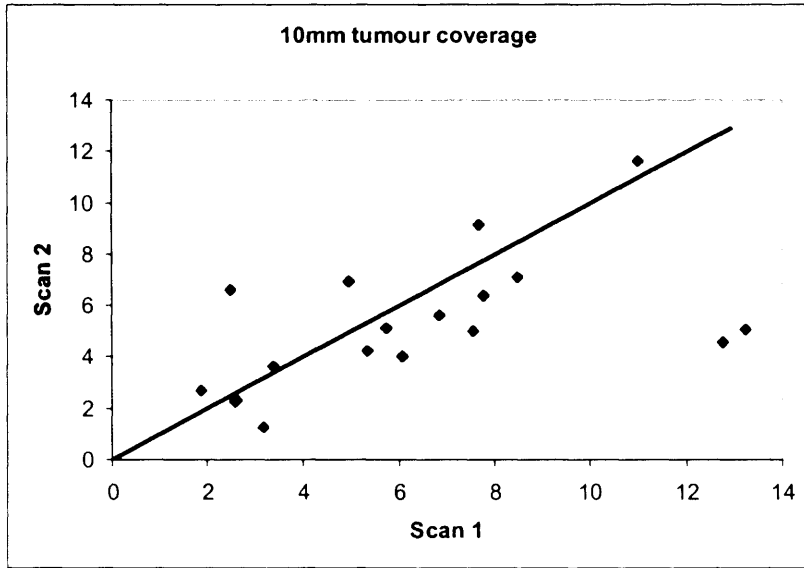


Figure 3.6 Bland-Altman agreement plots (a) of the difference in blood volume (BV) between the two scans against the mean of the BV values for a 10mm, 40mm and whole tumour coverage. The narrowing of the 95% limits of agreement with whole tumour coverage compared to 10mm and 40mm coverage indicates an improvement in measurement repeatability. Scatter plots (b) of BV measurements from the two scans with a line of perfect agreement, for a 10mm, 40mm and whole tumour coverage. As tumour coverage increases from 10mm to 40mm to whole tumour, the measurements become closer to the line of equality, indicating an improvement in agreement, and hence the precision of the measurements.

3.4.3 Observer Variability

Inter and intra-observer variability was evaluated in the first 10 patients recruited onto the study. There was good agreement between and within observers for both vascular parameters (Table 3.3), as indicated by a coefficient of variation between 3.5% and 3.6% for inter-observer variation and 3.3 % and 6.3% for intra-observer variation. Intraclass correlation coefficient for inter and intra-observer variability for both vascular parameters ranged from 0.97 to 0.99.

Table 3.3 Inter- and Intra-observer agreement from ten patients for whole tumour transfer constant (K) and blood volume (BV) measurements

Vascular measurement	Agreement	Mean difference (95% limits of agreement)	WCV	ICC
K (ml/100ml/min)	<i>Inter-observer</i>	0.07 (-1.01 to +1.08)	3.47%	0.99
	<i>Intra-observer 1</i>	0.49 (-2.08 to +1.11)	6.34%	0.97
	<i>Intra-observer 2</i>	0.15 (-0.87 to +1.17)	3.50%	0.99
BV (ml/100ml)	<i>Inter-observer</i>	0.44 (-0.59 to +0.68)	3.64%	0.99
	<i>Intra-observer 1</i>	0.09 (-0.64 to +0.45)	3.30%	0.99
	<i>Intra-observer 2</i>	0.01 (-0.68 to +0.70)	3.95%	0.99

WCV – within subject coefficient of variation; ICC – intraclass correlation coefficient

3.5 Discussion

Volumetric perfusion CT allows the measurement of tumour vascular parameters throughout an entire tumour volume, thus providing a more accurate representation of the spatial heterogeneity of the tumour microcirculation. Bland and Altman statistics were applied as a means of quantifying measurement variability, and hence the repeatability of the perfusion CT technique. This study has shown that vascular measurements derived from the whole tumour volume are repeatable, and indeed, improves on measurement repeatability when compared to conventional single level analysis. This is particularly salient when serial measurements are made on the same patient, for example when assessing response after therapy.

Measurement repeatability can be evaluated using several indices. The 95% limits of agreement represents the boundaries within which the true measurement is expected to lie 95 percent of the time; the narrower the limits, the more precise the measurement being made. The repeatability coefficient indicates the 95% confidence limits that might occur spontaneously in an individual. The WCV quantifies the measurement error with respect to the mean, and provides an estimation of precision. The variance ratio compares the between patient variance and within patient variance, and a parameter with a larger variance in the patient population and a smaller variance within individual patients (and thus a higher ratio) is ideal for therapeutic monitoring. Finally, the

intra-class correlation coefficient provides a measure of the reliability of the measurement method.

We found that both K and BV measurements were repeatable, although K measurements were less variable than those for BV. This may be related to the mathematical basis of Patlak analysis where smaller changes in the gradient of the Patlak plot will produce greater changes in the y-intercept and BV measurements will show greater variability compared with K.

The repeatability results derived from whole tumour volume measurements are comparable with published CT data of repeatability for both animal and human subjects. Our WCV of 10.4% and 23.6% for K and BV respectively is similar to variability in cranial perfusion of 12 to 35% in dogs (Nabavi et al 1999), and 13 to 33% in rabbits (Purdie et al 2001), and cerebral tumour perfusion of 14 to 24% in rabbits (Cenic et al 2000). Indeed, our results compare favourably to single level DCE-MRI repeatability in a variety of human tumours (Galbraith et al 2002) where the WCV in $\log_{10}K_{trans}$, a measurement akin to K, was 24%. Furthermore, there was good agreement between and within observers, and the intraclass correlation coefficient of between 0.97 and 0.99 compare favourably to previous studies of observer variability where intraclass correlations of about 0.75 were achieved (Fiorella et al 2004, Goh et al 2005); this bodes well for clinical utility of this technique.

The results also demonstrate that the variability is within the accepted limits for therapeutic agents currently being assessed in clinical trials. In a phase 1 study of the anti-angiogenic agent bevacizumab in rectal cancers, mean reduction in blood volume of 26% in four patients was demonstrated using single level perfusion CT (Willett et al 2004). In a phase 1 study of CA4P assessed using single level DCE-MRI, mean $\log_{10}K_{trans}$ value, was reduced by 37% for nine patients after drug administration (Galbraith et al 2003). Using the repeatability statistics for the same number of patients, volumetric perfusion CT would be sensitive to reductions in BV of greater than 18.9%, and would be able to detect significant reductions in K greater than 8.3%. Therefore, the level of therapeutic change seen in these two studies is greater than the measurement variability of whole tumour perfusion CT.

This study has demonstrated that measurement repeatability can be improved by increasing tumour volume coverage. For example, an improvement in the repeatability coefficient from 0.54 to 0.33 to 0.27 was demonstrated for tumour K when tumour coverage increased from 10mm to 40mm to the whole tumour volume, indicating a decrease in measurement variability. This was also supported by the ratio of between-patient variance to within-patient variance, which increased from 11.0 to 15.1 to 19.5, indicating that vascular measurements derived from a greater tumour volume may be more sensitive to population variations in the parameter studied, and less variable when repeated studies are performed on the same individual.

The sample size for this repeatability study is small. However, a recent study looking at the effects of increasing number of patients on measurement repeatability of DCE-MRI vascular parameters concluded that there was little improvement in repeatability once 20 patients were recruited (Taylor et al 2006). Furthermore, the number of patients in this study is consistent with repeatability studies on functional imaging of vascular physiology reported in the literature, where the majority of studies recruited between 10 and 20 patients (Laking et al 2006). Nevertheless, it is clearly important to incorporate repeatability analysis into future studies of functional imaging in order to be confident that the measurements obtained are reliable.

While we have established that repeatability of perfusion CT measurements can be improved with increasing tumour coverage, one limitation of this analysis is that it merely provides an overall measure of measurement variability. It does not distinguish between the extrinsic factors that contribute to this variability, including acquisition technique, patient compliance with breath-holding and observer variability, and the intrinsic factors such as tumour heterogeneity. However, on a practical level, identical scan acquisition parameters and technique were employed in each of the paired studies, and analysis was performed by a single observer using the same software package, minimising variability from these factors. It is therefore a reasonable assumption that

compensation for intrinsic spatial heterogeneity is a major factor contributing to this improvement.

In summary, we have shown that perfusion CT measurements derived from whole tumour volume evaluation are repeatable and that measurement repeatability improves with increasing tumour coverage. Assessing tumour vasculature over a greater tumour volume may provide more reliable assessment, and should be considered in clinical practice.

CHAPTER 4

TUMOUR VASCULAR EFFECTS OF FRACTIONATED RADIOTHERAPY IN HUMAN NON-SMALL CELL LUNG CANCER

4.1 Introduction

Nearly 50% of patients with cancer will undergo radiotherapy as part of their treatment (Jemal et al 2005). Radiotherapy is an important component of the radical treatment of many localised cancers. For lung cancer, radiotherapy is a major treatment modality; radical radiotherapy is offered for potentially curable tumours, and palliative radiotherapy for symptomatic relief of advanced disease. In the palliative setting, lower doses may be employed to achieve tumour regression and growth delay rather than hope to completely eradicate all tumour cells; this is achieved using fewer larger fractions over a shorter overall time, for example, two to three weeks, compared to four to six weeks for radical treatment. However, even for radical regimens, treatment failure will occur in a significant number of patients, and manipulation of the tumour vasculature has emerged as a promising therapeutic strategy over the past few years (Herbst et al 2005). Anti-angiogenic agents that impede tumour neo-vascularisation and vascular disrupting agents that target established tumour blood vessels are currently in clinical trials, and are being integrated with fractionated radiotherapy regimens, with the aim of improving treatment effectiveness.

There has been little human data on the effects of radiation on tumour vasculature. Recent pre-clinical data has indicated that the tumour response to radiation may be regulated by the degree of apoptosis in tumour endothelial cells, suggesting that the tumour vasculature may be an important therapeutic target for radiation (Garcia-Barros et al 2003). There is also evidence that radiation induced tumour regression may involve destruction of tumour vessels. It is also well recognised that tumour perfusion, through its effects on oxygenation, plays an important role in modulating responses to radiotherapy (Thomlinson and Gray 1955).

To date, the acute *in vivo* effects of fractionated radiotherapy on tumour vessels have not been evaluated for human lung cancer. Assessment of the acute tumour vascular effects of ionising radiation in human tumours is needed to corroborate data suggesting that the tumour vasculature may be an important therapeutic target for radiation. It is also important to establish a baseline for future evaluation of combined therapy with vascular targeting drugs in human lung cancer.

4.2 Aim

The aims of this study was firstly, to measure *in vivo* the acute vascular effects of fractionated radiotherapy on an entire human lung cancer using volumetric

perfusion CT. Secondly, to describe the spatial distribution of these vascular effects by measuring the vascular changes at the rim and the centre of the tumour.

4.3 Patients and methods

4.3.1 Study design

Local research ethics committee approval was obtained, with explicit approval for radiation exposure of patients for research purposes as required under the Ionising Radiation (Medical Exposure) Regulations (IR(ME)R). Each patient gave written informed consent; this included information on the radiation exposure from both the CT examinations (7.5mSv per examination), and subsequent radiotherapy (27Gy total dose). Sixteen patients (nine males, seven females, mean age 71 years) with histologically proven, inoperable non-small cell lung cancer were enrolled prospectively into the study. All patients were treated with a course of hypo-fractionated palliative radiotherapy delivering 27Gy in six fractions of radiotherapy over three weeks (4.5Gy per fraction, two fractions per week). Using volumetric perfusion CT, all sixteen patients were scanned after the second fraction (9Gy total dose) of radiotherapy. Eight patients had additional scans after the fourth (18Gy total dose) and sixth (27Gy total dose) fractions of radiotherapy. All scans were performed within two hours of patients receiving radiotherapy.

4.3.2 Volumetric perfusion CT

The CT methodology, image post-processing and data analysis have been described in Chapter 2. Apart from whole tumour measurements, additional image analysis was carried out on both the tumour rim and the tumour centre. The tumour rim was defined as the area less than 20% of the diameter from the tumour edge, and the tumour centre was defined as the area more than 30% of the diameter from the tumour edge. Because of difficulty in defining the tumour rim and the centre at the ends of the tumour volume, analysis was only carried out on a single central representative 10mm tumour axial level. As before, Patlak analysis (1983 and 1985) was used to quantify (i) transfer constant (K; ml/100ml/min) which provides information on permeability surface area product and blood flow, and (ii) relative vascular blood volume (BV; ml/100ml) on a pixel-by-pixel basis.

4.3.3 Statistical analysis

Paired t test was performed to compare mean changes in BV and K. In addition, Bland and Altman repeatability statistics (1986), as described in Chapter 3, were used to assess if an observed response following therapy is meaningful. The 95% limits of change for a group of 'n' patients can be estimated from the value of the mean squared differences (dSD) derived from the repeatability data set using the following formula: $(1.96 \cdot dSD) / \sqrt{n}$. From the repeatability data derived previously from 17 patients, the dSD values for BV and logarithmically

transformed K were 1.05ml/100ml and 0.13ml/100ml/min respectively. Hence, for a group of sixteen patients, any change in tumour vascular BV of more than $\pm 9.4\%$ as a consequence of treatment would be over and above intrinsic measurement variability, that is, the probability of this change being random is less than 5%. Similarly, an increase in tumour vessel K of more than 6.7%, or reduction more than 6.3% for a group of sixteen patients would be statistically significant at the 5% level. Likewise, for a group of eight patients, any change in BV of more than $\pm 13.4\%$, or an increase in K of more than 9.6%, or reduction of more than 8.8% would be statistically significant at the 5% level.

4.4 Results

4.4.1 Whole tumour vascular changes

All 16 patients completed their radiation treatment and were scanned successfully. Mean tumour vascular BV and K measurements are summarised in Table 4.1.

Table 4.1 Mean (\pm standard deviation) values for tumour transfer constant (K) and blood volume (BV) at baseline and after fractionated radiotherapy

	Baseline	9Gy	18Gy	27Gy
K (ml/100ml/min)				
<i>Whole tumour</i>	11.8 \pm 3.3	13.0 \pm 2.0	13.5 \pm 3.0	13.7 \pm 5.3
<i>Tumour rim</i>	14.3 \pm 4.2	16.9 \pm 5.6	20.7 \pm 3.4	17.2 \pm 6.4
<i>Tumour centre</i>	8.6 \pm 3.8	8.9 \pm 3.0	9.0 \pm 2.6	8.3 \pm 5.1
BV (ml/100ml)				
<i>Whole tumour</i>	5.8 \pm 1.9	7.1 \pm 3.0	7.4 \pm 2.5	6.5 \pm 2.0
<i>Tumour rim</i>	7.0 \pm 2.6	9.3 \pm 4.9	10.5 \pm 5.8	10.2 \pm 3.8
<i>Tumour centre</i>	3.4 \pm 2.0	3.9 \pm 2.0	4.1 \pm 2.1	3.5 \pm 1.1

At baseline, whole tumour BV and K were 5.8ml/100ml and 11.8ml/100ml/min respectively. Both mean BV and K increased following radiotherapy (Figure 4.1). BV increased significantly from baseline by 21.5% (paired t-test, $p=0.025$), 27.1% ($p=0.018$) and 11.2% ($p=0.0020$) after the second (9Gy total dose), fourth (18Gy total dose), and sixth (27Gy total dose) fractions of radiotherapy respectively. These BV changes were greater than the 95% limits of change. K increased from baseline by 10.2% ($p=0.065$), 14.5% ($p=0.37$) and 16.2% ($p=0.31$) after the second, fourth and sixth fractions of radiotherapy. These changes in K were greater than the 95% limits of change derived from our repeatability data, but were not significant on paired t-testing.

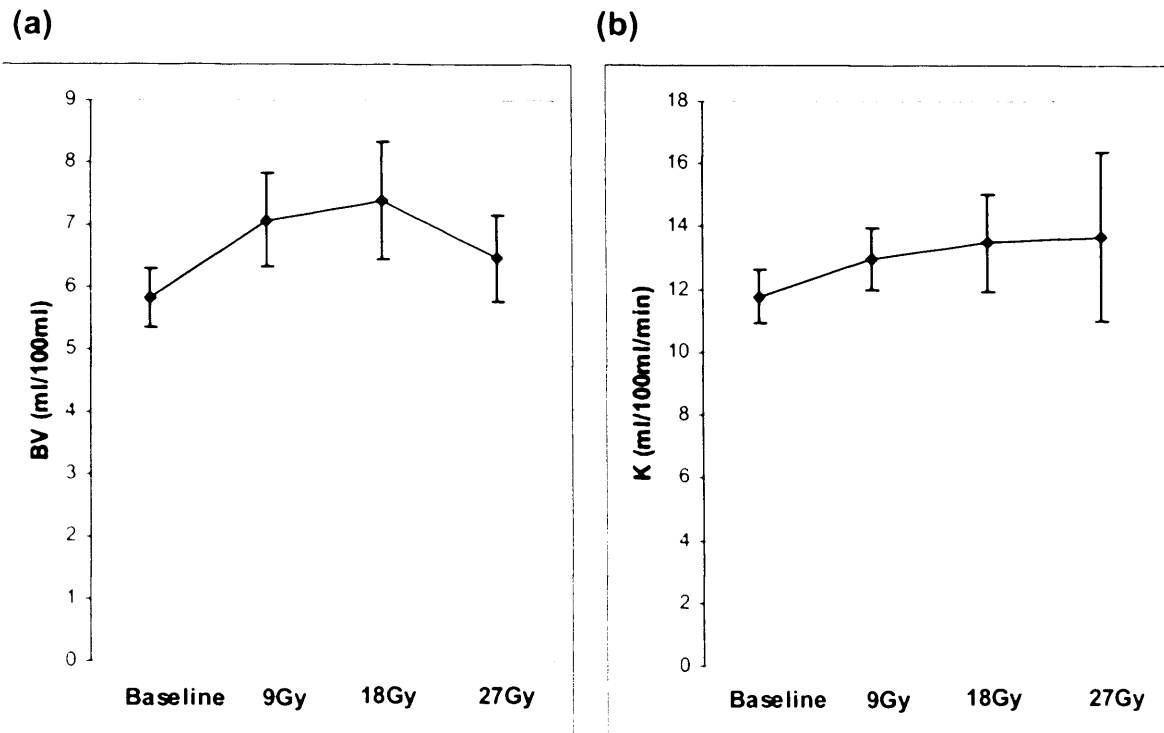


Figure 4.1 Line graphs showing mean changes (± 1 standard error) in whole tumour vascular blood volume (BV) (a) and transfer constant (K) (b) after fractionated radiotherapy. Measurements are derived from pixel-by-pixel analysis of whole lung tumour volumes and included pixels from both the more vascularised tumour rim as well as the relatively poorly perfused tumour centre.

4.4.2 Vascular changes in the tumour rim compared to the centre

The tumour vasculature was noted to be spatially heterogeneous with the tumour rim showing a higher BV and K than the centre. At baseline, the ratio of BV at the tumour rim to BV at the tumour centre was 2.1:1. For K, this was 1.7:1. Following radiotherapy, changes in vascular BV were greater at the tumour rim compared to the centre (Figure 4.2 and Figure 4.3). After the second fraction of radiotherapy, vascular BV increased by 31.6% ($p=0.10$) and 16.4% ($p=0.29$) at the rim and centre of the tumour respectively. These changes were greater than the 95% limits of change but were not significant on paired t-testing. After the fourth and sixth fractions of radiotherapy, vascular BV at the tumour rim increased significantly by 49.3% ($p=0.034$) and 44.6% ($p=0.0012$) respectively. Increase in vascular BV at the tumour centre was 19.9% ($p=0.029$) and 4.0% ($p=0.0050$) respectively. Again these changes were greater than the 95% limits of change.

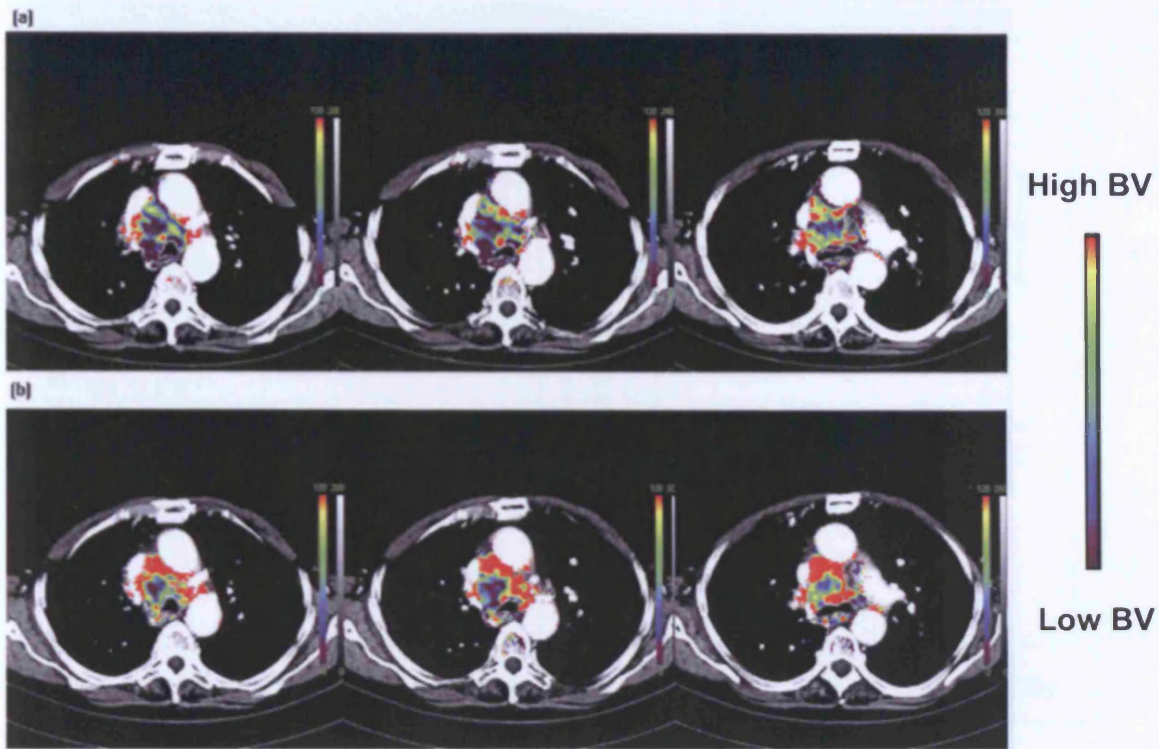
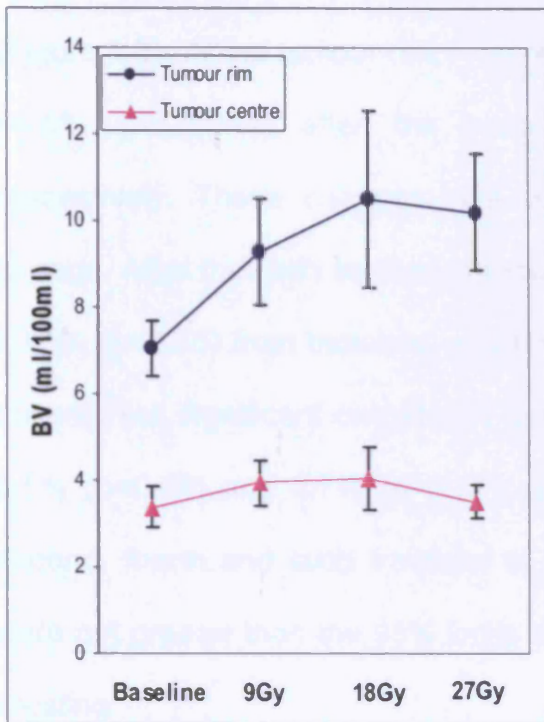


Figure 4.2 Coloured parametric maps depicting vascular blood volume (BV) at three contiguous axial levels from a lung tumour, at baseline (a) and after four fractions (18Gy total dose) of radiation therapy (b). Baseline tumour vascularity was spatially heterogeneous with the tumour rim being more vascular than the centre. A greater increase in BV after radiotherapy is observed at the tumour rim compared to the centre.

(a)



(b)

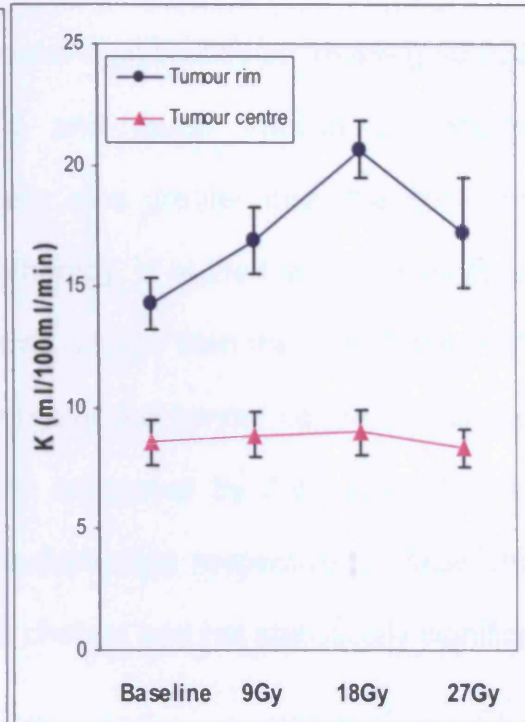


Figure 4.3 Line graphs showing mean changes (± 1 standard error) in tumour blood volume (BV) (a) and transfer constant (K) (b) at the tumour rim and the tumour centre following fractionated radiation therapy. Increases in both vascular parameters were greater at the tumour rim compared to the tumour centre.

Changes in K after radiotherapy were greater at the tumour rim than the centre (Figure 4.3). At the tumour rim, K increased significantly by 18.4% ($p=0.022$) and 44.8% ($p=0.0048$) after the second and fourth fraction of radiotherapy respectively. These changes in K were also greater than the 95% limits of change. After the sixth fraction of radiotherapy, K at the tumour rim increased by 20.5% ($p=0.25$) from baseline, which was greater than the 95% limits of change but was not significant on paired t-testing. At the tumour centre, K increased by 3.5% ($p=0.69$) and 4.7% ($p=0.27$), and decreased by 2.9% ($p=0.65$) after the second, fourth and sixth fractions of radiotherapy respectively. These changes were not greater than the 95% limits of change and not statistically significant on t-testing.

4.5 Discussion

The spatial distribution of K and BV on the baseline coloured parametric maps of the lung tumours in this study demonstrate that the tumour periphery is more vascular relative to the centre. This is consistent with pre-clinical studies in rat sarcomas showing that macroscopically, the tumour vasculature, although chaotic, and lacking the branching pattern of normal vessels, is ordered in distinct spatial regions (Endrich et al 1979). The centre of the tumour is relatively avascular, and is surrounded by a semi-necrotic region; a relatively stable microcirculation is evident at the periphery of the tumour, with an advancing vascular front at the tumour rim.

Ionising radiation causes cell death through accumulated single and double strand DNA damage mediated by both a direct effect of the photon passage through a cell and an indirect effect due to the production of free radicals, in particular the hydroxyl free radical; this latter effect is considered the dominant mode of DNA damage after therapeutic radiation. The interaction between ionising radiation and tumour vasculature has been studied in the laboratory. Recent *in vitro* studies have shown that the tumour response to radiation may be regulated by tumour endothelial cell apoptosis, indicating that the tumour endothelium is an important therapeutic target for radiation (Garcia-Barros et al 2003). Up-regulation of VEGF, either directly, or through activation of endothelium HIF-1, has also been reported in various cancer cell lines after ionising radiation, which may result in increased perfusion and neo-vessel formation (Moeller et al 2004, Lund et al 2004, Ando et al 1998). In mice, increase in tumour perfusion and subsequent increase in oxygenation were observed within four hours of fractionated radiation (Crokart et al 2005). This was thought to be due to an acute tumour inflammatory response. It has also been shown that tumour perfusion increases about 24 hours after radiation, which is mediated by endothelial nitric oxide (Sonveaux et al 2002). The mechanism of tumour re-oxygenation, which is essential to the enhancement of radio-sensitivity following irradiation, is therefore partly due to decrease in oxygen consumption and better diffusion secondary to tumour cell loss, as well as an increase in tumour perfusion.

Our findings bear out these pre-clinical findings of increased perfusion following ionising radiation. Whole tumour BV increased *in vivo* following radiotherapy. BV changes were evident as early on as the first two fractions of radiotherapy, indicating that a dose of 9Gy was sufficient to cause measurable increases, and remained significantly raised compared to baseline following 18Gy and 27Gy of radiotherapy. There did not appear to be a radiation dose response in terms of vascular changes as BV increased after two fractions without further significant increase after the fourth and sixth fractions of radiotherapy. The vascular changes were spatially heterogeneous. Although significant increases were noted both for the tumour rim and centre, changes were greater at the tumour rim. This may in part reflect the distribution of the vascularisation, but may also reflect the mechanism of radiation effect: vasodilatation of perfused established vessels secondary to release of inflammatory cytokines, opening up previously non-perfused vessels, and neovessel formation due to upregulation of VEGF, and expression of endothelial NOS.

Changes in K did not closely parallel changes in BV. Whole tumour K did not appear to increase significantly following radiotherapy. When changes at the tumour rim were compared with the centre, significant changes were found, suggesting that K change was more spatially dependent than BV change. Significant K change occurred at the tumour rim after the second and fourth fractions of radiotherapy, possibly reflecting increased vessel leakiness and

endothelial cell damage. However no significant change in K was identified following the sixth fraction of radiotherapy, which may be due to establishment of equilibrium between vessel permeability and interstitial pressure.

While there have been no *in vivo* human studies monitoring the acute tumour vascular effects over an entire course of fractionated radiotherapy, our results are broadly in line with the few studies that have evaluated vascular changes in patients treated with radiotherapy or chemo-radiation. An increase in tumour permeability and blood volume, measured with perfusion CT, has been reported in a variety of solid tumours following radiotherapy (Harvey et al 1999). However, the heterogeneous group of tumours and different radiotherapy schedules make results difficult to compare and interpret. Tumour perfusion changes may be dose dependent, and may vary according to fraction size. It may also vary across different tumour sites, and different tumour types. In patients with rectal carcinoma receiving pre-operative chemo-radiotherapy, DCE-MRI measurements of tumour perfusion showed significant increases after the first and second week of treatment but not after the third and fourth week (de Vries et al 2000). In a separate study, also in patients with rectal carcinoma receiving pre-operative chemo-radiotherapy, significant decreases in perfusion CT measurements of blood flow were observed upon completion of treatment (Sahani et al 2005). However, in both these studies, the vascular changes observed might be confounded by the potential anti-vascular effects of the chemotherapeutic agents used (Miller et al 2001).

In conclusion, this study has demonstrated for the first time *in vivo* using a non-invasive whole tumour perfusion CT technique that fractionated radiotherapy has tumour vascular activity. Radiotherapy increases tumour vascular BV and K in human non-small cell lung cancer, and these vascular changes are more pronounced at the tumour rim.

CHAPTER 5

TUMOUR VASCULAR EFFECTS OF COMBRETASTATIN A4 PHOSPHATE IN COMBINATION WITH RADIOTHERAPY

5.1 Introduction

Combretastatin A4 Phosphate (CA4P) is a vascular disrupting agent that targets immature tumour blood vessels. Phase 1 clinical trials of CA4P as a single agent have demonstrated reduction in tumour vascularity within four hours of patients receiving CA4P, with partial recovery by 24 hours (Galbraith et al 2003, Anderson et al 2003, Stevenson et al 2003). In animal models, CA4P causes haemorrhagic necrosis in the central region of tumours, and despite adequate doses, leaves a rim of viable tumour cells, which may re-perfuse and re-populate the tumour (Dark et al 1997). In contrast, radiation has shown greater tumour cell killing activity in better oxygenated tumour areas, such as the tumour rim (Steel et al 1983). The combination of radiotherapy with CA4P has been shown to achieve a reduction in tumour cell survival, and synergy between the two agents has been demonstrated in animal tumour models (Li et al 1998, Murata et al 2001). However, the potential vascular interaction between radiotherapy and CA4P has yet to be studied in humans.

5.2 Aim

A phase 1b clinical trial of radiotherapy combined with CA4P in patients with advanced lung cancer was designed to include the *in vivo* assessment of the tumour vascular effects after radiotherapy in combination with CA4P using volumetric perfusion computed tomography (CT).

5.3 Patients and Methods

5.3.1 Study design

Local research ethics committee approval was obtained, with explicit approval for radiation exposure of patients for research purposes as required under the Ionising Radiation (Medical Exposure) Regulations (IR(ME)R). Each patient gave written informed consent; this included information on the radiation exposure from both the CT examinations (7.5mSv per examination), and subsequent radiotherapy (27Gy total dose). This Phase 1b study was primarily designed to evaluate the safety and toxicity of the combination of radiotherapy with CA4P. Functional imaging using perfusion CT was incorporated to assess the tumour vascular changes that occur after radiotherapy in combination with CA4P, and the results form the basis of this chapter.

Patients with histologically confirmed, inoperable non-small cell lung cancer, who were due to receive palliative radiotherapy, were eligible for the study. In addition, patients must not have clinically significant cardiac abnormality including uncontrolled hypertension, history of angina or myocardial infarction, arrhythmias, or prolongation of QTc interval. Other requirements included age 18 years or older, World Health Organisation performance status of 0 to 2, life expectancy of more than 12 weeks, minimum 4 weeks interval between prior chemotherapy, immunotherapy, and radiotherapy and receiving CA4P, and adequate renal, hepatic, and haematological function. Patients were also excluded if they had major surgery in the preceding 4 weeks, active brain metastases, grade 2 or greater peripheral neuropathy, symptomatic peripheral vascular disease or cerebrovascular disease.

Eligible patients were recruited prospectively into two treatment cohorts with six patients in each cohort. All patients were treated with a course of hypofractionated palliative radiotherapy, delivering 27Gy in six fractions of radiotherapy over three weeks (two fractions per week). Six patients in the first cohort received a single 50mg/m² dose of CA4P after the second fraction of radiotherapy. Six patients in the second cohort received weekly CA4P at the same dose after the second, fourth and sixth fractions of radiotherapy (Table 5.1).

Table 5.1 Treatment schedule for study patients receiving combretastatin A4 Phosphate (CA4P) at 50mg/m² in combination with radiotherapy (RT) at 4.5Gy per fraction

Cohort	Week	Mon	Tues	Wed	Thurs	Fri	Sat	Sun
1	1	RT			RT + CA4P			
	2	RT			RT			
	3	RT			RT			
2	1	RT			RT+ CA4P			
	2	RT			RT+ CA4P			
	3	RT			RT+ CA4P			

Approximately two hours after completion of radiotherapy, CA4P was administered intravenously over 10 minutes using a volumetric pump. The dose of CA4P corresponds to the weight of the free acid; the dose representing the free acid is equal to 90% of the dose representing the disodium salt. Thus, 50mg/m² of CA4P as the free acid is equivalent to a dose of 55.5mg/m² of the disodium salt, which is above the threshold dose of 52mg/m² where CA4P was

shown to have tumour anti-vascular activity as a single agent, and is below the maximum tolerated dose (Galbraith et al 2003, Anderson et al 2003, Stevenson et al 2003). Volumetric perfusion CT scans were performed at (i) baseline, (ii) after the second, fourth and sixth fractions of radiotherapy prior to CA4P, (iii) four hours following CA4P administration to assess for acute vascular changes, and (iv) 72 hours after CA4P to determine the duration of the vascular response.

5.3.2 Volumetric perfusion CT

The CT methodology, image post-processing and data analysis have been described in Chapter 2. Apart from whole tumour vascular measurements, additional image analysis was carried out for both the tumour rim and the tumour centre in order to assess the spatial distribution of the vascular changes after treatment. The tumour rim was defined as the area less than 20% of the diameter from the tumour edge, and the tumour centre was defined as the area more than 30% of the diameter from the tumour edge. Because of difficulty in defining the tumour rim and the centre at the ends of the tumour volume, analysis was only carried out on a single central representative 10mm tumour axial level. As before, Patlak analysis (1983) was used to quantify (i) transfer constant (K; ml/100ml/min) which provides information on permeability surface area product and blood flow, and (ii) relative blood volume (BV; ml/100ml) on a pixel-by-pixel basis.

5.3.3 Statistical analysis

Paired t test was performed to compare mean changes in BV and K. In addition, Bland and Altman repeatability statistics (1986), as described in Chapter 3, were used to assess if an observed response following therapy is meaningful. The 95% limits of change for a group of 'n' patients can be estimated from the value of the mean squared differences (dSD) derived from the repeatability data set using the following formula: $(1.96 \cdot dSD) / \sqrt{n}$. From the repeatability data derived previously from 17 patients, the dSD values for BV and logarithmically transformed K were 1.05ml/100ml and 0.13ml/100ml/min respectively. Hence, for a group of eight patients, any change in tumour BV of more than $\pm 13.4\%$, or an increase in tumour K of more than 9.6%, or reduction of more than 8.8% as a consequence of treatment would be over and above intrinsic measurement variability, that is, the probability of this change being random is less than 5%. Similarly, for a group of four patients, any change in BV of more than $\pm 18.9\%$, or increase in K of more than 13.9%, or reduction more than 12.2% would be statistically significant at the 5% level.

5.4 Results

Twelve patients were treated in the study. Four patients did not take part in the CT study for logistical reasons. Patients 1 and 2 were recruited before the CT was fully developed for clinical use. Patients 8 and 11 were treated during Bank

Holidays when the CT was unfortunately unavailable for research purposes. The remaining eight patients (six males, two females; mean age 66 years; six stage IIIB, two stage IV) completed all CT scans. Thus, eight patients received CA4P following the second fraction of radiotherapy (9Gy total dose), and four of these patients received further doses of CA4P after the fourth (18Gy total dose) and sixth (27Gy total dose) fractions of radiotherapy. Whole tumour vascular measurements were performed for all scans, while vascular measurements from the tumour rim and centre were carried out for scans performed during the first week of treatment only.

5.4.1 Vascular changes from the whole tumour during the first week of treatment

Baseline mean tumour K and BV were 11.6ml/100ml/min and 6.8ml/100ml respectively. Following the second fraction of radiotherapy (9Gy total dose), mean K increased by 11.7% which was just greater than the 95% limits of change but was not significant on paired t-testing ($p=0.20$) (Figure 5.1). Mean BV increased by 10.6% ($p=0.16$) which was not statistically significant. Four hours after CA4P, there was a decrease in BV (16.4%; $p=0.029$), which was sustained to 72 hours (21.3%; $p=0.025$) (Figure 5.2). At four and 72 hours after CA4P, K decreased by 6.2% ($p=0.51$) and 7.7% ($p=0.23$) respectively which were not statistically significant.

On an individual patient basis, it was observed that six of the eight patients achieved reductions in tumour BV (22.9%, $p < 0.001$) four hours after CA4P (Figure 5.3). It was also noted that all six patients had increases in K after radiotherapy (23.6%, $p = 0.011$; Figure 5.3). The two patients who did not have a vascular response to CA4P did not show an initial increase in tumour K following radiotherapy. Indeed, for all eight patients, there was a significant correlation between increase in K following radiotherapy and the reduction in vascular BV four hours following CA4P administration ($r = 0.77$, $p = 0.026$) (Figure 5.4). At 72 hours after CA4P, there was a sustained reduction in tumour vascular BV of 29.6% ($p < 0.001$) in the same six patients.

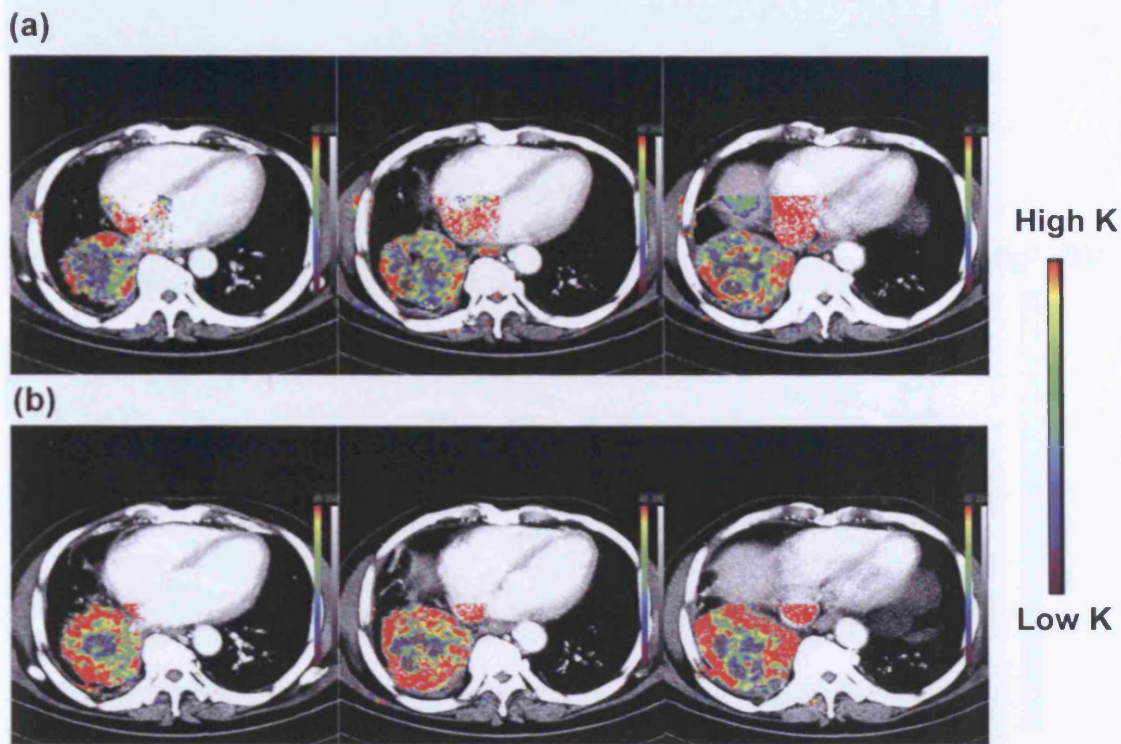


Figure 5.1 CT images of a lung tumour from three representative axial levels showing coloured parametric map of transfer constant (K) at baseline (a) and after two fractions (9Gy total dose) of radiotherapy (b). Increases in K were seen predominantly at the rim of the tumour.

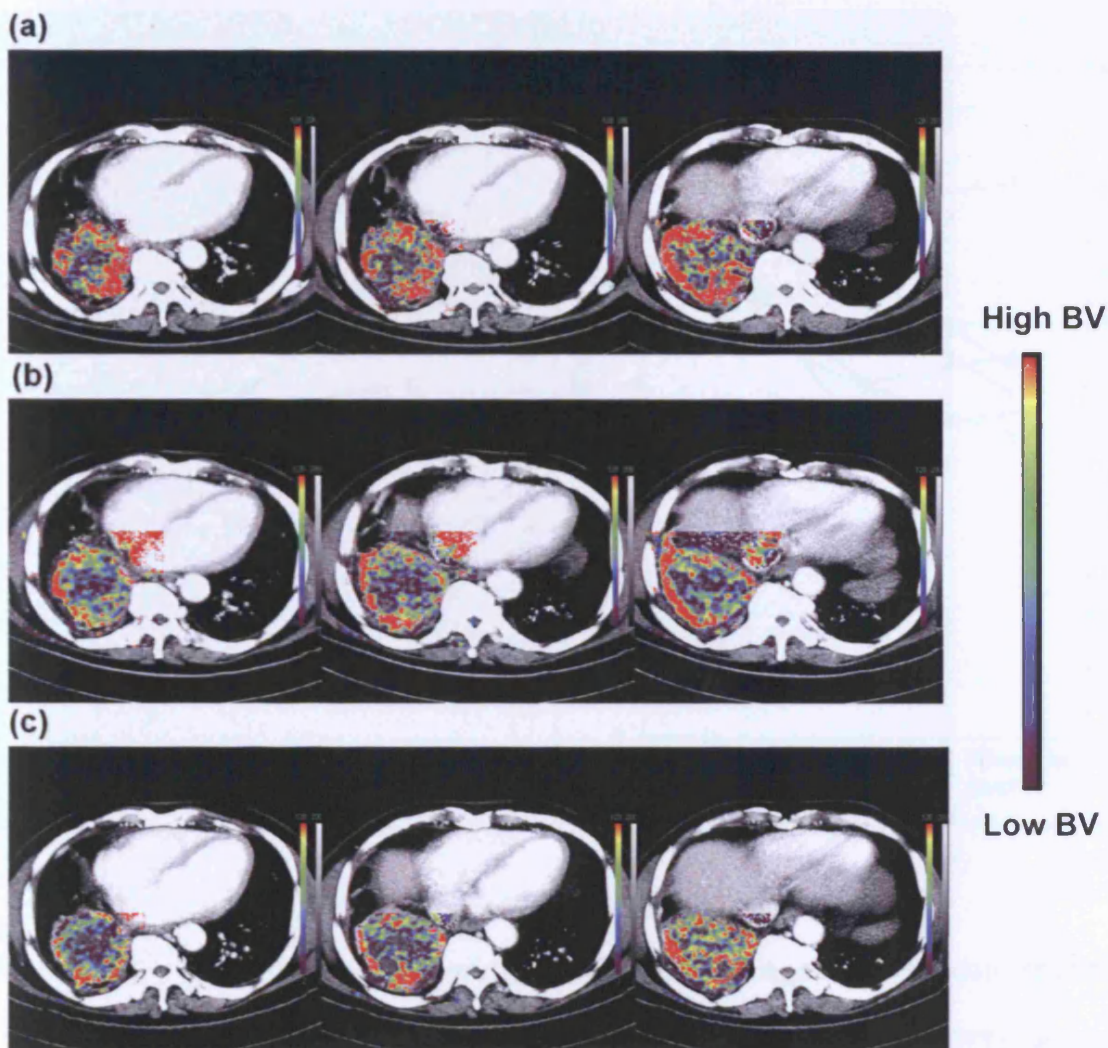


Figure 5.2 CT images of a lung tumour from three representative axial levels showing coloured parametric map of tumour blood volume (BV) before CA4P (a), 4 hours (b), and 72 hours (c) after a single dose of CA4P. Reduction in BV seen after CA4P at 4 hours was sustained to 72 hours and most evident at the tumour rim.

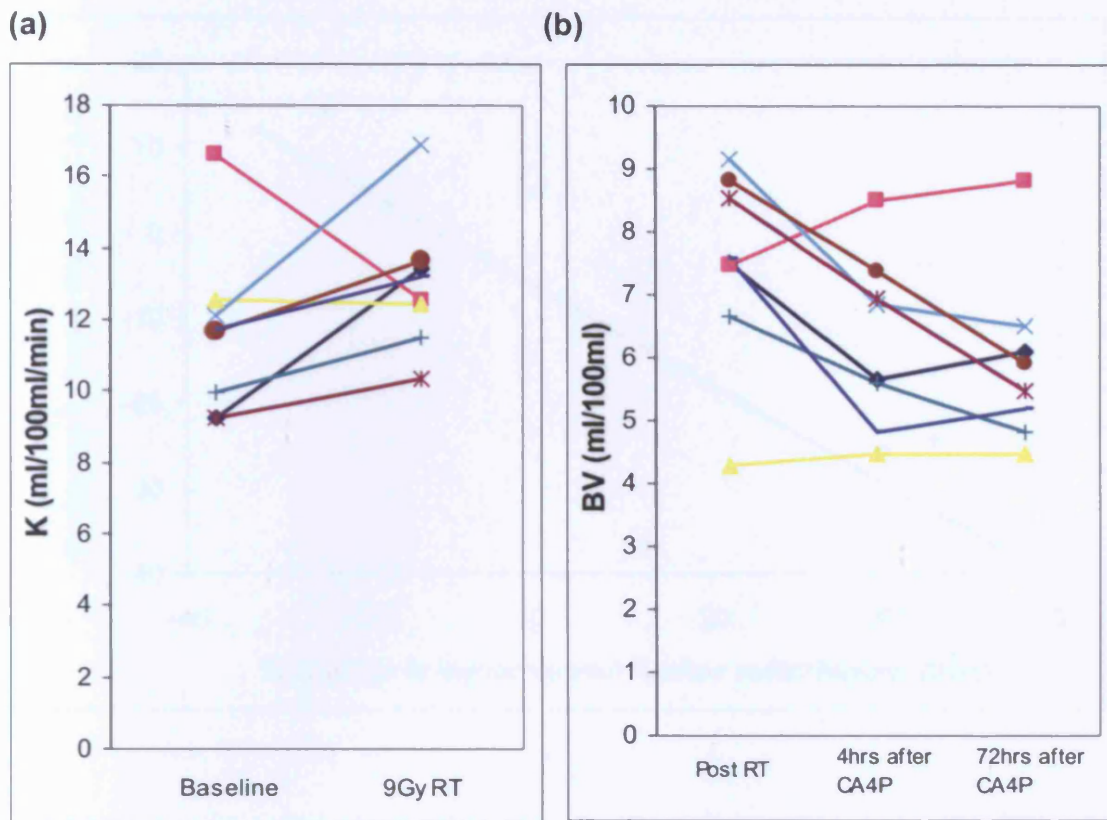


Figure 5.3 Line graphs showing individual changes in tumour transfer constant (K) after two fractions of radiotherapy (RT) (a), and tumour blood volume (BV) at four and 72 hours after combretastatin A4 Phosphate (CA4P) (b). The six patients who had increases in K after RT had a vascular response to CA4P

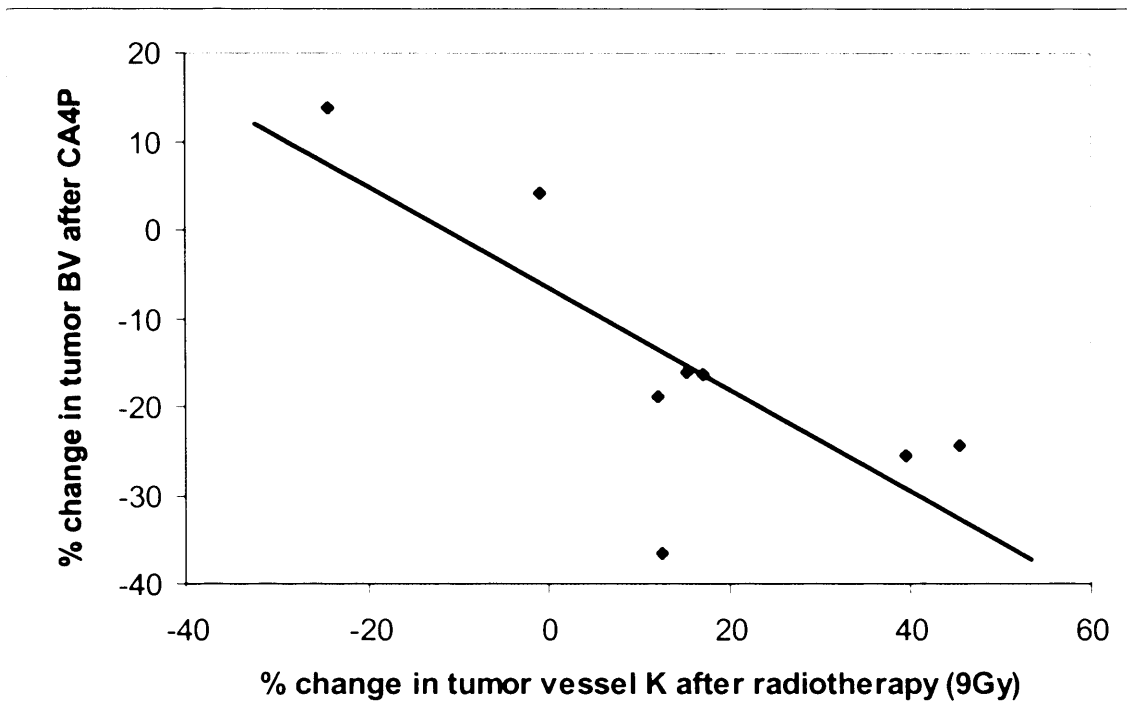


Figure 5.4 Regression plot showing change in whole tumour blood volume (BV) after combretastatin A4 Phosphate (CA4P) against change in the transfer constant (K) after radiotherapy. Increase in K after radiotherapy correlated to reduction in BV after CA4P ($r=0.77$, $p=0.026$)

5.4.2 Vascular changes in the tumour rim compared to the centre during the first week of treatment

Baseline tumour vascularity was spatially heterogeneous; the tumour rim demonstrated a higher K and BV than the tumour centre. The ratio of BV at the tumour rim to the tumour centre was 2.0:1. Similarly, for K, this was 1.5:1. Following the second fraction of radiotherapy, mean K increased by 12.7% ($p=0.36$) at the tumour rim but decreased by 2.2% ($p=0.84$) at the centre. Four hours after CA4P, mean BV decreased by 32.0% ($p=0.16$) at the tumour rim and 10.6% ($p=0.41$) at the tumour centre. At 72 hours after CA4P, a reduction in BV of 39.3% ($p=0.097$) was measured at the tumour rim, and 14.6% ($p=0.15$) at the tumour centre. Increase in K after radiotherapy correlated to reduction in BV after CA4P ($r=0.75$, $p=0.020$) at the tumour rim only.

Analysis was then carried out on the six patients who had a vascular response to CA4P. For these patients, increases in K following the second fraction of radiotherapy were also greater at the tumour rim than the tumour centre (34.2%, $p=0.0073$ versus 11.3%, $p=0.28$) (Figure 5.5). Four hours following CA4P administration, there was a greater reduction in BV at the tumour rim than the tumour centre (45.5%, $p=0.035$ versus 22.7%, $p=0.0077$) (Figure 5.5). Reduction in BV at the tumour rim and centre were sustained to 72 hours (51.4%, $p=0.014$ versus 22.8%, $p=0.012$).

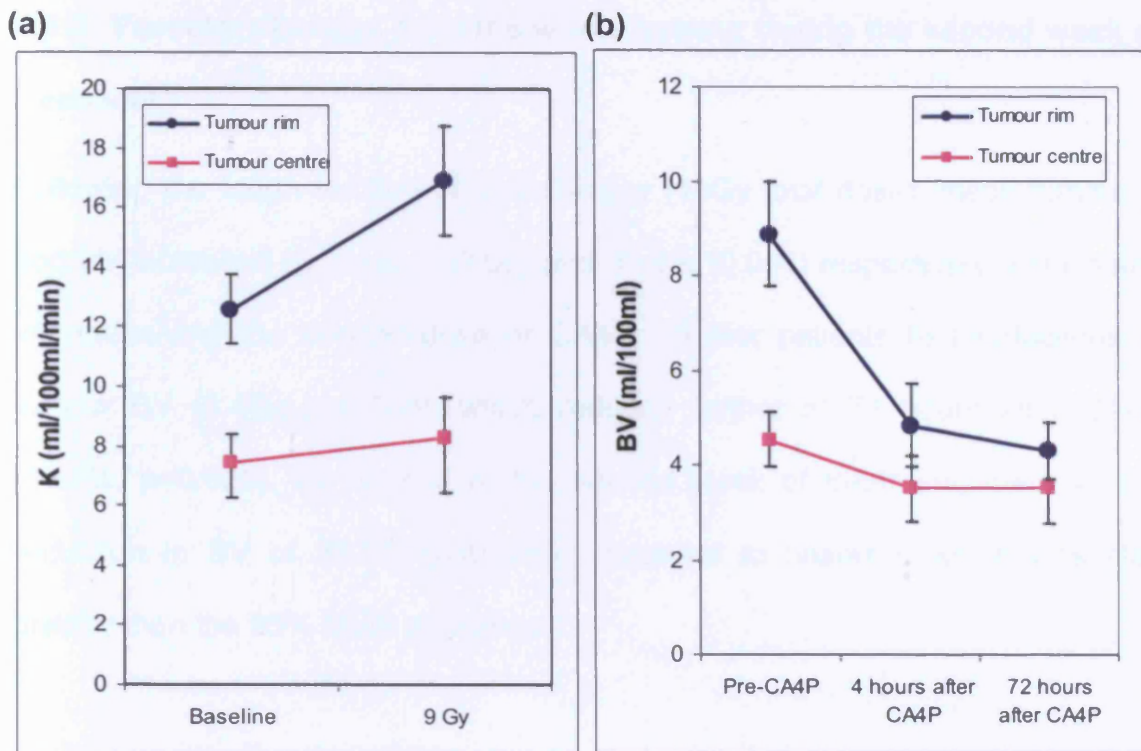


Figure 5.5 Line graphs showing mean vascular changes (± 1 standard error) at the tumour rim and the tumour centre for transfer constant (K) after two fractions of radiotherapy (a), and blood volume (BV) at four and 72 hours after combretastatin A4 phosphate (CA4P) (b). Changes in both vascular parameters were greater at the tumour rim compared to the tumour centre.

5.4.3 Vascular changes from the whole tumour during the second week of treatment

Following the fourth fraction of radiotherapy (18Gy total dose), mean tumour K and BV increased by 3.4% ($p=0.59$) and 33.1% (0.064) respectively. Four hours after receiving the second dose of CA4P, all four patients had reductions in tumour BV (8.4%, $p=0.038$), which reduced further at 72 hours after CA4P (31.7%, $p=0.025$). At the end of the second week of treatment, there was a reduction in BV of 28.5% ($p=0.029$) compared to baseline. which was also greater than the 95% limits of change.

5.4.4 Vascular changes from the whole tumour during the third week of treatment

Following the sixth fraction of radiotherapy (27Gy total dose), K decreased by 8.4% ($p=0.49$), while tumour BV increased by 27.1% ($p=0.049$). Four and 72 hours after the third dose of CA4P, tumour BV decreased by 8.7% ($p=0.34$) and 22.2% ($p=0.061$) respectively. Overall, a reduction in tumour BV of 30.3% ($p=0.044$), which was also greater than the 95% limits of change, was observed at the end of treatment compared to baseline (Figure 5.6).

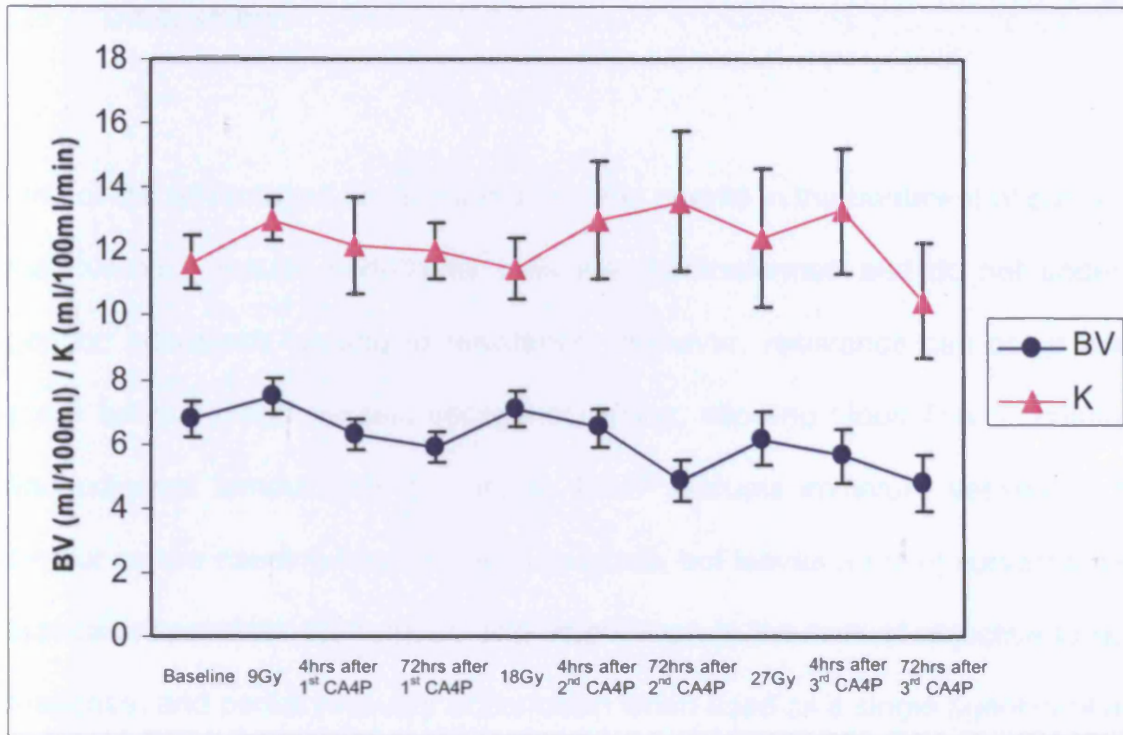


Figure 5.6 Changes in mean (± 1 standard error) tumour blood volume (BV) and transfer constant (K) during the course of treatment.

5.5 Discussion

One of the advantages of vascular disrupting agents in the treatment of cancer is that tumour vascular endothelial cells are untransformed and do not undergo genetic alterations leading to resistance. However, resistance can occur when some tumour blood vessels escape occlusion, allowing blood flow to continue and adjacent tumour cells to survive. CA4P disrupts immature vessels in the tumour centre causing haemorrhagic necrosis, but leaves a rim of surviving cells that can repopulate the tumour. This might explain the lack of objective tumour response, and partial recovery of perfusion when used as a single agent in phase 1 clinical trials. In order to overcome this resistance, CA4P was administered in combination with radiotherapy in this study.

At the dose used in this study, the vascular disrupting effect of CA4P is through its action on tumour endothelial cells. Within minutes of exposure to CA4P, there is a change in the cytoskeletal network within immature tumour endothelial cells resulting in a marked change in the endothelial cell shape, and an increase in vascular permeability. This leads to an additional increase in the already high interstitial fluid pressure in tumours, resulting in vascular collapse (Galbraith et al 2001, Kanthou and Tozer 2002, Tozer et al 2005). Recent *in vitro* studies have shown that both radiation and CA4P increase tumour permeability through a similar effect on tumour endothelial cells, by activating the Rho/Rho kinase signal pathway, and causing reorganisation of actin filaments (Kanthou et al 2005).

Tumours with greater permeability have been shown to be more susceptible to the effects of CA4P (Tozer et al 2001, Beauregard et al 2001). Radiotherapy, by increasing vessel permeability through the same pathway as CA4P, might therefore augment the vascular disrupting activity of CA4P. The positive correlation between radiation induced increase in K and reduction in BV after CA4P also appear to uphold the hypothesis, proposed by pre-clinical data, that radiotherapy may enhance the effect of CA4P.

In pre-clinical studies, the enhancement of CA4P by radiation appears to be dependent on timing and scheduling. In the C3H mammary carcinoma, improvement in tumour control was only observed when CA4P was administered at the same time or after radiation (Murata et al 2001, Horsman and Murata 2002). There are two possible reasons for this. Firstly, as we have shown in this clinical study, radiotherapy induces changes in the tumour vasculature that appear to increase the vascular shutdown caused by subsequent administration of CA4P. Secondly, CA4P when administered before radiation may induce acute tumour hypoxia and render the tumour radioresistant. In this clinical study, CA4P was administered to patients about two hours after receiving radiotherapy. Furthermore, the fractionated regimen used here potentially allows tumour re-oxygenation to occur, as there is a 72 hours interval between radiation fractions. It was shown recently that there was significant re-perfusion and re-oxygenation at the periphery of the syngeneic 13762NF rat breast carcinoma by 24 hours following CA4P treatment (Zhao et al 2005).

During the first week of treatment, CA4P caused a greater reduction in tumour BV at the tumour rim compared to the centre. This spatial distribution of vascular shutdown following CA4P appears inconsistent with preclinical data where CA4P has been shown to be more effective at the tumour centre than the rim. However, increases in K following 9Gy of radiation were also predominantly at the tumour rim; further supporting the hypothesis that radiation enhances vascular shut down after CA4P. At the tumour centre, increase in K following radiotherapy was not statistically significant (11.3%, $p=0.28$), while at 4 hours after CA4P administration, there was a significant reduction in BV (22.7%, $p=0.0077$). This explains why increase in K after radiotherapy did not significantly correlate to reduction in BV after CA4P at the tumour centre. This suggests that while radiotherapy might enhance the vascular disrupting effects of CA4P at the tumour rim, CA4P is able to target the vasculature at the tumour centre independent of the effects of radiation. The reduction in tumour vascular BV observed after the combination of radiotherapy and CA4P is in contrast to the increase in BV that has been demonstrated after radiotherapy alone in Chapter 4. Furthermore, the sustained vascular shutdown at 72 hours is in contrast to the partial recovery in tumour vascularity seen within 24 hours of single agent CA4P, and suggests a positive interaction between radiation and CA4P.

All four patients in the second cohort had increases in tumour K after the second fraction of radiotherapy, followed by a vascular response to the first dose of

CA4P. However, the changes in K after the fourth and sixth fractions of radiotherapy were not statistically significant, and there was a decrease in K after the sixth radiation fraction. These findings are similar to the K changes after radiotherapy alone (Chapter 4), and might be due to establishment of equilibrium between vessel permeability and interstitial pressure following repeated fractions of radiation. Despite the small number of patients, there were significant reductions in mean tumour BV after the second and third doses of CA4P when compared to baseline. Each additional week of treatment resulted in a further cumulative decrease in BV; by the end of treatment, there was a 30.3% overall reduction in tumour BV. Increases in BV after radiotherapy were also observed during the second and third week of treatment, which might have contributed to increasing drug delivery to the tumour vessels, thus further enhancing the vascular disrupting effect of CA4P.

In summary, we have used a non-invasive perfusion CT technique to demonstrate the vascular interaction between radiation and CA4P. The positive correlation between increase in tumour K after radiotherapy and reduction in vascular BV after CA4P, together with the sustained vascular shutdown, and the spatial distribution of blood volume change may provide a mechanistic rationale for the enhanced tumour anti-vascular activity between radiation and CA4P.

CHAPTER 6

TUMOUR VASCULAR EFFECTS OF NITRIC OXIDE SYNTHESIS INHIBITION

6.1 Introduction

Nitric oxide (NO) is an important signalling compound that is synthesised during the conversion of L-arginine to citrulline, catalysed by the nitric oxide synthase (NOS) enzymes (Alderton et al 2001). NO has complex functions in tumour biology, with apparently opposing roles depending on its concentration, redox status and the local microenvironment. Increased expression of NOS has been demonstrated in experimental tumour models, and higher levels of NOS expression in human tumours may be correlated with worse prognosis (Thomsen et al 1994, Cobbs et al 1995, Vakkala et al 2000, Klotz et al 1998, Fujimoto et al 1997, Gallo et al 1998). The effects of NO on the tumour vasculature has been widely investigated in pre-clinical studies, and NO has been implicated in tumour angiogenesis, as well as maintaining the vasodilator tone of tumour blood vessels, thus making it an attractive target for anti-cancer therapy (Fukumara et al 2006, Lala et al 2001). NO has been shown to act downstream from angiogenic factors such as vascular endothelial growth factor (VEGF) which activate endothelial NOS in vascular endothelial cells (Ziche et al 1997, Veikkola et al 2000, Fukumara et al 2001). Competitive inhibition of NOS using analogues of L-arginine results in a decrease in blood flow to experimental tumours as a result of vasoconstriction (Tozer et al 1997). The NOS inhibitor N-nitro L-arginine

(L-NNA) has been shown in BD9 rats bearing the P22 carcinosarcoma to selectively reduce tumour blood flow. In man, NOS inhibition has been shown to increase blood pressure in healthy volunteers, and critically ill patients with septic shock (Haynes et al 1993, Lorente et al 1993). However, the potential anti-vascular tumour effects of NOS inhibition have not been investigated in patients with cancer.

6.2 Aim

A phase I clinical study of L-NNA in patients with cancer was designed to include assessment of the *in vivo* tumour vascular effects of L-NNA using volumetric perfusion CT.

6.3 Patients and Methods

6.3.1 Study Design

Local research ethics committee approval was obtained for the study and all patients provided written informed consent, which included information on the radiation exposure from the CT examinations (7.5mSv per examination). Patients were enrolled prospectively onto a phase 1 dose escalation study. Main inclusion criteria were patients ≥ 18 years old with a World Health Organization performance status ≤ 2 and histologically confirmed cancer. Patients with hypertension or any significant cardiac medical history were excluded from the

study. The starting dose was 0.1mg/kg, escalating stepwise to 0.2mg/kg, 0.3mg/kg, 0.5mg/kg, 0.7mg/kg and 0.9mg/kg. A total of three patients were studied at each of the six dose levels. L-NNA was supplied as a lyophilised powder and reconstituted in 0.9% sodium chloride to provide a 5.85mg/ml solution. All patients received a single intravenous dose of L-NNA administered as a one minute infusion.

Cardiovascular monitoring was carried out on all patients in the study. Pulse, systolic and diastolic blood pressures were monitored at five minute intervals for the first hour, and hourly for six hours after L-NNA. Any adverse event that occurred while a patient was enrolled onto the trial was recorded and graded according to the National Cancer Institute common toxicity criteria (CTC) version 2.0 (Appendix 1). All patients had blood sampled for pharmacokinetic measurements. In addition, perfusion CT scans were performed on the final eight patients in the study. Scans were performed (i) prior to receiving L-NNA, (ii) one hour after L-NNA to measure the acute vascular changes, and (iii) 24 hours following L-NNA administration to determine the duration of the vascular response.

6.3.2 Pharmacokinetics

Blood samples in 7ml heparinised blood tubes were taken before treatment and at 2 minutes after the end of infusion, then at 5, 10, 15, 30, 45, 60, 75, 90, 105,

120, 150, 180, 240, and 360 minutes. When possible, blood samples were also taken 24 hours after treatment. Samples were immediately placed on ice. After centrifugation, plasma was removed with a pipette and transferred to a -20°C freezer. Pharmacokinetic analysis was performed by Dr Michael Stratford at the Gray Cancer Institute. Concentration of L-NNA was measured using high performance liquid chromatography with absorbance detection using a method based on that of Tabrizi-Fard and Fung (1996). Half-lives were calculated by weighted nonlinear least squares regression, area under the curve (AUC) and area under the first moment curve (AUMC) were calculated using the linear trapezoidal rule, extrapolated to infinity using the terminal half life, clearance (Cl) was calculated as dose/AUC, and the volume of distribution at steady state (Vdss) as $Cl \times AUMC/AUC$.

6.3.3 Volumetric perfusion CT

The CT methodology, image post-processing and data analysis have been described in Chapter 2. As before, Patlak analysis (1983 and 1985) was used to quantify (i) transfer constant (K; ml/100ml/min) which provides information on permeability surface area product and blood flow, and (ii) relative blood volume (BV; ml/100ml) on a pixel-by-pixel basis. For this study, an upgraded version of the prototype perfusion CT software was used, which allows the estimation of the percentage of non-perfused pixels. When BV was calculated as zero, these pixels were considered to be non-perfused, as opposed to pixels that fail to

model mathematically. These were assumed to represent non-functioning vessels. The percentage of non-perfused pixels in each ROI was recorded.

6.3.4 Statistical analysis

Paired t test was performed to compare mean changes in BV and K. In addition, Bland and Altman repeatability statistics (1986), as described in Chapter 3, were used to assess if an observed response following therapy is meaningful. The 95% limits of change for a group of 'n' patients can be estimated from the value of the mean squared differences (dSD) derived from the repeatability data set using the following formula: $(1.96 \cdot dSD) / \sqrt{n}$. From the repeatability data derived previously from 17 patients, the dSD values for BV and logarithmically transformed K were 1.05ml/100ml and 0.13ml/100ml/min respectively. Hence, for a group of eight patients, any change in tumour vascular BV of more than $\pm 13.4\%$ as a consequence of treatment would be over and above intrinsic measurement variability, that is, the probability of this change being random is less than 5%. Similarly, an increase in tumour vessel K of more than 9.6%, or reduction of more than 8.8% would be statistically significant at the 5% level.

6.4 Results

Eighteen patients (seven females and 11 males; age range 36 to 76 years; 12 non-small cell lung, five prostate, and one cervical cancer) were recruited onto

the study. All patients were assessed for toxicity and had plasma sampled for pharmacokinetic measurements. Eight patients from the final three dose levels (seven non-small cell lung cancer and one cervical cancer) underwent perfusion CT examinations.

6.4.1 Cardiovascular changes following L-NNA

A decrease of 6.1% ($p < 0.001$) of mean pulse rate was observed by five minutes after L-NNA from baseline of 81.2 (SD 15.4) beats per minute to 76.2 (SD 15.3) beats per minute, further decreasing by 11.2% ($p = 0.0069$) below baseline to 72.1 (SD 15.3) beats per minute. Mean systolic blood pressure increased by 6.1% ($p < 0.001$) from baseline of 133.2 (SD 19.6) mmHg to 141.4 mmHg (SD 19.0) mmHg at 40 minutes after L-NNA. Similarly, mean diastolic blood pressure increased by 10.4% ($p < 0.001$) from baseline of 75.3 (SD 8.9) mmHg to 83.2 (SD 11.7) mmHg at 50 minutes after L-NNA. All cardiovascular changes returned to baseline levels by three hours after L-NNA (Figure 1). Three patients, treated at the 0.2mg/kg, 0.3mg/kg and 0.7mg/kg dose levels respectively, had CTC grade 1 hypertension. Two patients had grade 1 sinus bradycardia. One patient at the first dose level reported transient grade 1 palpitation at 45 minutes following L-NNA, without 12-lead electrocardiography changes. No other adverse effects were observed or reported.

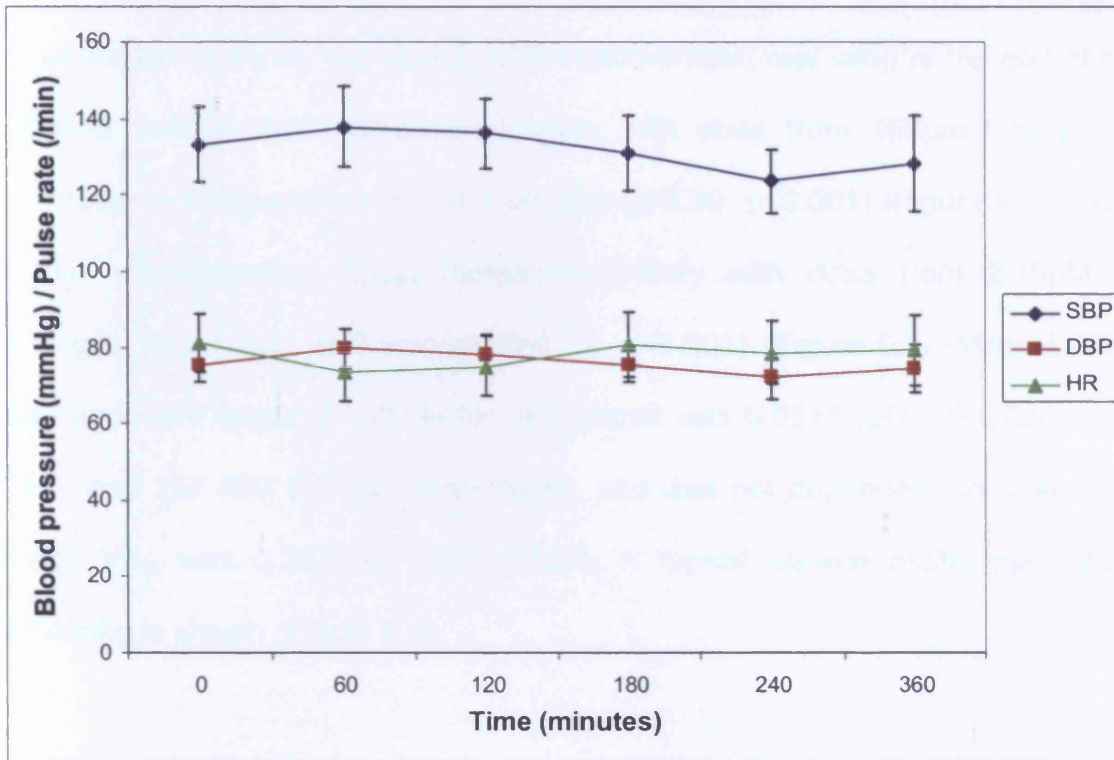
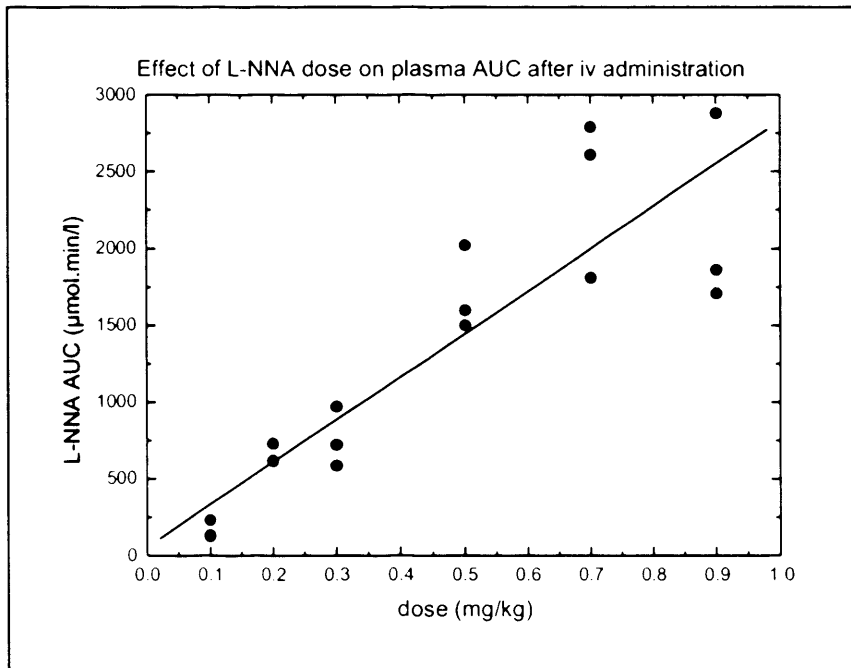


Figure 6.1 Mean cardiovascular changes (\pm 95% confidence intervals) in systolic blood pressure (SBP), diastolic blood pressure (DBP) and pulse rate (HR) after a single dose of N-nitro L-arginine (L-NNA).

6.4.2 Pharmacokinetics

In all but two patients, the peak L-NNA concentration was seen at the end of the infusion. L-NNA AUC increased linearly with dose from $163\mu\text{mol}\cdot\text{min}\cdot\text{L}^{-1}$ at $0.1\text{mg}/\text{kg}$ to $2150\mu\text{mol}\cdot\text{min}\cdot\text{L}^{-1}$ at $0.9\text{mg}/\text{kg}$ ($r=0.89$, $p<0.001$) (Figure 6.2). Peak L-NNA concentration (C_{max}) increased linearly with dose from $2.15\mu\text{M}$ at $0.1\text{mg}/\text{kg}$ to $24.5\mu\text{M}$ at $0.9\text{mg}/\text{kg}$ ($r=0.71$, $p<0.001$) (Figure 6.2). Mean L-NNA clearance and terminal half-life for all patients was 0.0018 (SD 0.00072) $\text{L}\cdot\text{min}^{-1}\cdot\text{kg}^{-1}$ and 197 (SD 82) min respectively, and was not dependent on dose. The mean $V_{\text{d}_{\text{ss}}}$ was $0.267\text{L}\cdot\text{kg}^{-1}$ (SD 0.092). A typical plasma profile seen after $0.9\text{mg}/\text{kg}$ is shown (Figure 6.3).

(a)



(b)

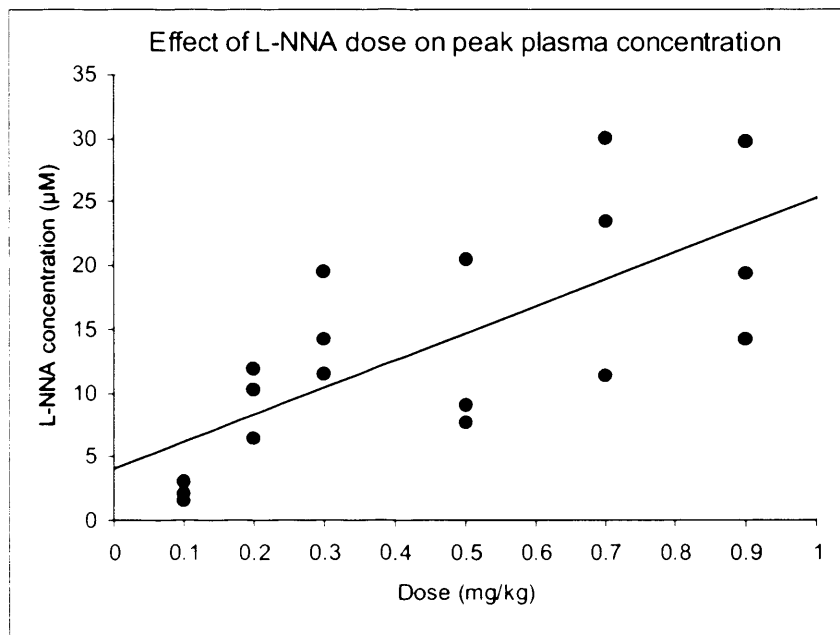


Figure 6.2 Relationship between N-nitro L-arginine (L-NNA) dose in mg/kg and L-NNA plasma area under the curve (AUC) (a), and peak concentration (b).

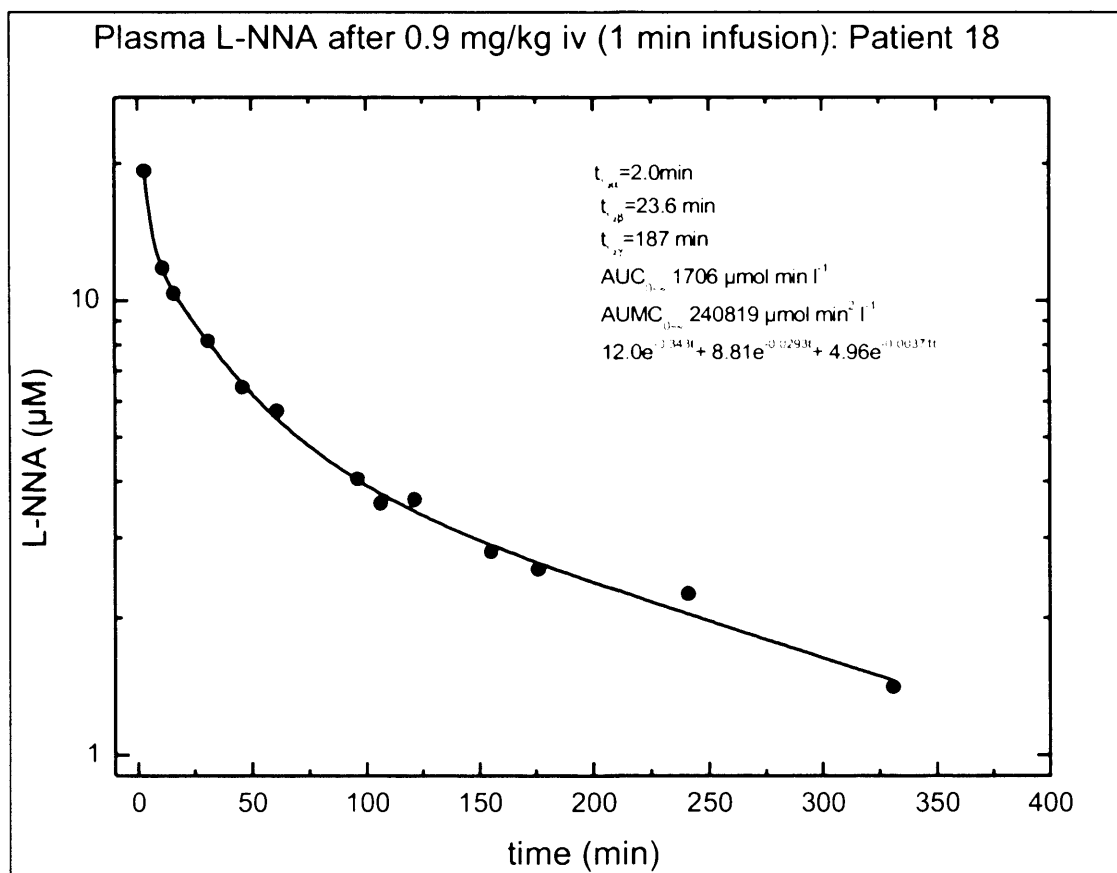


Figure 6.3 Typical plasma profile after 0.9mg/kg of N-nitro L-arginine (L-NNA)

6.4.3 Tumour vascular changes following L-NNA

The final eight patients recruited onto the study underwent perfusion CT examinations. Two patients were treated at the 0.5mg/kg dose level, three patients at 0.7mg/kg, and three patients at 0.9mg/kg. The mean baseline tumour vascular BV was 9.2 (SD 3.7) ml/100ml and mean baseline tumour vessel K was 14.9 (SD 5.73) ml/100ml/min. One hour after receiving L-NNA, all eight patients had reductions in tumour vascular BV (mean 42.9%; range 12.0 to 62.1%; paired t-test $p=0.0070$), which was greater than the 95% limits of change (Figure 6.4 and Figure 6.5). This was associated with an increase in the number of non-perfused tumour pixels from 7.3% at baseline to 25.1% ($p=0.0089$) (Figure 6.5), indicating a decrease in functional vascularity. Mean tumour K decreased by 9.3% one hour after L-NNA which was just greater than the 95% limits of change but did not reach statistical significance on t-testing ($p=0.11$).

At 24 hours following L-NNA, all eight patients had sustained reductions in tumour vascular BV (mean 33.9%; range 6.5 to 64.9%; $p=0.035$), which was also greater than the 95% limits of change (Figure 6.5). The number of non-perfused pixels remained increased above baseline at 18.1% ($p=0.050$) (Figure 6.5). A 10.6% increase in K was observed at 24 hours, which was greater than the 95% limits of change but did not reach statistical significance on paired t-testing ($p=0.24$) (Figure 6.5). There was a significant correlation between L-NNA plasma AUC and the reduction in tumour vascular BV at 24 hours after L-NNA ($r=0.83$; $p=0.010$) (Figure 6.6) but not at one hour.

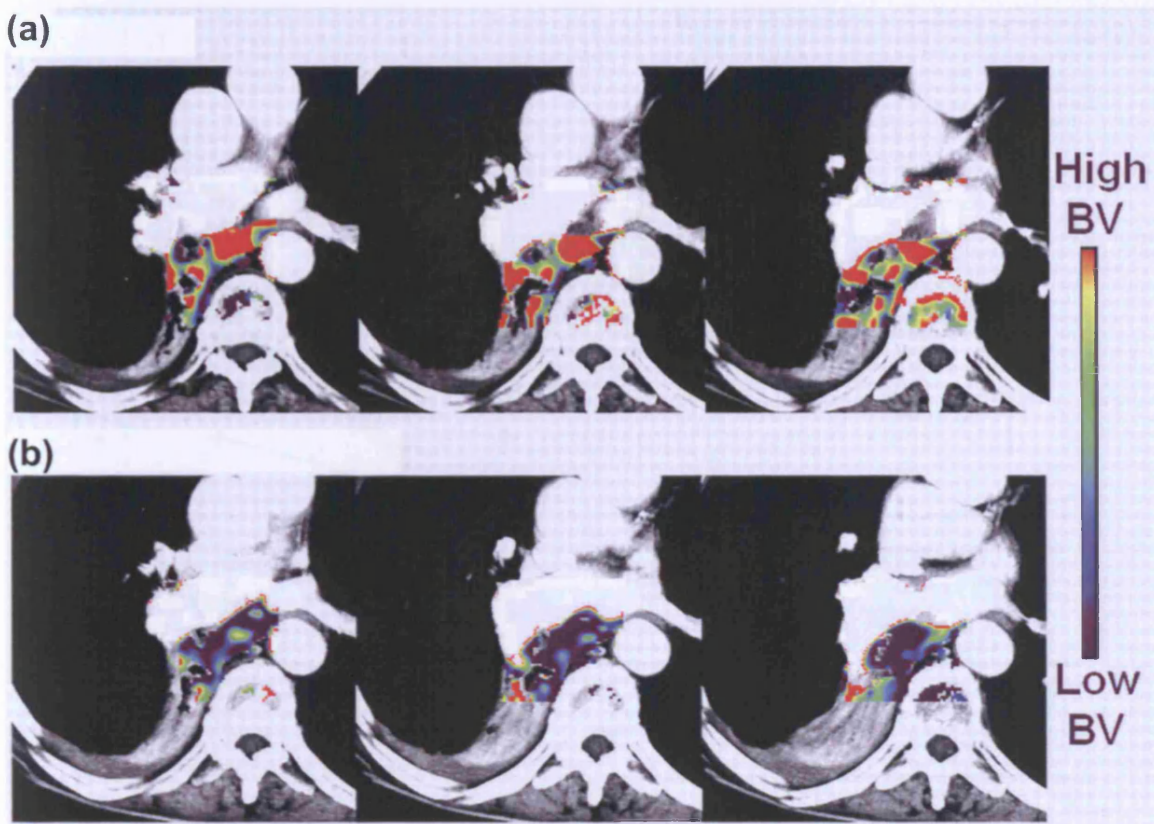
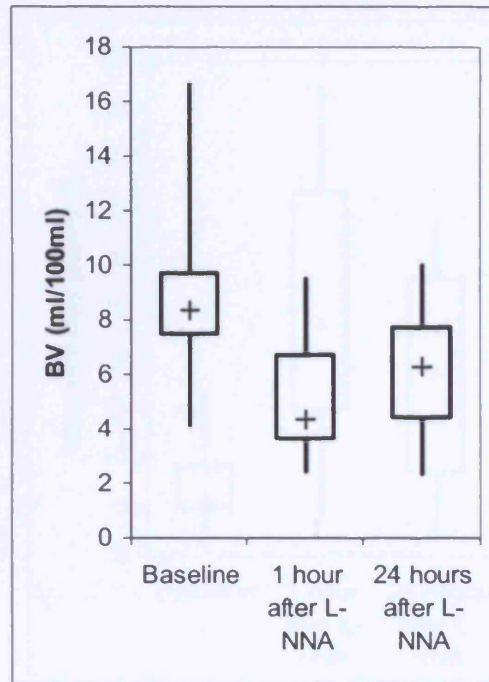
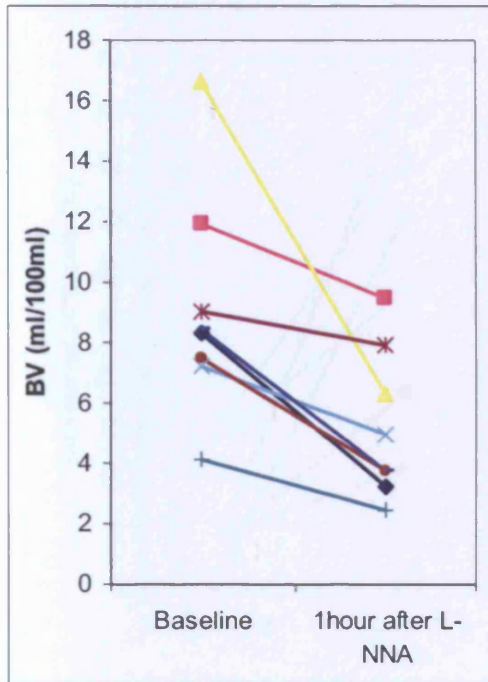
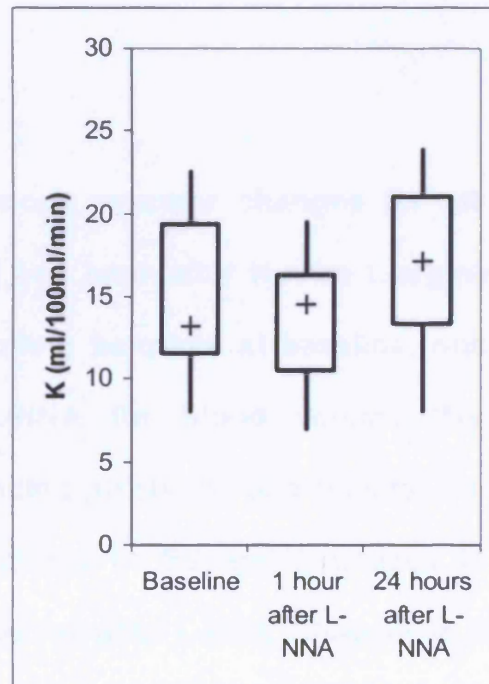
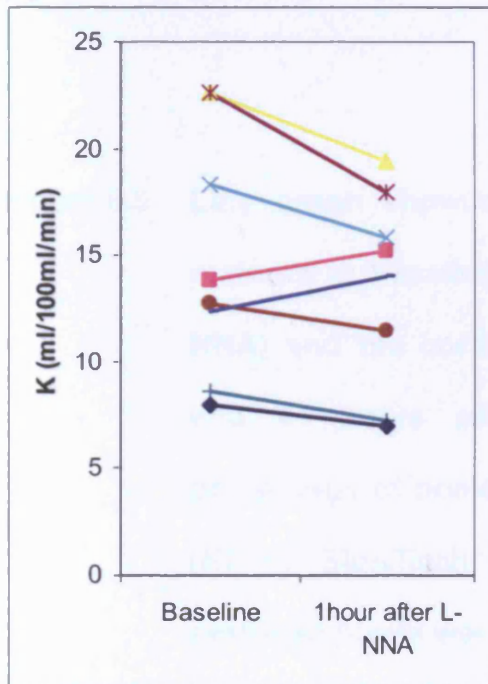


Figure 6.4 Coloured parametric maps of tumour blood volume (BV) representing three contiguous axial levels of a lung tumour before (a), and one hour after a single 0.5mg/kg infusion of N-nitro L-arginine (L-NNA) (b). Each pixel within the tumour map represents a single vascular parameter value; the colour scale indicates red pixels as high BV values and purple pixels as low BV values.

(a)



(b)



(c)

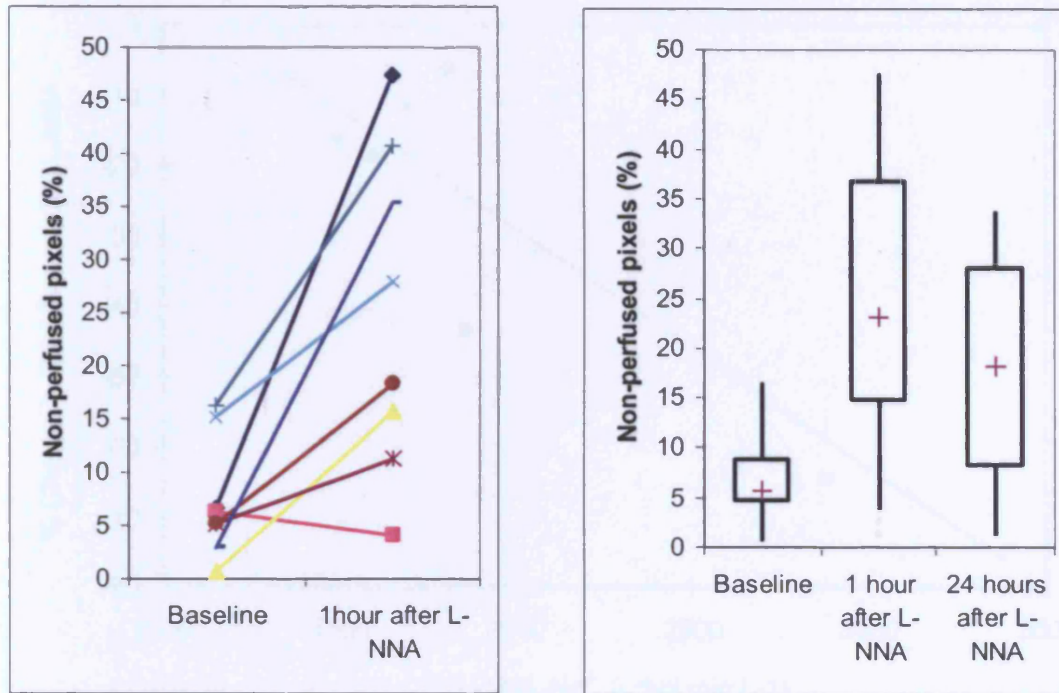


Figure 6.5. Relationship between plasma L-arginine (L-Arg) and L-nitro L-arginine (L-NNA) and

Figure 6.5 Line graph showing tumour vascular changes for all eight patients at baseline and one hour after N-nitro L-arginine (L-NNA) and the corresponding boxplots at baseline, one hour and 24 hours after L-NNA for blood volume (BV) (a), percentage of non-enhancing pixels (b), and transfer constant (K) (c). Significant reductions in BV and increases in non-perfused pixels were observed after L-NNA. Changes in K were not statistically significant.

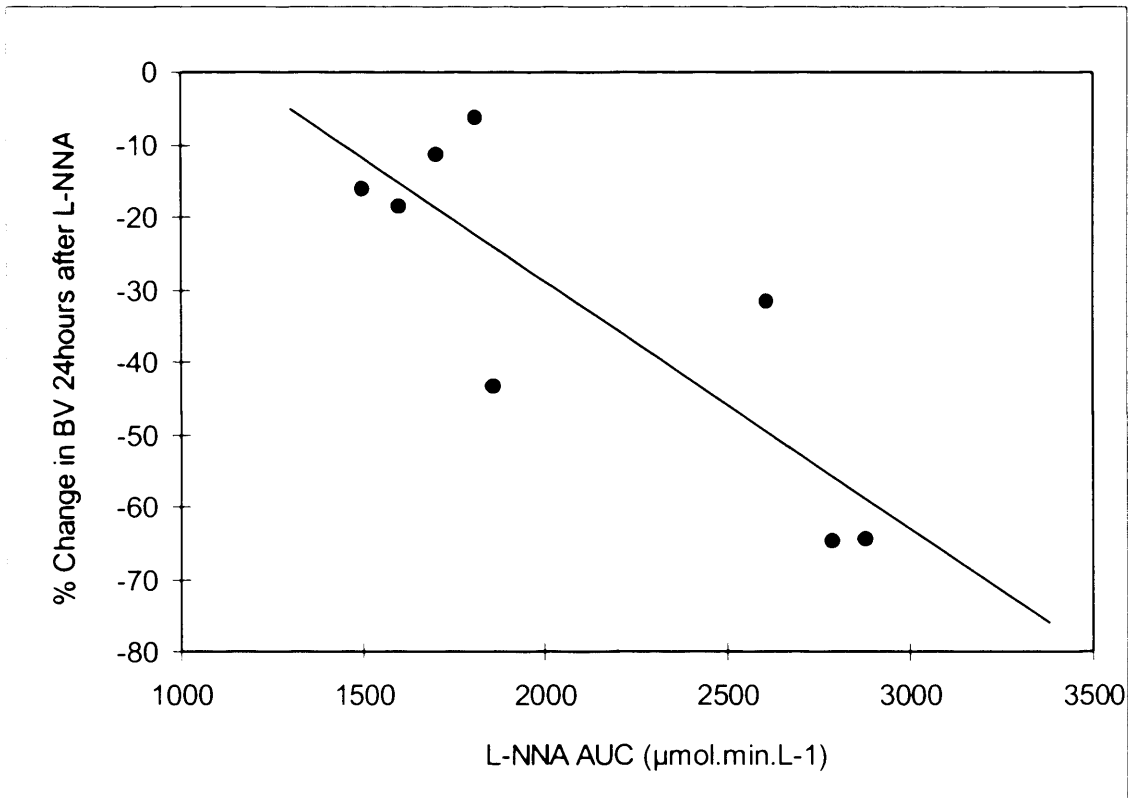


Figure 6.6 Relationship between plasma N-nitro L-arginine (L-NNA) area under the curve (AUC) and reduction in tumour blood volume (BV) at 24 hours after L-NNA.

6.5 Discussion

For the first time in man, the results from this study show that inhibition of NOS results in an acute reduction in tumour BV which is sustained to 24 hours. The sustained reduction in tumour vascular BV and the increase in the number of non-perfused pixels up to 24 hours following L-NNA are consistent with prolonged vascular shutdown, which has been shown to reduce tumour growth in animal models (Orucevic et al 1995, Camp et al 2006). This unexpected finding of sustained vascular shutdown could be due to endothelial cell damage and development of microthrombi resulting from platelet aggregation and leucocyte adhesion, both known effects of reduction in vascular NO (Kubes et al 1991, Moncada et al 1991). The observed correlation between increasing L-NNA plasma AUC and vascular shutdown observed at 24 hours is consistent with a dose effect, and not as a result of prolonged drug exposure. There was no correlation between vascular changes and half-life or clearance. Indeed, L-NNA has a terminal half-life of less than four hours, so the vascular changes seen at 24 hours reflect the consequence of events initiated by drug exposure. There was no correlation between L-NNA AUC and BV reduction at one hour suggesting that the acute BV reduction after L-NNA might not be dependent on amount of drug exposure.

NO increases tumour vascularisation through the process of angiogenesis and this has been found to correlate with increased tumour growth (Jenkins et al

1995). NO is the final mediator of angiogenesis stimulated by VEGF, the major factor implicated in angiogenesis of many human tumours (Ziche et al 1997, Veikkola et al 2000, Fukumara et al 2001). NO has been shown to mediate VEGF-induced permeability in tumour vessels, although its effects are variable. NOS inhibition has been shown to reduce vascular permeability to albumin in some experimental tumour models but not others (Fukumara et al 1997). In our study, tumour K reductions following L-NNA were not significant, which may be due to the heterogeneity of NOS expression. Our results also appear consistent with the tumour vascular response to the anti-angiogenic agent bevacizumab measured using perfusion CT, where significant changes in BV but not PS were reported (Willett et al 2004). The reason for this is unclear; it has been suggested that this might be due to the balance between a reduction in vascular surface area and decrease in blood volume against the effects of improved extravasation of contrast from normalised vasculature.

To date, clinical studies using inhibitors of NO have focused on its cardiovascular effects. In healthy human volunteers, the NOS inhibitor N-monomethyl L-arginine (L-NMMA) did not have an effect on blood pressure at doses under 3mg/kg (infused over 20 minutes). However at doses more than 1mg/kg (infused over one hour), there was a significant reduction in heart rate and cardiac index (Haynes et al 1993). In patients diagnosed with septic shock, 20mg/kg of L-NNA was shown to increase mean arterial blood pressure, associated with a decrease in cardiac index and oxygen delivery (Lorente et al 1993). It is noted that the

NOS inhibitors and doses used in these two human studies are different, and L-NNA has been shown to be more potent than L-NMMA (Alderton et al 2001). Both L-NNA and L-NMMA are non-selective inhibitors of the NOS isoforms, although L-NNA has a minor selectivity to eNOS compared to iNOS of just under ten-fold (Alderton et al 2001). The role of eNOS derived NO in promoting tumour angiogenesis and maintaining tumour blood flow is well studied and therefore the vascular changes seen here are likely to be dominated by the effects of eNOS inhibition. A more recent randomised trial using the non-selective NOS inhibitor 546C88 in patients with septic shock achieved adequate maintenance of mean blood pressure with a reduction in the requirement for conventional inotropic agents. However, recruitment into the study was discontinued because of increased mortality in the 546C88 arm (Watson et al 2004, Lopez et al 2004).

In BD9 rats bearing subcutaneous P22 carcinosarcoma, L-NNA, up to a dose of 1mg/kg, selectively reduced tumour blood flow, without any significant changes in heart rate or mean arterial blood pressure in the rat (Tozer et al 1997), suggesting that tumour vessels are more sensitive than normal vessels to NOS inhibition. The cardiovascular changes observed in our study are therefore consistent with previous studies of NO synthesis inhibition in both animals and humans, and are possibly the result of a homeostatic response to increase in vascular resistance caused by NOS inhibition. In this study, the significant reduction in tumour BV relative to the mild and self-limiting cardiovascular changes suggests a degree of selectivity to the effects of NOS inhibition in

tumour vessels. This might be because tumour vessel patency is particularly dependent on NO (Peterson 1991), and NOS is over-expressed in tumours, thus the inhibition of this potent vasodilator results in vascular collapse due to the immature tumour vascular walls and high interstitial fluid pressure (Boucher et al 1990). However, the cardiovascular system is subjected to tightly regulated homeostatic controls and cardiovascular changes are not the ideal marker to determine selectivity to NOS inhibition. CT can potentially be used to measure changes in BV and K in normal tissues, thus estimating the effects of L-NNA on the peripheral vascular system. Most of the patients in this study had lung tumours, and the most consistent normal tissue included in the scan plane was the erector spinae muscle. However, measurement repeatability for skeletal muscle measurements is quite variable, with coefficient of variation ranging from 27 to 70%, making it very difficult to assess vascular changes reliably (Goh et al 2006).

In summary, the results from this study have demonstrated that NO plays a role in maintaining tumour blood supply and that inhibition of NO synthesis results in a sustained reduction in tumour BV at doses that are well tolerated, providing early clinical evidence that NOS inhibition has tumour anti-vascular activity in cancer patients.

CHAPTER 7

CONCLUDING DISCUSSION

The arsenal in the treatment of cancer now includes chemotherapy, radiotherapy, immunotherapy, antibody, and gene therapy. With the recognition that growth of solid tumours is dependent on its blood supply, the last few years have seen an increase in the use of vascular targeting drugs in the clinic. A greater understanding of tumour vascular biology has led to the development of vascular disrupting agents that selectively destroy existing tumour vessels and anti-angiogenic agents that prevent new vessel formation. Many of these novel agents have shown enhancement of anti-tumour activity when combined with conventional treatment modalities such as radiation and cytotoxics. There is also evidence that radiotherapy and chemotherapy may exert their anti-tumour effects partially through damage to the tumour vasculature.

Functional imaging techniques, such as perfusion CT, are increasingly used to quantify the tumour vascularity *in vivo*. A significant limitation of perfusion CT as an *in vivo* clinical technique has been its inability to quantify vascular measurements for a large tumour volume without a significant radiation burden. It is well recognised that the tumour microcirculation is spatially heterogeneous. A conventional single level scanning technique that only assesses a limited tumour volume is unrepresentative of the tumour as a whole, and consequently, might be prone to measurement variability. As the aim of this research was to describe the

vascular changes after anti-cancer therapy in whole human tumours, we needed to develop a scanning technique that could encompass a large tumour volume and depict this spatial heterogeneity, yet be a straightforward and clinically repeatable technique. We were aided by developments in multi-detector CT technology enabling faster scanning with isotropic resolution, thus allowing us to encompass the entire tumour volume in such a manner to allow quantification of blood volume and vascular leakage.

We found that the measurements obtained provided a more accurate representation of the spatial heterogeneity of tumour vasculature. More importantly, this whole tumour technique improves on measurement repeatability when compared to conventional single level techniques, increasing confidence that any changes observed following therapy are real, and not simply due to the intrinsic variability of the tumour microcirculation. This improvement in repeatability reflects, to a certain extent, the care that was taken to minimise variability from technical aspects. Patients were educated carefully prior to each scan to ensure the breath-holding technique was optimal, the same senior radiographers performed each scan, and the scans were supervised by a consultant CT radiologist with experience of perfusion CT techniques to ensure proper patient positioning and adequate anatomical coverage. Also, the patients recruited onto this study had lung cancer, and suffered with varying degrees of dyspnoea. It is truly a credit to their helpfulness, resolve, and good humour that such reliable results were achieved.

Further developments are being carried out on the CT technique. The isotropic resolution of current multi-detector CT scanners allows vascular measurements to be obtained from sagittal and coronal imaging planes following reconstructions of the native axial CT images. For perfusion CT to be truly volumetric, vascular measurements should be consistent regardless of which plane the measurements are derived from, thus has the potential for the development of a true 3-dimensional vascular measurement technique. This CT technique has many potential applications in addition to therapeutic assessment. For example, this technique can potentially be integrated into sophisticated radiotherapy planning systems. Major advances in radiation therapy have resulted from improved imaging techniques that can define anatomical volumes more accurately. The introduction of intensity modulated radiotherapy where the dose is varied across the beam of radiotherapy enables different doses to be given to different parts of the volume at the same time. Therefore, varying radiation doses can be administered across the tumour volume depending on the biological characteristics within the tumour. Clinical trials are currently being conducted to assess whether biological information derived from functional imaging can assist in defining the tumour volume during radiotherapy planning, and ultimately, improve patient outcome (ClinicalTrials.gov identifier NCT00122252).

Radiotherapy has been shown to cause tumour vascular changes in human lung cancer. Fractionated radiotherapy increases tumour vascular leakage and blood

volume, especially at the tumour rim. A better understanding of the *in vivo* changes in tumour vascularity after ionising radiation is clinically relevant. The vascular effects of radiotherapy may influence radio-sensitivity of both tumours and normal tissues with potential implications for acute and late radiation side effects (Anscher et al 2005). Most radical radiotherapy is now given in combination with chemotherapy; novel radiation schedules are also being developed incorporating new agents such as monoclonal antibodies and vascular targeting drugs. The therapeutic success of these combinations is dependent on its scheduling (Glynne-Jones et al 2002, Zips et al 2003, Williams et al 2004), and a better understanding of the tumour vascular changes after radiotherapy may better guide the timing of both chemotherapy and other novel drugs.

The vascular disrupting agent CA4P selectively destroys the tumour vasculature by exploiting the morphological and functional differences between normal and tumour blood vessels. It is currently being studied in a phase 1 trial combined with radiotherapy. The results presented here have described the mechanistic vascular interaction between CA4P and radiation, and demonstrated potential enhancements of anti-vascular activity between the two treatments. CA4P when combined with radiotherapy causes a sustained reduction in tumour blood volume, which is in contrast to the partial recovery in perfusion and blood flow seen after single agent CA4P, and in contrast to the increase in blood volume seen after radiation alone. These initial findings provide the basis for further clinical studies using this novel combination. Currently, CA4P in combination with

radiotherapy is being offered to additional cohorts of patients with different tumour sites including prostate and head and neck cancers. Dose escalation will be carried out such that each subsequent cohort of patients will receive either a greater dose of CA4P, or radiation, or both. Functional imaging will continue to be used to evaluate the vascular responses after treatment, and it will be interesting to see if the higher doses and different tumour sites result in a greater enhancement of tumour anti-vascular activity.

For the first time in man, the NOS inhibitor L-NNA has been shown to cause a significant and sustained reduction in tumour vascular blood volume, providing clinical evidence that NO plays a role in maintaining tumour blood supply. Although there is probably limited potential in retarding tumour growth using NOS inhibitors alone, the sustained tumour vascular shutdown after just a single dose of L-NNA appear to show promise for its use as a novel vascular targeting agent. However, the biological role of NO in cancer remains unclear. Future studies incorporating direct measurements of NO biosynthesis and NOS activity will provide corroborating data on the potential of NOS inhibition as a vascular targeting anti-cancer agent. The effects of inhibitors of specific NOS isoforms as well as the potential for anti-angiogenic activity by NOS inhibition in man also remains to be fully evaluated.

There is pre-clinical evidence that NO exerts a protective effect on endothelial cells against CA4P, and combining CA4P with NOS inhibitors results in enhanced vascular disrupting activity and cytotoxicity, even in CA4P resistant tumour models (Parkins et al 2000, Davis et al 2002). There is clearly potential for combining CA4P with NOS inhibitors such as L-NNA, although care has to be taken to closely monitor the possible cardiovascular effects of this combination, and further pre-clinical studies are needed. The role of NO as a hypoxic cell radiosensitiser and as a mediator of chemosensitivity in tumour cells has also been previously discussed. Thus, further investigation into the use of NO, and NOS inhibitors as cancer therapeutics, and in combination with radiotherapy, chemotherapy, anti-angiogenic and vascular disrupting agents are warranted.

While this work has demonstrated that functional imaging can be used reliably to assess the tumour vasculature, further studies will be needed to show that tumour vascular changes observed after treatment with vascular targeting drugs correlate with clinical response in terms of survival or even with conventional response criteria in terms of tumour shrinkage. Such data will be useful in confirming the value of functional imaging in clinical practice, and more importantly, will allow one to define the level and duration of vascular change needed to improve clinical outcome after vascular targeting therapy.

In conclusion, the vascular effects of cancer treatment in whole tumours can be measured using a repeatable, non-invasive perfusion CT technique. The results presented here have provided further evidence that targeting the tumour vasculature is a promising approach to the treatment of cancer. These findings will hopefully expand our knowledge of tumour vascular biology, and stimulate the development of new therapeutic strategies for cancer.

APPENDIX 1

National Cancer Institute common toxicity criteria (CTC) version 2.0

Hypertension	
Grade 0	None
Grade 1	Asymptomatic, transient increase by >20mmHg (diastolic) or to >150/100 if previously within normal limits (WNL); not requiring treatment
Grade 2	Recurrent or persistent or symptomatic increase by >20mmHg (diastolic) or to >150/100 if previously WNL; not requiring treatment
Grade 3	Requiring therapy or more intensive therapy than previously
Grade 4	Hypertensive crisis

Palpitations	
Grade 0	None
Grade 1	Present
Grade 2	-
Grade 3	-
Grade 4	-

Sinus bradycardia	
Grade 0	None
Grade 1	asymptomatic, not requiring treatment
Grade 2	symptomatic, but not requiring treatment
Grade 3	symptomatic and requiring treatment
Grade 4	life-threatening (e.g. arrhythmia associated with congestive heart failure, hypotension, syncope, shock)

REFERENCES

Alderton WK, Cooper CE, Knowles RG (2001) Nitric oxide synthases: structure, function and inhibition. *Biochem J* 357:593-615.

Anderson HL, Yap JT, Miller MP, Robbins A, Jones T, Price PM (2003) Assessment of pharmacodynamic vascular response in a Phase I trial of Combretastatin A4 Phosphate. *J Clin Oncol* 1:2823-2830.

Ando S, Nojima K, Majima H, Ishihara H, Suzuki M, Furusawa Y, Yamaguchi H, Koike S, Ando K, Yamauchi M, Kuriyama T (1998) Evidence for mRNA expression of vascular endothelial growth factor by X-ray irradiation in a lung squamous carcinoma cell line. *Cancer Lett* 132:75-80.

Anscher MS, Chen L, Rabbani Z, Kang S, Larrier N, Huang H, Samulski TV, Dewhirst MW, Brizel DM, Folz RJ, Vujaskovic Z (2005) Recent progress in defining mechanisms and potential targets for prevention of normal tissue injury after radiation therapy. *Int J Radiat Oncol Biol Phys* 62:255-259.

Antoch G, Kanja J, Bauer S, Kuehl H, Renzing-Koehler K, Schuette J, Bockisch A, Debatin JF, Freudenberg LS (2004) Comparison of PET, CT, and dual-modality PET/CT imaging for monitoring of imatinib (STI571) therapy in patients with gastrointestinal stromal tumors. *J Nucl Med* 45:357-365.

Attard G, Greystoke A, Kaye S, De Bono J (2006) Update on tubulin-binding agents. *Pathol Biol (Paris)* 54:72-84.

Baguley BC (2003) Antivascular therapy of cancer: DMXAA. *Lancet Oncol*;4:141-148.

Baguley BC, Holdaway KM, Thomsen LL, Zhuang L, Zwi LJ (1991) Inhibition of growth of colon 38 adenocarcinoma by vinblastine and colchicine: evidence for a vascular mechanism. *Eur J Cancer* 27:482-487.

Baguley BC, Zhuang L, Kestell P (1997) Increased plasma serotonin following treatment with flavone-8-acetic acid, 5,6-dimethylxanthenone-4-acetic acid, vinblastine, and colchicine: relation to vascular effects. *Oncol Res* 9:55-60.

Baluk P, Morikawa S, Haskell A, Mancuso M, McDonald DM (2003) Abnormalities of basement membrane on blood vessels and endothelial sprouts in tumours. *Am. J. Pathol* 163:1801-1815

Beauregard DA, Hill SA, Chaplin DJ, Brindle KM (2001) The susceptibility of tumours to the antivascular drug combretastatin A4 phosphate correlates with vascular permeability. *Cancer Res* 61:6811-6815.

Beauregard DA, Thelwall PE, Chaplin DJ, Hill SA, Adams GE, Brindle KM (1998) Magnetic resonance imaging and spectroscopy of combretastatin A4 prodrug-induced disruption of tumour perfusion and energetic status. *Br J Cancer* 77:1761-1767.

Beerepoot LV, Radema SA, Witteveen EO, Thomas T, Wheeler C, Kempin S, Voest EE (2006) Phase I clinical evaluation of weekly administration of the novel vascular-targeting agent, ZD6126, in patients with solid tumours. *J Clin Oncol* 24:1491-1498.

Bilenker JH, Flaherty KT, Rosen M, Davis L, Gallagher M, Stevenson JP, Sun W, Vaughn D, Giantonio B, Zimmer R, Schnall M, O'Dwyer PJ (2005) Phase I trial of combretastatin a-4 phosphate with carboplatin. *Clin Cancer Res* 11:1527-1533.

Blakey DC, Westwood FR, Walker M, Hughes GD, Davis PD, Ashton SE, Ryan AJ (2002) Antitumour activity of the novel vascular targeting agent ZD6126 in a panel of tumour models. *Clin Cancer Res* 8:1974-1983.

Bland JM, Altman DG (1986) Statistical methods for assessing agreement between two methods of clinical measurement. *Lancet* 1:307-310.

Bonavida B, Khineche S, Huerta-Yepez S, Garban H (2006) Therapeutic potential of nitric oxide in cancer. *Drug Resist Updat* 9:157-173.

Boucher Y, Baxter LT, Jain RK (1990) Interstitial pressure gradients in tissue-isolated and subcutaneous tumours: implications for therapy. *Cancer Res* 50:4478-4484.

British Standards Institution. Precision of test methods, part 1: guide for the determination of repeatability and reproducibility for a standard test method. BS 5497, Part 1. London: BSI, 1979.

Buckley DL, Drew PJ, Mussurakis S, Monson JR, Horsman A (1997) Microvessel density of invasive breast cancer assessed by dynamic Gd-DTPA enhanced MRI. *J Magn Reson Imaging* 7:461-464.

Camp ER, Yang A, Liu W, Fan F, Somcio R, Hicklin DJ, Ellis LM (2006) Roles of nitric oxide synthase inhibition and vascular endothelial growth factor receptor-2 inhibition on vascular morphology and function in an in vivo model of pancreatic cancer. *Clin Cancer Res* 12:2628-2633.

Cao Z, Baguley BC, Ching L-M (2001) Interferon-inducible protein 10 induction and inhibition of angiogenesis in vivo by the antitumour agent 5,6-dimethylxanthenone-4-acetic acid (DMXAA). *Cancer Res* 61:1517-1521.

Cenic A, Nabavi DG, Craen RA, Gelb AW, Lee TY (1999) Dynamic CT measurement of cerebral blood flow: a validation study. *Am J Neuroradiol* 20:63-73.

Cenic A, Nabavi DG, Craen RA, Gelb AW, Lee TY (2000) A CT method to measure hemodynamics in brain tumors: validation and application of cerebral blood flow maps. *Am J Neuroradiol* 21:462-470.

Chaplin DJ, Hill SA (1995) Temporal heterogeneity in microregional erythrocyte flux in experimental solid tumors. *Br J Cancer* 71:1210-1213.

Chaplin DJ, Hill SA (2002) The development of combretastatin A4 phosphate as a vascular targeting agent. *Int J Radiat Oncol Biol Phys* 54:1491-1496.

Chaplin DJ, Pettit GR, Hill SA (1999) Anti-vascular approaches to solid tumour therapy: evaluation of combretastatin A4 phosphate. *Anticancer Res* 19:189-195.

Ching LM, Cao Z, Kieda C, Zwain S, Jameson MB, Baguley BC (2002) Induction of endothelial cell apoptosis by the antivascular agent 5,6-dimethylxanthenone-4-acetic acid. *Br J Cancer* 86:1937-1942.

Ching LM, Joseph WR, Crosier KE, Baguley BC (1994) Induction of tumour necrosis factor-alpha messenger RNA in human and murine cells by the flavone

acetic acid analogue 5,6-dimethylxanthenone-4-acetic acid (NSC 640488).
Cancer Res 54:870-872.

Cionini L, Bianco AR, Tortora G, Ciardiello F, Bunn P (2004) Antitumour activity of ZD6126, a novel vascular-targeting agent, is enhanced when combined with ZD1839, an epidermal growth factor receptor tyrosine kinase inhibitor, and potentiates the effects of radiation in a human non-small cell lung cancer xenograft model. Mol Cancer Ther 3:977-983.

Cliffe S, Taylor ML, Rutland M, Baguley BC, Hill RP, Wilson WR (1994) Combining bioreductive drugs (SR 4233 or SN 23862) with the vasoactive agents flavone acetic acid or 5,6-dimethylxanthenone acetic acid. Int J Radiat Oncol Biol Phys 29:373-377.

Cobbs CS, Brenman JE, Aldape KD, Bredt DS, Israel MA (1995) Expression of nitric oxide synthase in human central nervous system tumours. Cancer Res 55:727-730.

Cooney MM, Radivoyevitch T, Dowlati A, Overmoyer B, Levitan N, Robertson K, Levine SL, DeCaro K, Buchter C, Taylor A, Stambler BS, Remick SC (2004) Cardiovascular safety profile of combretastatin a4 phosphate in a single-dose phase I study in patients with advanced cancer. Clin Cancer Res 10:96-100.

Corbett TH, Bissery MC, Wozniak A, Plowman J, Polin L, Tapazoglou E, Dieckman J, Valeriote F (1986) Activity of flavone acetic acid (NSC-347512) against solid tumours of mice. *Invest New Drugs* 4:207-220.

ClinicalTrials.gov identifier NCT00122252: Biological imaging for optimising clinical target volume (CTV) and gross tumour volume (GTV) contouring in prostate cancer to improve the possibilities for intensity modulated radiotherapy (IMRT) dose escalation.

Crocart N, Jordan BF, Baudelet C, Ansiaux R, Sonveaux P, Gregoire V, Beghein N, DeWever J, Bouzin C, Feron O, Gallez B (2005) Early reoxygenation in tumors after irradiation: determining factors and consequences for radiotherapy regimens using daily multiple fractions. *Int J Radiat Oncol Biol Phys* 63:901-910.

Crone C (1963) The permeability of capillaries in various organs as determined by use of the 'indicator diffusion' method. *Acta Physio Scand* 58:292-305

Dark GG, Hill SA, Prise VE, Tozer GM, Pettit GR, Chaplin DJ (1997) Combretastatin A-4, an agent that displays potent and selective toxicity toward tumor vasculature. *Cancer Res* 57:1829-1834.

Davis PD, Tozer GM, Naylor MA, Thomson P, Lewis G, Hill SA (2002) Enhancement of vascular targeting by inhibitors of nitric oxide synthase. *Int J Radiat Oncol Biol Phys* 54:1532-1536.

Dawson P and Peters M (1993) Dynamic contrast bolus computed tomography for the assessment of renal function. *Invest Radiol* 28:1039-1042.

Dawson P (2006) Functional imaging in CT. *Eur J Radiol* doi:10.1016/j.ejrad.2006.06.023

de Vries A, Griebel J, Kremser C, Judmaier W, Gneiting T, Debbage P, Kremser T, Pfeiffer KP, Buchberger W, Lukas P (2000) Monitoring of tumor microcirculation during fractionated radiation therapy in patients with rectal carcinoma: preliminary results and implications for therapy. *Radiology* 217:385-391.

Dehdashti F, Mintun MA, Lewis JS, Bradley J, Govindan R, Laforest R, Welch MJ, Siegel BA (2003) In vivo assessment of tumor hypoxia in lung cancer with ⁶⁰Cu-ATSM. *Eur J Nucl Med Mol Imaging* 30:844-850.

Denekamp J (1982) Endothelial cell proliferation as a novel approach to targeting tumour therapy. *Br J Cancer* 45:136-139.

Denekamp J (1984) Vascular endothelium as the vulnerable element in tumours. *Acta Radiol Oncol* 23:217-225.

Dugdale PE, Miles KA, Kelley BB, Bunce IH, Leggett DAC (1999) CT measurements of perfusion and permeability within lymphoma masses: Relationship to grade, activity and chemotherapeutic response. *J Comput Tomogr* 23:540-547.

Dvorak HF, Nagy JA, Dvorak AM (1991) Structure of solid tumours and their vasculature: implications for therapy with monoclonal antibodies. *Cancer Cells* 3:77-85

Eberhard A, Kahlert S, Goede V, Hemmerlein B, Plate KH, Augustin HG (2000) Heterogeneity of angiogenesis and blood vessel maturation in human tumours: implications for antiangiogenic tumour therapies. *Cancer Res* 60:1388-1393. Erratum in: *Cancer Res* 2000;60:3668.

Endrich B, Reinhold HS, Gross JF, Intaglietta M (1979) Tissue perfusion inhomogeneity during early tumor growth in rats. *J Natl Cancer Inst* 62:387-395.

Evelhoch JL, LoRusso PM, He Z, DelProposto Z, Polin L, Corbett TH, Langmuir P, Wheeler C, Stone A, Leadbetter J, Ryan AJ, Blakey DC, Waterton JC (2004) Magnetic resonance imaging measurements of the response of murine and

human tumours to the vascular-targeting agent ZD6126. *Clin Cancer Res* 10:3650-3657.

Fiorella D, Heiserman J, Prenger E, Partovi S (2004) Assessment of the reproducibility of postprocessing dynamic CT perfusion data. *AJNR Am J Neuroradiol* 25:97-107.

Folkman J (1971) Tumour angiogenesis: therapeutic implications. *N Engl J Med* 285:1182-1186.

Folkman J (1992) The role of angiogenesis in tumour growth. *Semin Cancer Biol* 3:65-71.

Folkman J, Merler E, Abernathy C, Williams G (1971) Isolation of a tumour factor responsible for angiogenesis. *J Exp Med* 133:275-288.

Ford J, Miles K, Hayball M, Bearcroft P, Bleehan N, Osborn C (1996) A simplified method for measurement of blood-brain barrier permeability using CT: Preliminary results and the effect of RMP-7. In: K. Faulkner, et al., eds. *Quantitative imaging in Oncology*, British Institute of Radiology: London 1-5.

Frederiksen LJ, Siemens DR, Heaton JP, Maxwell LR, Adams MA, Graham CH (2003) Hypoxia induced resistance to doxorubicin in prostate cancer cells is inhibited by low concentrations of glyceryl trinitrate. *J Urol* 170:1003-1007.

Fujimoto H, Ando Y, Yamashita T, Terazaki H, Tanaka Y, Sasaki J, Matsumoto M, Suga M, Ando M (1997) Nitric oxide synthase activity in human lung cancer. *Jpn J Cancer Res* 88:1190-1198.

Fukumura D, Gohongi T, Kadambi A, Izumi Y, Ang J, Yun CO, Buerk DG, Huang PL, Jain RK (2001) Predominant role of endothelial nitric oxide synthase in vascular endothelial growth factor-induced angiogenesis and vascular permeability. *Proc Natl Acad Sci USA* 98:2604-2609.

Fukumura D, Gohongi T, Kadambi A, Izumi Y, Ang J, Yun CO, Buerk DG, Huang PL, Jain RK (2001) Predominant role of endothelial nitric oxide synthase in vascular endothelial growth factor-induced angiogenesis and vascular permeability. *Proc Natl Acad Sci USA* 98:2604-2609.

Fukumura D, Kashiwagi S, Jain RK (2006) The role of nitric oxide in tumor progression. *Nat Rev Cancer* 6:521-534.

Fukumura D, Yuan F, Endo M, Jain RK (1997) Role of nitric oxide in tumor microcirculation. Blood flow, vascular permeability, and leukocyte-endothelial interactions. *Am J Pathol* 150:713-725.

Furchgott RF, Zawadzki JV (1980) The obligatory role of endothelial cells in the relaxation of arterial smooth muscle by acetylcholine. *Nature* 288:373-376.

Gabra H; AS1404-202 Study Group Investigators (2006) Phase II study of DMXAA combined with carboplatin and paclitaxel in recurrent ovarian cancer. *American Society of Clinical Oncology Annual Meeting Proceedings* 24:5032.

Gadgeel SM, LoRusso PM, Wozniak AJ, Wheeler C (2002) A dose-escalation study of the novel vascular-targeting agent, ZD6126, in patients with solid tumours. *American Society of Clinical Oncology Annual Meeting Proceedings* 21:438.

Galbraith SM, Chaplin DJ, Lee F, Stratford MR, Locke RJ, Vojnovic B, Tozer GM (2001) Effects of combretastatin A4 phosphate on endothelial cell morphology in vitro and relationship to tumor vascular targeting activity in vivo. *Anticancer Res* 21:93-102.

Galbraith SM, Lodge MA, Taylor NJ, Rustin GJ, Bentzen S, Stirling JJ, Padhani AR (2002) Reproducibility of dynamic contrast-enhanced MRI in human muscle

and tumors: comparison of quantitative and semi-quantitative analysis. *NMR in Biomed* 15:132-142.

Galbraith SM, Maxwell RJ, Lodge MA, Tozer GM, Wilson J, Taylor NJ, Stirling JJ, Sena L, Padhani AR, Rustin GJ (2003) Combretastatin A4 Phosphate has tumour antivasular activity in rat and man as demonstrated by dynamic magnetic resonance imaging. *J Clin Oncol* 21:2831-2842.

Galbraith SM, Rustin GJ, Lodge MA, Taylor NJ, Stirling JJ, Jameson M, Thompson P, Hough D, Gumbrell L, Padhani AR (2002) Effects of 5,6-dimethylxanthenone-4-acetic acid on human tumour microcirculation assessed by dynamic contrast-enhanced magnetic resonance imaging. *J Clin Oncol* 20:3826-3840

Gallo O, Masini E, Morbidelli L, Franchi A, Fini-Storchi I, Vergari WA, Ziche M (1998) Role of nitric oxide in angiogenesis and tumour progression in head and neck cancer. *J Natl Cancer Inst* 90:587-596.

Gandhi D, Chepeha DB, Miller T, Carlos RC, Bradford CR, Karamchandani R, Worden F, Eisbruch A, Teknos TN, Wolf GT, Mukherji SK (2006) Correlation between initial and early follow-up CT perfusion parameters with endoscopic tumor response in patients with advanced squamous cell carcinomas of the

oropharynx treated with organ-preservation therapy. *AJNR Am J Neuroradiol* 27:101-106.

Garcia-Barros M, Paris F, Cordon-Cardo C, Lyden D, Rafii S, Haimovitz-Friedman A, Fuks Z, Kolesnick R (2003) Tumor response to radiotherapy regulated by endothelial cell apoptosis. *Science* 300:1155-1159.

Gerhardt H, Betsholtz C (2003) Endothelial-pericyte interactions in angiogenesis. *Cell Tissue Res* 314:15-23.

Gillard JH, Minhas PS, Hayball MP, Bearcroft PW, Antoun NM, Freer CE, Mathews JC, Miles KA, Pickard JD (2000) Assessment of quantitative computed tomographic cerebral perfusion imaging with H₂(¹⁵O) positron emission tomography. *Neurol Res* 22:457-464.

Glynne-Jones R, Sebag-Montefiore D (2002) Chemoradiation schedules - what radiotherapy? *Eur J Cancer* 38:258-269

Gobbel GT, Cann CE, Fike JR (1993) Comparison of xenon-enhanced CT with ultrafast CT for measurement of regional cerebral blood flow. *Am J Neuroradiol* 14:543-550.

Gobbel GT, Cann CE, Iwamoto HS, Fike JR (1991) Measurement of regional cerebral blood flow in dog using ultrafast computed tomography: Experimental validation. *Stroke* 22:772-779.

Goh V, Halligan S, Hugill JA, Bassett P, Bartram CI (2005) Quantitative assessment of colorectal perfusion using MDCT: inter- and intra observer agreement. *AJR Am J Roentgenol* 185:225-231.

Goh V, Halligan S, Hugill JA, Bartram CI (2006) Quantitative assessment of tissue perfusion using MDCT: comparison of colorectal cancer and skeletal muscle measurement reproducibility. *AJR Am J Roentgenol* 187:164-169.

Griffin RJ, Makepeace CM, Hur WJ, Song CW (1996) Radiosensitization of hypoxic tumor cells in vitro by nitric oxide. *Int J Radiat Oncol Biol Phys* 36:377-383.

Grosios K, Loadman PM, Swaine DJ, Pettit GR, Bibby MC (2000) Combination chemotherapy with combretastatin A-4 phosphate and 5-fluorouracil in an experimental murine colon adenocarcinoma. *Anticancer Res* 20:229-233.

Hanahan D, Folkman J (1996) Patterns and emerging mechanisms of the angiogenic switch during tumourigenesis. *Cell* 86:353-364.

Harvey C, Dooher A, Morgan J, Blomley M, Dawson P (1999) Imaging of tumour therapy responses by dynamic CT. *Eur J Radiol* 30:221-226.

Hashizume H, Baluk P, Morikawa S, McLean JW, Thurston G, Roberge S, Jain RK, McDonald DM (2000) Openings between defective endothelial cells explain tumour vessel leakiness. *Am J Pathol* 156:1363-1380.

Havlin KA, Kuhn JG, Craig JB, Boldt DH, Weiss GR, Koeller J, Harman G, Schwartz R, Clark GN, Von Hoff DD (1991) Phase I clinical and pharmacokinetic trial of flavone acetic acid. *J Natl Cancer Inst* 83:124-128.

Hawighorst H, Knapstein PG, Weikel W, Knopp MV, Zuna I, Knof A, Brix G, Schaeffer U, Wilkens C, Schoenberg SO, Essig M, Vaupel P, van Kaick G (1997) Angiogenesis of uterine cervical carcinoma: characterization by pharmacokinetic magnetic resonance parameters and histological microvessel density with correlation to lymphatic involvement. *Cancer Res* 57:4777-4786.

Haynes WG, Noon JP, Walker BR, Webb DJ (1993) Inhibition of nitric oxide synthesis increases blood pressure in healthy humans. *J Hypertens* 11:1375-1380.

Herbst RS, Onn A, Sandler A (2005) Angiogenesis and lung cancer: prognostic and therapeutic implications. *J Clin Oncol* 23:3243-3256.

Hill SA, Lonergan SJ, Denekamp J, Chaplin DJ (1993) Vinca alkaloids: anti-vascular effects in a murine tumour. *Eur J Cancer* 29A:1320-134.

Hill SA, Lonergan SJ, Denekamp J, Chaplin DJ (1994) The effect of vinca alkaloids on tumour blood flow. *Adv Exp Med Biol* 345:417-422.

Hill SA, Toze GM, Pettit GR, Chaplin DJ (2002) Preclinical evaluation of the antitumour activity of the novel vascular targeting agent Oxi 4503. *Anticancer Res* 22:1453-1458.

Hodivala-Dilke KM, Reynolds AR, Reynolds LE (2003) Integrins in angiogenesis: multitasking molecules in a balancing act. *Cell Tissue Res* 314:131-144.

Hori K, Saito S (2003) Microvascular mechanisms by which the combretastatin A-4 derivative AC7700 (AVE8062) induces tumour blood flow stasis. *Br J Cancer* 89:1334-1344.

Hori K, Saito S, Kubota K (2002) A novel combretastatin A-4 derivative, AC7700, strongly stanches tumour blood flow and inhibits growth of tumours developing in various tissues and organs. *Br J Cancer* 86:1604-1614.

Hori K, Saito S, Nihei Y, Suzuki M, Sato Y (1999) Antitumour effects due to irreversible stoppage of tumour tissue blood flow: evaluation of a novel combretastatin A-4 derivative, AC7700. *Jpn J Cancer Res* 90:1026-1038.

Horsman MR, Ehrnrooth E, Ladekarl M, Overgaard J (1998) The effect of combretastatin A-4 disodium phosphate in a C3H mouse mammary carcinoma and a variety of murine spontaneous tumors. *Int J Radiat Oncol Biol Phys* 42:895-898.

Horsman MR, Murata R (2002) Combination of vascular targeting agents with thermal or radiation therapy. *Int J Radiat Oncol Biol Phys* 54:1518-1523.

Horsman MR, Murata R (2003) Vascular targeting effects of ZD6126 in a C3H mouse mammary carcinoma and the enhancement of radiation response. *Int J Radiat Oncol Biol Phys* 57:1047-1055.

Hua J, Sheng Y, Pinney KG, Garner CM, Kane RR, Prezioso JA, Pettit GR, Chaplin DJ, Edvardsen K (2003) Oxi4503, a novel vascular targeting agent: effects on blood flow and antitumour activity in comparison to combretastatin A-4 phosphate. *Anticancer Res* 23:1433-1440.

Hurwitz H, Fehrenbacher L, Novotny W, Cartwright T, Hainsworth J, Heim W, Berlin J, Baron A, Griffing S, Holmgren E, Ferrara N, Fyfe G, Rogers B, Ross R,

Kabbinavar F (2004) Bevacizumab plus irinotecan, fluorouracil, and leucovorin for metastatic colorectal cancer. *N Engl J Med* 350:2335-2342.

Jain RK (1987) Transport of molecules across tumour vasculature. *Cancer Metastasis Rev* 6:559-593.

Jameson MB, Thompson PI, Baguley BC, Evans BD, Harvey VJ, Porter DJ, McCrystal MR, Small M, Bellenger K, Gumbrell L, Halbert GW, Kestell P; Phase I/II Trials Committee of Cancer Research UK (2003) Clinical aspects of a phase I trial of 5,6-dimethylxanthenone-4-acetic acid (DMXAA), a novel antivasculature agent. *Br J Cancer* 88:1844-1850.

Janssens MY, Van den Berge DL, Verovski VN, Monsaert C, Storme GA (1998) Activation of inducible nitric oxide synthase results in nitric oxide-mediated radiosensitization of hypoxic EMT-6 tumor cells. *Cancer Res* 58:5646-5648.

Jemal A, Murray T, Ward E, Samuels A, Tiwari RC, Ghafoor A, Feuer EJ, Thun MJ (2005) Cancer statistics, 2005. *CA Cancer J Clin* 55:10-30. Erratum in: *CA Cancer J Clin* 55:259.

Jenkins DC, Charles IG, Thomsen LL, Moss DW, Holmes LS, Baylis SA, Rhodes P, Westmore K, Emson PC, Moncada S (1995) Roles of nitric oxide in tumor growth. *Proc Natl Acad Sci USA* 92:4392-4396.

Jinzaki M, Tanimoto A, Mukai M, Ikeda E, Kobayashi S, Yuasa Y, Narimatsu Y, Murai M (2000) Double phase helical CT of small renal parenchymal neoplasms: correlation with pathologic findings and tumor angiogenesis. *J Comput Assist Tomogr* 24:835-842.

Kanthou C, Tozer GM (2002) The tumor vascular targeting agent combretastatin A-4-phosphate induces reorganization of the actin cytoskeleton and early membrane blebbing in human endothelial cells. *Blood* 99:2060-2066.

Kanthou C, Gabrys D and Tozer G (2005) Effects of the vascular disrupting agent combretastatin A-4-phosphate and radiation on the endothelial cytoskeleton and on endothelial monolayer permeability. *American Association of Cancer Research Annual Meeting Proceedings* 46:3419.

Karin M, Ben-Neriah Y (2000) Phosphorylation meets ubiquitination: the control of NF-kappa B activity. *Annu Rev Immunol* 18:621-663.

Kawasaki K, Smith RS Jr, Hsieh CM, Sun J, Chao J, Liao JK (2003) Activation of the phosphatidylinositol 3-kinase/protein kinase Akt pathway mediates nitric oxide-induced endothelial cell migration and angiogenesis. *Mol Cell Biol* 23:5726-5737.

Kaye SB, Clavel M, Dodion P, Monfardini S, ten Bokkel-Huinink W, Wagener DT, Gundersen S, Stoter G, Smith J, Renard J, et al (1990) Phase II trials with flavone acetic acid (NCS. 347512, LM975) in patients with advanced carcinoma of the breast, colon, head and neck and melanoma. *Invest New Drugs* 8:S95-99.

Kerbel R, Folkman J (2002) Clinical translation of angiogenesis inhibitors. *Nat Rev Cancer* 2:727-739.

Kerr DJ, Kaye SB (1989) Flavone acetic acid d preclinical and clinical activity. *Eur J Cancer Clin Oncol* 25:1271-1272.

Kerr DJ, Kaye SB, Cassidy J, Bradley C, Rankin EM, Adams L, Setanoians A, Young T, Forrest G, Soukop M, et al (1987) Phase I and pharmacokinetic study of flavone acetic acid. *Cancer Res* 47:6776-6781.

Kerr DJ, Maughan T, Newlands E, Rustin G, Bleehen NM, Lewis C, Kaye SB (1989) Phase II trials of flavone acetic acid in advanced malignant melanoma and colorectal carcinoma. *Br J Cancer* 60:104-106.

Kiessling F, Boese J, Corvinus C, Ederle JR, Zuna I, Schoenberg SO, Brix G, Schmahl A, Tuengerthal S, Herth F, Kauczor HU, Essig M (2004) Perfusion CT in patients with advanced bronchial carcinomas: a novel chance for characterization and treatment monitoring? *Eur Radiol* 14:1226-1233.

Kimura H, Braun RD, Ong ET, Hsu R, Secomb TW, Papahadjopoulos D, Hong K, Dewhirst MW (1996) Fluctuations in red cell flux in tumor microvessels can lead to transient hypoxia and reoxygenation in tumor parenchyma. *Cancer Res* 56:5522-5528.

Klotz T, Bloch W, Volberg C, et al: Selective expression of inducible nitric oxide synthase in human prostate carcinoma. *Cancer*;2:2897-1903,1998.

Kubes P, Suzuki M, Granger DN (1991) Nitric oxide: an endogenous modulator of leukocyte adhesion. *Proc Natl Acad Sci USA* 88:4651-4655.

Krause BJ, Beck R, Souvatzoglou M, Piert M (2006) PET and PET/CT studies of tumor tissue oxygenation. *Q J Nucl Med Mol Imaging* 50:28-43.

Laking GR, Price PM (2003) Positron emission tomographic imaging of angiogenesis and vascular function. *Br J Radiol* 76:S50-59.

Laking GR, West C, Buckley DL, Matthews J, Price PM (2006) Imaging vascular physiology to monitor cancer treatment. *Crit Rev Oncol Hematol* 58:95-113.

Lala PK, Chakraborty C (2001) Role of nitric oxide in carcinogenesis and tumor progression. *Lancet Oncol* 3:149-156.

Landuyt W, Ahmed B, Nuyts S, Theys J, Op de Beeck M, Rijnders A, Anne J, van Oosterom A, van den Bogaert W, Lambin P (2001) In vivo antitumour effect of vascular targeting combined with either ionizing radiation or anti-angiogenesis treatment. *Int J Radiat Oncol Biol Phys* 49:443-450.

Lash CJ, Li AE, Rutland M, Baguley BC, Zwi LJ, Wilson WR (1998) Enhancement of the anti-tumour effects of the antivascular agent 5,6-dimethylxanthenone-4-acetic acid (DMXAA) by combination with 5-hydroxytryptamine and bioreductive drugs. *Br J Cancer* 78:439-445.

Li L, Rojiani A, Siemann DW (1998) Targeting the tumor vasculature with combretastatin A-4 disodium phosphate: effects on radiation therapy. *Int J Radiat Oncol Biol Phys* 42:899-903.

Li L, Rojiani AM, Siemann DW (2002) Preclinical evaluations of therapies combining the vascular targeting agent combretastatin A-4 disodium phosphate and conventional anticancer therapies in the treatment of Kaposi's sarcoma. *Acta Oncol* 41:91-97.

Li S, Peck-Radosavljevic M, Koller E, Koller F, Kaserer K, Kreil A, Kapiotis S, Hamwi A, Weich HA, Valent P, Angelberger P, Dudczak R, Virgolini I (2001) Characterization of (123)I-vascular endothelial growth factor-binding sites

expressed on human tumour cells: possible implication for tumour scintigraphy. *Int J Cancer* 91:789-796.

Lopez A, Lorente JA, Steingrub J, Bakker J, McLuckie A, Willatts S, Brockway M, Anzueto A, Holzapfel L, Breen D, Silverman MS, Takala J, Donaldson J, Arneson C, Grove G, Grossman S, Grover R (2004) Multiple-center, randomized, placebo-controlled, double-blind study of the nitric oxide synthase inhibitor 546C88: effect on survival in patients with septic shock. *Crit Care Med* 32:21-30.

Lorente JA, Landin L, De Pablo R, Renes E, Liste D (1993) L-arginine pathway in the sepsis syndrome. *Crit Care Med* 21:1287-1295.

Ludford RJ (1945) Colchicine in the experimental chemotherapy of cancer. *J Natl Cancer Inst* 6:89-101.

Ludford RJ (1948) Factors determining the action of colchicine on tumour growth. *Br J Cancer* 2:75-86.

Lund EL, Hog A, Olsen MW, Hansen LT, Engelholm SA, Kristjansen PE (2004) Differential regulation of VEGF, HIF1alpha and angiopoietin-1, -2 and -4 by hypoxia and ionizing radiation in human glioblastoma. *Int J Cancer* 108:833-838.

Matthews NE, Adams MA, Maxwell LR, Gofton TE, Graham CH (2001) Nitric oxide-mediated regulation of chemosensitivity in cancer cells. *J Natl Cancer Inst* 93:1879-1885.

McIntyre DJ, Robinson SP, Howe FA, Griffiths JR, Ryan AJ, Blakey DC, Peers IS, Waterton JC (2004) Single dose of the antivascular agent, ZD6126 (N-acetylcolchicol-O-phosphate), reduces perfusion for at least 96 hours in the GH3 prolactinoma rat tumor model. *Neoplasia* 6:150-157.

McKeage M; AS1404-201 Study Group Investigators (2006) Phase Ib/II study of DMXAA combined with carboplatin and paclitaxel in non-small cell lung cancer (NSCLC). *American Society of Clinical Oncology Annual Meeting Proceedings* 24:7102.

McKeage MJ, Fong P, Jeffery M, Baguley BC, Kestell P, Ravic M, Jameson MB (2006) 5,6-Dimethylxanthenone-4-acetic acid in the treatment of refractory tumours: a phase I safety study of a vascular disrupting agent. *Clin Cancer Res* 12:1776-1784.

McPhail LD, McIntyre DJ, Ludwig C, Kestell P, Griffiths JR, Kelland LR, Robinson SP (2006) Rat tumour response to the vascular-disrupting agent 5,6-dimethylxanthenone-4-acetic acid as measured by dynamic contrast-enhanced

magnetic resonance imaging, plasma 5-hydroxyindoleacetic acid levels, and tumour necrosis. *Neoplasia* 8:199-206.

Miles KA (2003) Perfusion CT for the assessment of tumour vascularity: which protocol? *Br J Radiol* 76:S36-42.

Miles KA, Griffiths MR, Fuentes MA (2001) Standardized perfusion value: universal CT contrast enhancement scale that correlates with FDG-PET in lung nodules. *Radiology* 220:548-553.

Miles KA, Leggett DA, Bennett GA (1999) CT derived Patlak images of the human kidney. *Br J Radiol* 72:153-158.

Miller KD, Sweeney CJ, Sledge GW Jr (2001) Redefining the target: chemotherapeutics as antiangiogenics. *J Clin Oncol* 19:1195-1206.

Mitchell JB, Wink DA, DeGraff W, Gamson J, Keefer LK, Krishna MC (1993) Hypoxic mammalian cell radiosensitization by nitric oxide. *Cancer Res* 53:5845-5848.

Moeller BJ, Cao Y, Li CY, Dewhirst MW (2004) Radiation activates HIF-1 to regulate vascular radiosensitivity in tumors: role of reoxygenation, free radicals, and stress granules. *Cancer Cell* 5:429-441.

Moncada S, Palmer RM, Higgs EA (1989) Biosynthesis of nitric oxide from L-arginine. A pathway for the regulation of cell function and communication. *Biochem Pharmacol* 38:1709-1715.

Moncada S, Palmer RM, Higgs EA (1991) Nitric oxide: physiology, pathophysiology, and pharmacology. *Pharmacol Rev* 43:109-142.

Muir CP, Adams MA, Graham CH (2006) Nitric oxide attenuates resistance to doxorubicin in three-dimensional aggregates of human breast carcinoma cells. *Breast Cancer Res Treat* 96:169-176.

Murata R, Overgaard J, Horsman MR (2001) Comparative effects of combretastatin A-4 disodium phosphate and 5,6-dimethylxanthenone-4-acetic acid on blood perfusion in a murine tumour and normal tissues. *Int J Radiat Biol* 77:195-204.

Murata R, Siemann DW, Overgaard J, Horsman MR (2001) Interaction between combretastatin A-4 disodium phosphate and radiation in murine tumors. *Radiother Oncol* 60:155-161.

Nabavi DG, Cenic A, Dool J, Smith RM, Espinosa F, Craen RA, Gelb AW, Lee TY (1999) Quantitative assessment of cerebral hemodynamics using CT: stability, accuracy, and precision studies in dogs. *J Comput Assist Tomogr* 23:506-515.

Nelkin BD, Ball DW (2001) Combretastatin A-4 and doxorubicin combination treatment is effective in a preclinical model of human medullary thyroid carcinoma. *Oncol Rep* 8:157-160.

Ng QS, Carnell D, Milner D, Meer K, Saunders MI, Hoskin PJ (2005) Phase Ib trial of Combretastatin A4 Phosphate (CA4P) in combination with radiotherapy (RT): Initial clinical results. *American Society of Clinical Oncology Annual Meeting Proceedings* 23:3117.

Orucevic A, Lala PK (1996) NG-nitro-L-arginine methyl ester, an inhibitor of nitric oxide synthesis, ameliorates interleukin 2-induced capillary leakage and reduces tumor growth in adenocarcinoma-bearing mice. *Br J Cancer* 73:189-196.

Padhani AR (2003) MRI for assessing antivasular cancer treatments. *Br J Radiol* 76:S60-80.

Palmer RM, Ferrige AG, Moncada S (1987) Nitric oxide release accounts for the biological activity of endothelium-derived relaxing factor. *Nature* 327:524-526.

Pang JH, Cao Z, Joseph WR, Baguley BC, Ching LM (1998) Antitumour activity of the novel immune modulator 5,6-dimethylxanthenone-4-acetic acid (DMXAA) in mice lacking the interferon-gamma receptor. *Eur J Cancer* 34:1282-1289.

Parkins CS, Holder AL, Hill SA, Chaplin DJ, Tozer GM (2000) Determinants of anti-vascular action by combretastatin A-4 phosphate: role of nitric oxide. *Br J Cancer* 83:811-816.

Patlak CS, Blasberg RG, Fernstmacher JD (1983) Graphical evaluation of blood to brain transfer constants from multiple time uptake data. *J Cereb Blood Flow Metab* 3:1-7.

Patlak CS, Blasberg RG (1985) Graphical evaluation of blood-to-brain transfer constants from multiple-time uptake data. Generalizations. *J Cereb Blood Flow Metab* 5:584-590

Pedley RB, Boden JA, Boden R, Boxer GM, Flynn AA, Keep PA, Begent RH (1996) Ablation of colorectal xenografts with combined radioimmunotherapy and tumour blood flow modifying agents. *Cancer Res* 56:3293-3300.

Pedley RB, Sharma SK, Boxer GM, Boden R, Stribbling SM, Davies L, Springer CJ, Begent RH (1999) Enhancement of antibody directed enzyme prodrug

therapy in colorectal xenografts by an antivascular agent. *Cancer Res* 59:3998-4003.

Pedley RB, El-Emir E, Flynn AA, Boxer GM, Dearling J, Raleigh JA, Hill SA, Stuart S, Motha R, Begent RH (2002) Synergy between vascular targeting agents and antibody-directed therapy. *Int J Radiat Oncol Biol Phys* 54:1524-1531.

Pedley RB, Hill SA, Boxer GM, Flynn AA, Boden R, Watson R, Dearling J, Chaplin DJ, Begent RH (2001) Eradication of colorectal xenografts by combined radioimmunotherapy and combretastatin a-4 3-O-phosphate. *Cancer Res* 61:4716-4722.

Peterson HI (1991) Modification of tumour blood flow--a review. *Int J Radiat Biol* 60:201-210.

Policastro L, Duran H, Henry Y, Molinari B, Favaudon V (2006) Selective radiosensitization by nitric oxide in tumor cell lines. *Cancer Lett* doi:10.1016/j.canlet.2006.06.009.

Pollard RE, Garcia TC, Stieger SM, Ferrara KW, Sadlowski AR, Wisner ER (2004) Quantitative evaluation of perfusion and permeability of peripheral tumours using contrast-enhanced computed tomography. *Invest Radiol* 39:340-349.

Pruijn FB, van Daalen M, Holford NH, Wilson WR (1997) Mechanisms of enhancement of the antitumour activity of melphalan by the tumour blood-flow inhibitor 5,6-dimethylxanthenone-4-acetic acid. *Cancer Chemother Pharmacol* 39:541-546.

Purdie TG, Henderson E, Lee TY (2001) Functional CT imaging of angiogenesis in rabbit VX2 soft-tissue tumor. *Phy Med Biol* 46:3161-3175.

Raben D, Bianco C, Damiano V, Bianco R, Melisi D, Mignogna C, D'Armiento FP, Cionini L, Bianco AR, Tortora G, Ciardiello F, Bunn P (2004) Antitumor activity of ZD6126, a novel vascular-targeting agent, is enhanced when combined with ZD1839, an epidermal growth factor receptor tyrosine kinase inhibitor, and potentiates the effects of radiation in a human non-small cell lung cancer xenograft model. *Mol Cancer Ther* 3:977-983.

Raben D, Bianco C, Damiano V, Bianco R, Melisi D, Mignogna C, D'Armiento FP, Raghunand N, Gatenby RA, Gillies RJ (2003) Microenvironmental and cellular consequences of altered blood flow in tumours. *Br J Radiol* 76:S11-22.

Renkin EM (1959) Transport of potassium-42 from blood to tissue in isolated mammalian skeletal muscle. *Am J Physiol* 197:1205-1210

Ridnour LA, Isenberg JS, Espey MG, Thomas DD, Roberts DD, Wink DA (2005) Nitric oxide regulates angiogenesis through a functional switch involving thrombospondin-1. *Proc Natl Acad Sci U S A* 102:13147-13152.

Robinson SP, McIntyre DJ, Checkley D, Tessier JJ, Howe FA, Griffiths JR, Ashton SE, Ryan AJ, Blakey DC, Waterton JC (2003) Tumour dose response to the antivascular agent ZD6126 assessed by magnetic resonance imaging. *Br J Cancer* 88:1592-1597.

Rustin GJ, Bradley C, Galbraith S, Stratford M, Loadman P, Waller S, Bellenger K, Gumbrell L, Folkes L, Halbert G; Phase I/II Trials Committee of Cancer Research UK (2003) 5,6-dimethylxanthenone-4-acetic acid (DMXAA), a novel antivascular agent: phase I clinical and pharmacokinetic study. *Br J Cancer* 88:1160-1167.

Rustin GJ, Nathan PD, Boxall J, Saunders L, Ganesan TS, Shreeves GE (2005) A phase Ib trial of combretastatin A-4 phosphate (CA4P) in combination with carboplatin or paclitaxel chemotherapy in patients with advanced cancer. *American Society of Clinical Oncology Annual Meeting Proceedings* 23:3103.

Rustin GJ, Galbraith SM, Anderson H, Stratford M, Folkes LK, Sena L, Gumbrell L, Price PM (2003) Phase I clinical trial of weekly combretastatin A4 phosphate: clinical and pharmacokinetic results. *J Clin Oncol* 21:2815-2822.

Sahani DV, Kalva SP, Hamberg LM, Hahn PF, Willett CG, Saini S, Mueller PR, Lee TY (2005) Assessing tumor perfusion and treatment response in rectal cancer with multisection CT: initial observations. *Radiology* 234:785-792.

Seed L, Slaughter DP, Limarzi LR (1940) Effect of colchicine on human carcinoma. *Surgery* 7:696-709.

Senan S, van Sornsen de Koste J, Samson M, Tankink H, Jansen P, Nowak PJ, Krol AD, Schmitz P, Lagerwaard FJ (1999) Evaluation of a target contouring protocol for 3D conformal radiotherapy in non-small cell lung cancer. *Radiother Oncol* 53:247-255.

Senger DR, Van de Water L, Brown LF, Nagy JA, Yeo KT, Yeo TK, Berse B, Jackman RW, Dvorak AM, Dvorak HF (1993) Vascular permeability factor (VPF, VEGF) in tumour biology. *Cancer Metastasis Rev* 12:303-324.

Seshadri M, Mazurchuk R, Sperryak JA, Bhattacharya A, Rustum YM, Bellnier DA (2006) Activity of the vascular-disrupting agent 5,6-dimethylxanthenone-4-acetic acid against human head and neck carcinoma xenografts. *Neoplasia* 8:534-542.

Shaked Y, Ciarrocchi A, Franco M, Lee CR, Man S, Cheung AM, Hicklin DJ, Chaplin D, Foster FS, Benezra R, Kerbel RS (2006) Therapy-induced acute recruitment of circulating endothelial progenitor cells to tumours. *Science* 313:1785-1787.

Siemann DW, Horsman MR (2002) Enhancement of radiation therapy by vascular targeting agents. *Curr Opin Investig Drugs* 3:1660-1665.

Siemann DW, Rojiani AM (2002) Antitumour efficacy of conventional anticancer drugs is enhanced by the vascular targeting agent ZD6126. *Int J Radiat Oncol Biol* 54:1512-1517.

Siemann DW, Rojiani AM (2002) Enhancement of radiation therapy by the novel vascular targeting agent ZD6126. *Int J Radiat Oncol Biol Phys* 53:164-171.

Siemann DW, Mercer E, Lepler S, Rojiani AM (2002) Vascular targeting agents enhance chemotherapeutic agent activities in solid tumor therapy. *Int J Cancer* 99:1-6.

Siemann DW (2002) Vascular targeting agents. *Horizons in Cancer Therapeutics: From Bench to Bedside* 3:4-14.

Siim BG, Laux WT, Rutland MD, Palmer BN, Wilson WR (2000). Scintigraphic imaging of the hypoxia marker (99m)technetium-labeled 2,2'-(1,4-

diaminobutane)bis(2-methyl-3-butanone) dioxime (99mTc-labeled HL-91; prognox): noninvasive detection of tumour response to the antivasular agent 5,6-dimethylxanthenone-4-acetic acid. *Cancer Res* 60:4582-4588.

Steel G, Adama C, Peckham M (1983) *The biological basis of radiotherapy*. Amsterdam: Elsevier Science.

Stevenson JP, Rosen M, Sun W, Gallagher M, Haller DG, Vaughn D, Giantonio B, Zimmer R, Petros WP, Stratford M, Chaplin D, Young SL, Schnall M, O'Dwyer PJ (2003) Phase I Trial of the antivasular agent Combretastatin A4 Phosphate on a 5-day schedule to patients with cancer: magnetic resonance imaging evidence for altered tumor blood flow. *J Clin Oncol* 21:4428-4438.

Tabrizi-Fard MA, Fung HL (1996) Reversed-phase high-performance liquid chromatography method for the analysis of nitro-arginine in rat plasma and urine. *J Chromatogr B Biomed Appl* 679:7-12.

Tateishi U, Nishihara H, Tsukamoto E, Morikawa T, Tamaki N, Miyasaka K (2002) Lung tumors evaluated with FDG-PET and dynamic CT: the relationship between vascular density and glucose metabolism. *J Comput Assist Tomogr* 26:185-190.

Taylor NJ, d'Arcy JA, Walker-Samuel S, Collins DJ, Knowles B, Stirling JJ, Wallace T, Koh DM, Tang A, Lee C, Leach MO, Rustin GJ, Padhani AR (2006) What is the optimal cohort size for a reproducibility study of dynamic contrast-enhanced MRI? International Society for Magnetic Resonance in Medicine Annual Meeting Proceedings.

Therasse P, Arbuck SG, Eisenhauer EA, Wanders J, Kaplan RS, Rubinstein L, Verweij J, Van Glabbeke M, van Oosterom AT, Christian MC, Gwyther SG (2000) New guidelines to evaluate the response to treatment in solid tumors. J Natl Cancer Inst 92:205-216.

Thomas JP, Arzoomanian RZ, Alberti D, Marnocha R, Lee F, Friedl A, Tutsch K, Dresen A, Geiger P, Pluda J, Fogler W, Schiller JH, Wilding G (2003) Phase I pharmacokinetic and pharmacodynamic study of recombinant human endostatin in patients with advanced solid tumors. J Clin Oncol 21:223-231.

Thomlinson RH, Gray LH (1955) The histological structure of some human lung cancers and the possible implications for radiotherapy. Br J Cancer 9:539-549.

Thomsen LL, Lawton FG, Knowles RG, Beesley JE, Riveros-Moreno V, Moncada S. (1994) Nitric oxide synthase activity in human gynecological cancer. Cancer Res 54:1352-1354

Thorpe PE, Chaplin DJ, Blakey DC (2003) The first international conference on vascular targeting: meeting overview. *Cancer Res* 63:1144-1147.

Thurston G (2003) Role of Angiopoietins and Tie receptor tyrosine kinases in angiogenesis and lymphangiogenesis. *Cell Tissue Res* 314:61-68.

Tolcher AW, Forero L, Celio P, Hammond LA, Patnaik A, Hill M, Verat-Follet C, Haacke M, Besenval M, Rowinsky EK (2003) Phase I, pharmacokinetic, and DCE-MRI correlative study of AVE8062A, an antivascular combretastatin analogue, administered weekly for 3 weeks every 28-days. *American Society of Clinical Oncology Annual Meeting Proceedings* 22:834.

Tozer GM, Kanthou C, Baguley BC (2005) Disrupting tumor blood vessels. *Nat Rev Cancer* 5:423-435.

Tozer GM, Prise VE, Chaplin DJ (1997) Inhibition of nitric oxide synthase induces a selective reduction in tumor blood flow that is reversible with L-arginine. *Cancer Res* 57:948-955.

Tozer GM, Prise VE, Wilson J, Cemazar M, Shan S, Dewhirst MW, Barber PR, Vojnovic B, Chaplin DJ (2001) Mechanisms associated with tumor vascular shut-down induced by combretastatin A-4 phosphate: intravital microscopy and measurement of vascular permeability. *Cancer Res* 61:6413-6422.

Vakkala M, Kahlos K, Lakari E, Paakko P, Kinnula V, Soini Y (2000) Inducible nitric oxide synthase expression, apoptosis and angiogenesis in situ and invasive breast carcinomas. *Clin Cancer Res* 6:2408-2415.

Veikkola T, Karkkainen M, Claesson-Welsh L, Alitalo K (2000) Regulation of angiogenesis via vascular endothelial growth factor receptors. *Cancer Res* 60:203-212.

Vincent L, Kermani P, Young LM, Cheng J, Zhang F, Shido K, Lam G, Bompais-Vincent H, Zhu Z, Hicklin DJ, Bohlen P, Chaplin DJ, May C, Rafii S (2005) Combretastatin A4 phosphate induces rapid regression of tumour neovessels and growth through interference with vascular endothelial-cadherin signaling. *J Clin Invest* 115:2992-3006.

Walshe WH (1844) *The anatomy, physiology, pathology and treatment of cancer.* London.

Wang JH, Min PQ, Wang PJ, Cheng WX, Zhang XH, Wang Y, Zhao XH, Mao XQ (2006) Dynamic CT Evaluation of Tumor Vascularity in Renal Cell Carcinoma. *AJR Am J Roentgenol* 186:1423-1430.

Watson D, Grover R, Anzueto A, Lorente J, Smithies M, Bellomo R, Guntupalli K, Grossman S, Donaldson J, Le Gall JR; Glaxo Wellcome International Septic Shock Study Group (2004) Cardiovascular effects of the nitric oxide synthase inhibitor NG-methyl-L-arginine hydrochloride (546C88) in patients with septic shock: results of a randomized, double-blind, placebo-controlled multicenter study (study no. 144-002). *Crit Care Med* 32:13-20.

Sonveaux P, Dessy C, Brouet A, Jordan BF, Gregoire V, Gallez B, Balligand JL, Feron O (2002) Modulation of the tumor vasculature functionality by ionizing radiation accounts for tumor radiosensitization and promotes gene delivery. *FASEB J* 16:1979-81.

Weber WA (2005) Use of PET for monitoring cancer therapy and for predicting outcome. *J Nucl Med* 46:983-995.

Weiss RB, Greene RF, Knight RD, Collins JM, Pelosi JJ, Sulkes A, Curt GA. Phase I and clinical pharmacology study of intravenous flavone acetic acid (NSC 347512). *Cancer Res* 48:5878-5882.

Wildiers H, Ahmed B, Guetens G, De Boeck G, de Bruijn EA, Landuyt W, van Oosterom AT (2004) Combretastatin A-4 phosphate enhances CPT-11 activity independently of the administration sequence. *Eur J Cancer* 40:284-290.

Willett CG, Boucher Y, di Tomaso E, Duda DG, Munn LL, Tong RT, Chung DC, Sahani DV, Kalva SP, Kozin SV, Mino M, Cohen KS, Scadden DT, Hartford AC, Fischman AJ, Clark JW, Ryan DP, Zhu AX, Blaszkowsky LS, Chen HX, Shellito PC, Lauwers GY, Jain RK (2004) Direct evidence that the VEGF-specific antibody bevacizumab has antivasular effects in human rectal cancer. *Nat Med* 10:145-147.

Williams KJ, Telfer BA, Brave S, Kendrew J, Whittaker L, Stratford IJ, Wedge SR (2004) ZD6474, a potent inhibitor of vascular endothelial growth factor signaling, combined with radiotherapy: schedule-dependent enhancement of antitumor activity. *Clin Cancer Res* 10:8587-8593.

Wilson WR, Li AE, Cowan DS, Siim BG (1998) Enhancement of tumour radiation response by the antivasular agent 5,6-dimethylxanthenone-4-acetic acid. *Int J Radiat Oncol Biol Phys* 42:905-908.

Wintermark M, Maeder P, Verdun FR, Thiran JP, Valley JF, Schnyder P, Meuli R (2000) Using 80 kVp versus 120 kVp in perfusion CT measurement of regional cerebral blood flow. *AJNR Am J Neuroradiol* 21:1881-1884.

Wintermark M, Thiran JP, Maeder P, Schnyder P, Meuli R (2001) Simultaneous measurement of regional cerebral blood flow by perfusion CT and stable xenon CT: a validation study. *Am J Neuroradiol* 22:905-914.

Woon ST, Baguley BC, Palmer BD, Fraser JD, Ching LM (2002) Uptake of the antivasular agent 5,6-dimethylxanthenone-4-acetic acid (DMXAA) and activation of NF-kappa B in human tumour cell lines. *Oncol Res* 13:95-101.

World Health Organisation. WHO hand book for reporting results of cancer treatment. Geneva, Switzerland: World Health Organisation, 1979: WHO offset publication no. 48.

Xiong HQ, Herbst R, Faria SC, Scholz C, Davis D, Jackson EF, Madden T, McConkey D, Hicks M, Hess K, Charnsangavej CA, Abbruzzese JL (2004) A phase I surrogate endpoint study of SU6668 in patients with solid tumors. *Invest New Drugs* 22:459-466.

Yi CA, Lee KS, Kim EA, Han J, Kim H, Kwon OJ, Jeong YJ, Kim S (2004) Solitary pulmonary nodules: dynamic enhanced multidetector row CT study and comparison with vascular endothelial growth factor and microvessel density. *Radiology* 233:191-199.

Young H, Baum R, Cremerius U, Herholz K, Hoekstra O, Lammertsma AA, Pruim J, Price P (1999) Measurement of clinical and subclinical tumour response using [18F]-fluorodeoxyglucose and positron emission tomography: review and 1999

EORTC recommendations. European Organization for Research and Treatment of Cancer (EORTC) PET Study Group. *Eur J Cancer* 35:1773-1782.

Zhao D, Jiang L, Hahn EW, Mason RP (2005) Tumour physiologic response to combretastatin A4 phosphate assessed by MRI. *Int J Radiat Oncol Biol Phys* 62:872-880.

Ziche M, Morbidelli L, Choudhuri R, Zhang HT, Donnini S, Granger HJ, Bicknell R (1997) Nitric oxide synthase lies downstream from vascular endothelial growth factor-induced but not basic fibroblast growth factor-induced angiogenesis. *J Clin Invest* 99:2625-2634.

Ziche M, Morbidelli L, Masini E, Amerini S, Granger HJ, Maggi CA, Geppetti P, Ledda F (1994) Nitric oxide mediates angiogenesis in vivo and endothelial cell growth and migration in vitro promoted by substance P. *J Clin Invest* 94:2036-2044.

Zips D, Krause M, Hessel F, Westphal J, Bruchner K, Eicheler W, Dorfler A, Grenman R, Petersen C, Haberey M, Baumann M (2003) Experimental study on different combination schedules of VEGF-receptor inhibitor PTK787/ZK222584 and fractionated irradiation. *Anticancer Res* 23:3869-3876.

Zwi LJ, Baguley BC, Gavin JB, Wilson WR (1994) Correlation between immune and vascular activities of xanthenone acetic acid antitumour agents. *Oncol Res* 6:79-85.



Quantitative Assessment of Lung Cancer Perfusion Using MDCT: Does Measurement Reproducibility Improve with Greater Tumor Volume Coverage?

Quan Sing Ng¹
Vicky Goh²
Ernst Klotz³
Heinz Fichte³
Michele I. Saunders¹
Peter J. Hoskin¹
Anwar R. Padhani²

Lung Cancer Perfusion at Multi-Detector Row CT: Reproducibility of Whole Tumor Quantitative Measurements¹

Quan-Sing Ng, MBBS, MRCP
Vicky Goh, MA, MRCP, FRCR
Heinz Fichte, Dipl Inf
Ernst Klotz, Dipl Phys
Pat Fernie, DCR(R)
Michele I. Saunders, MD, FRCP, FRCR
Peter J. Hoskin, MD, FRCP, FRCR
Anwar R. Padhani, FRCP, FRCR

UNIVERSITY OF LONDON

SENATE HOUSE. MALET STREET, LONDON, WC1E 7HU



REPRODUCTION OF THESES

A thesis which is accepted by the University for the award of a Research Degree is placed in the Library of the College/Institution and in the University of London Library. The copyright of the thesis is retained by the author.

As you are about to submit a thesis for a Research Degree, you are required to sign the declaration below. This declaration is separate from any which may be made under arrangements with the College at which you have pursued your course (for internal candidates only). The declaration will be destroyed if your thesis is not approved by the examiners, being either rejected or referred for revision.

Academic Registrar

To be completed by the candidate

NAME IN FULL (Block Capitals)

QUAN SING NG

TITLE OF THESIS

THERAPEUTIC TARGETING AND CLINICAL ASSESSMENT
OF THE TUMOUR VASCULATURE

DEGREE FOR WHICH THESIS IS PRESENTED

M.D.

DATE OF AWARD OF DEGREE (To be completed by the University)

31 MAR 2008

DECLARATION

1. I authorise that the thesis presented by me in *[2007] for examination for the MPhil/PhD Degree of the University of London shall, if a degree is awarded, be deposited in the library of the appropriate College and in the University of London Library and that, subject to the conditions set out below, my thesis be made available for public reference, inter-library loan and copying.
2. I authorise the College or University authorities as appropriate to supply a copy of the abstract of my thesis for inclusion in any published list of theses offered for higher degrees in British universities or in any supplement thereto, or for consultation in any central file of abstracts of such theses.
3. I authorise the College and the University of London Libraries, or their designated agents, to make a microform or digital copy of my thesis for the purposes of inter-library loan and the supply of copies.
4. I understand that before my thesis is made available for public reference, inter-library loan and copying, the following statement will have been included at the beginning of my thesis: The copyright of this thesis rests with the author and no quotation from it or information derived from it may be published without the prior written consent of the author.
5. I authorise the College and/or the University of London to make a microform or digital copy of my thesis in due course as the archival copy for permanent retention in substitution for the original copy.
6. I warrant that this authorisation does not, to the best of my belief, infringe the rights of any third party.
7. I understand that in the event of my thesis being not approved by the examiners, this declaration would become void.

*Please state year.

DATE

4/1/07

SIGNATURE

Note: The University's Ordinances make provision for restriction of access to an MPhil/PhD thesis and/or the abstract but only in certain specified circumstances and for a maximum period of two years. If you wish to apply for such restriction, please enquire at your College/Institution about the conditions and procedures. External Students should enquire at the Research Degree Examinations Office, Room 261, Senate House.

THIS DECLARATION MUST BE COMPLETED AND RETURNED WITH THE EXAMINATION ENTRY FORM